

A HYBRID ANION EXCHANGER WITH NANOSCALE ZERO VALENT IRON FOR
TRACE HEXAVALENT CHROMIUM REMOVAL FROM DRINKING WATER

by

ANNABEL LIM MUNGAN

B.S., Johns Hopkins University, 2021

A thesis submitted to the
Faculty of the Graduate School of the
University of Colorado in partial fulfillment
of the requirement for the degree of
Master of Science
Environmental Engineering
2023

Committee Members:

Julie Korak, Ph.D., P.E.

Anthony Straub, Ph.D.

Anthony Kennedy, Ph.D., P.E.

Abstract

Mungan, Annabel L (M.S., Environmental Engineering)

A HYBRID ANION EXCHANGER WITH NANOSCALE ZERO VALENT IRON FOR
TRACE HEXAVALENT CHROMIUM REMOVAL FROM DRINKING WATER

Thesis directed by Assistant Professor Julie A. Korak

Hexavalent chromium, Cr(VI), is a human carcinogen that occurs in groundwater worldwide. While not federally regulated, the State of California has drafted a new Cr(VI) maximum contaminant level at 10 µg/L, expected to go into effect in early 2024. This study synthesizes, characterizes, and verifies performance of a hybrid strong base anion exchanger with nanoscale zero valent iron (NZVI-resin) for trace Cr(VI) removal from drinking water. NZVI-resin was synthesized by exchanging tetrachloroferrate ion, FeCl_4^- , onto the resin prior to sodium borohydride, NaBH_4 , reduction. Important synthesis variables included reagent concentrations and molar ratios, solvent selection, temperature, and drying procedure. Material characterization techniques (e.g. SEM-EDS and XPS) determined NZVI presence and distribution on the resin. Our work has shown 360% increased throughput by NZVI-resin compared to unmodified resin for trace Cr(VI) removal in column experimentation. This work presents a broad assessment of the material characteristics of NZVI-resin and its practicality for Cr(VI) treatment.

Acknowledgements

It is by the Lord's strength that I completed this work, and so I give all glory to him (Ephesians 3:20-21). I am thankful for my advisor Dr. Julie Korak for supporting me each step of the way during the past two years, providing fresh ideas and thoughtful encouragement through every setback. Julie poured countless hours into reviewing my work to make me a better researcher and writer, supported all my graduate school goals, and helped me in the lab by running analysis by IC and ICP-MS and troubleshooting experiments, and I am fortunate to call her a role model. I am also grateful to the other members of my thesis committee, Dr. Anthony Straub and Dr. Anthony Kennedy for their willingness to review my work and provide feedback. Next, I would like to thank my fellow graduate students who have stood by me. First, my labmate Ayush Raj Shahi for running analysis by IC and ICP-MS for my experiments and teaching me the fundamentals of batch and column experiments. Ayush has been a mentor to me, and I am grateful for all the encouragement and assistance he provided me throughout my project. Second, Elizabeth Hjelvik for running SEM-EDS and XPS characterization for this work, for assistance with synthesis techniques, and for her overall enthusiasm about my project. Third, my deskmate Lane Allen for assistance with dissecting microscopy. Additionally, I am grateful to the rest of the Korak lab group: Leah Flint, Emma Wilder, Lauren Magliozzi, Blair Hanson, Ida Clarke, and Landon Watts for their help and feedback through my master's. I am grateful for the support of my father, Carl Mungan, who first exhibited to me a love for research and encouraged me to pursue higher education; my mother, Peckbee Mungan, who prayed for me constantly through all the ups and downs of lab work; and my brother, Evan Mungan, for his encouragement along the way. Lastly, I thank the Colorado Groundwater Association and the National Science Foundation Graduate Research Fellowship for financially supporting this work.

Table of Contents

<i>1</i>	<i>CHAPTER 1: INTRODUCTION</i>	<i>1</i>
1.1	Hexavalent chromium.....	1
1.1.1	Toxicity.....	2
1.1.2	Occurrence.....	2
1.1.3	Drinking water regulations.....	4
1.2	Conventional Cr(VI) treatment technologies.....	4
1.2.1	RCF by ferrous iron.....	5
1.2.2	Stannous chloride.....	6
1.3	Ion exchange fundamentals.....	7
1.3.1	Resin properties.....	7
1.3.2	Capacity.....	12
1.3.3	Selectivity.....	13
1.3.4	Isotherm behavior.....	15
1.3.5	Mass transfer.....	17
1.3.6	Operation.....	19
1.3.7	Cr(VI) operation.....	23
1.4	Hybrid ion exchange.....	24
1.4.1	Nanoscale zero valent iron.....	26
1.4.2	Cr(VI) removal mechanism.....	27
1.4.3	Summary of previous findings.....	28
1.4.4	Research gap.....	30
<i>2</i>	<i>CHAPTER 2: METHODS</i>	<i>32</i>
2.1	Chemicals and reagents.....	32
2.2	Resins.....	32
2.3	Analytical methods.....	33
2.4	Synthesis.....	38
2.4.1	FeCl ₄ ⁻ -A600E optimization.....	42

2.4.2	NZVI-A600E optimization	44
2.5	Resin density change.....	46
2.6	Characterization	47
2.7	Batch experimentation	48
2.8	Fluidized bed column experimentation.....	48
3	<i>CHAPTER 3: RESULTS</i>	51
3.1	Synthesis	51
3.1.1	FeCl ₄ ⁻ -A600E optimization.....	57
3.1.2	NZVI-A600E optimization	59
3.1.3	Final synthesis procedure.....	66
3.2	Resin density change.....	68
3.3	Characterization	70
3.3.1	Visual inspection.....	70
3.3.2	Dissecting microscopy	71
3.3.3	SEM-EDS	72
3.3.4	XPS	74
3.4	Batch experiments.....	76
3.4.1	Capacity	76
3.4.2	Selectivity experiments.....	78
3.5	Fluidized bed column experimentation.....	81
4	<i>CHAPTER 4: CONCLUSION</i>	89
4.1	Summary	89
4.2	Practical implications.....	90
4.3	Future horizons	90
	<i>References</i>	92

List of Tables

Table 1. Types of resin and their pK_a values 8

Table 2. Previous studies using NZVI HIX for Cr(VI) removal..... 30

Table 3. Properties of selected resins as reported by manufacturers. 33

Table 4. Prior methodology for NZVI synthesis on SBA-IX resin..... 41

Table 5. Column engineering parameters. 48

Table 6. Column influent water quality. 49

Table 7. Synthesis of NZVI screening experiments using anion exchange resin, with each row documenting the incremental change in approach..... 51

Table 8. Freundlich fitted parameters for the A600E iron loading isotherm. 59

Table 9. Selected iron loading condition..... 59

Table 10. Dissecting microscopy images of NZVI-A600E over varied NaBH₄ conditions..... 61

Table 11. Resin cracking, Cr(VI) removal, and pH change from varying NaBH₄ parameters in replicate..... 65

Table 12. Resin mass change for 1 g of each resin in replicate. 69

Table 13. Resin capacities (with resin density correction)..... 77

Table 14. Column performance between resins. 81

Table 15. Expanded heights of A600E and NZVI-A600E in upflow column experiments..... 83

Table 16. Fluidized bed parameters. 84

List of Figures

Figure 1. log C–pH diagram showing the speciation of Cr(VI)..... 1

Figure 2. Tetrahedral structure of chromate and sulfate anions..... 2

Figure 3. Process flow of RCF Cr(VI) system..... 6

Figure 4. Schematic of SBA-IX resin bead..... 9

Figure 5. Polymetric matrices of SBA-IX resin..... 9

Figure 6. Functional groups of Type 1 and Type 2 SBA-IX resin..... 10

Figure 7. (A) Gel A600E Purolite® resin (B) Macroporous TP 107 Lanxess Lewatit® resin..... 11

Figure 8. Transmission electron microscopy (TEM) of (A) gel (B) macroporous anion exchange resin..... 11

Figure 9. Capacity isotherm for CrO₄²⁻ using a SBA-IX resin. 13

Figure 10. Selectivity isotherm for CrO₄²⁻ over SO₄²⁻ using a SBA-IX resin..... 15

Figure 11. (a) Linear, (b) rectangular, (c) favorable, and (d) unfavorable isotherms 16

Figure 12. Langmuir, Freundlich, and Linear equations..... 17

Figure 13. Mass transfer into a cation exchange resin..... 18

Figure 14. Mass transfer zone over time for a highly selective target ion such as CrO₄²⁻ in a downflow fixed-bed column IX system..... 20

Figure 15. Breakthrough curve of SO₄²⁻ in an anion exchange column. 21

Figure 16. Regeneration curve of SBA-IX for Cr(VI) removal at alkaline pH 22

Figure 17. Process flow of regenerable SBA-IX system 23

Figure 18. Purolite ArsenX^{np} HIX resin..... 26

Figure 19. Removal of HCrO₄⁻ using SBA-IX resin impregnated with NZVI 28

Figure 20. 1,5-Diphenylcarbazine method calibration curve for measuring Cr(VI) concentrations in water..... 35

Figure 21. Calibration curve for measuring Cr(VI) concentrations in water.....	36
Figure 22. Molar absorptivity of FeCl_4^- in an excess-chloride methanol solution	36
Figure 23. Full scan of 5.5 mg/L Fe^{3+} in an excess-chloride ethanol solution.	37
Figure 24. Calibration curve of Fe^{3+} concentrations at 362 nm.	38
Figure 25. NZVI-impregnated SBA-IX resin for CrO_4^{2-} removal.	39
Figure 26. Iron loading test matrix for FeCl_4^- -A600E.	43
Figure 27. Sodium borohydride loading test matrix for NZVI-A600E.	45
Figure 28. (A) Schematic and (B) photo of upflow fluidized bed column setup.	50
Figure 29. Isotherm of iron loading onto A600E resin.	58
Figure 30. NZVI-A600E produced gas bubbles at all 9 conditions tested.	60
Figure 31. Contour plot of dependence of resin cracking (%) on NaBH_4 conditions.....	64
Figure 32. FeCl_4^- exchange onto A600E resin.	66
Figure 33. Reduction of Fe^{3+} to Fe^0 by NaBH_4 on A600E resin.	67
Figure 34. (A) Pristine A600E (B) FeCl_4^- -A600E (C) NZVI-A600E.....	68
Figure 35. Freshly synthesized NZVI-A600E.	70
Figure 36. NZVI-A600E attracted to a metal stir bar in a round bottom flask.	71
Figure 37. Dissecting microscope images of (A) A600E (B) fresh NZVI-A600E (C) post- column NZVI-A600E.	71
Figure 38. SEM-EDS image of (A) A600E (B) fresh NZVI-A600E (C) post-column NZVI- A600E.	72
Figure 39. Elemental composition of (A) A600E (B) fresh NZVI-A600E (C) post-column NZVI-A600E.	73
Figure 40. XPS spectrum of A600E, fresh NZVI-A600E, and post-column NZVI-A600E.	74

Figure 41. XPS scan from 705-740 eV of (A) fresh NZVI-A600E (B) post-column NZVI-A600E.	75
Figure 42. Equilibrium isotherms of A600E and NZVI-A600E.....	77
Figure 43. (A) A600E and (B) NZVI-A600E batches after 24 hours.....	78
Figure 44. Separation factors α_{CrO_4/SO_4} of A600E and NZVI-A600E in 175 mg/L Cr(VI) and 2000 mg/L SO_4^{2-} solution.	79
Figure 45. Equilibrium isotherms with 2000 mg/L SO_4^{2-} of A600E and NZVI-A600E.....	80
Figure 46. Breakthrough curve for trace Cr(VI) in upflow column experiments.	82
Figure 47. Breakthrough curve for SO_4^{2-} in upflow column experiments.	83
Figure 48. Effluent iron during NZVI-A600E column experiment.	85
Figure 49. Approximate effluent boron concentrations during NZVI-A600E column experiment.	86
Figure 50. Effluent pH during NZVI-A600E column experiment.....	87
Figure 51. Images of post-column NZVI-A600E	88

1 CHAPTER 1: INTRODUCTION

1.1 Hexavalent chromium

Chromium occurs in surface and groundwater in two stable oxidation states: trivalent chromium, Cr(III), and hexavalent chromium, Cr(VI) (Saha et al., 2011). Cr(III), the reduced form, exists as cationic species, exhibiting low solubility and therefore low mobility in soils and water. Common forms of Cr(III) include Cr^{3+} , CrOH^{2+} , Cr(OH)_2^+ , and $\text{Cr(OH)}_3(\text{s})$ (Bryjak et al., 2016). Cr(VI), the oxidized form, exists in oxyanions and oxyacid forms and is comparatively more soluble and thus more mobile in water. Its exact species depends upon redox potential, concentration, and pH, shown in **Figure 1**. Above pH 6.5, which is the range relevant to groundwater, chromate (CrO_4^{2-}) is the prevalent form of Cr(VI) (Bryjak et al., 2016; Fendorf, 1995). Chromate has a tetrahedral structure, similar to that of sulfate, SO_4^{2-} , as shown in **Figure 2** (Bryjak et al., 2016). The differences between the CrO_4^{2-} and SO_4^{2-} ions will be further discussed in Section 1.3.3.

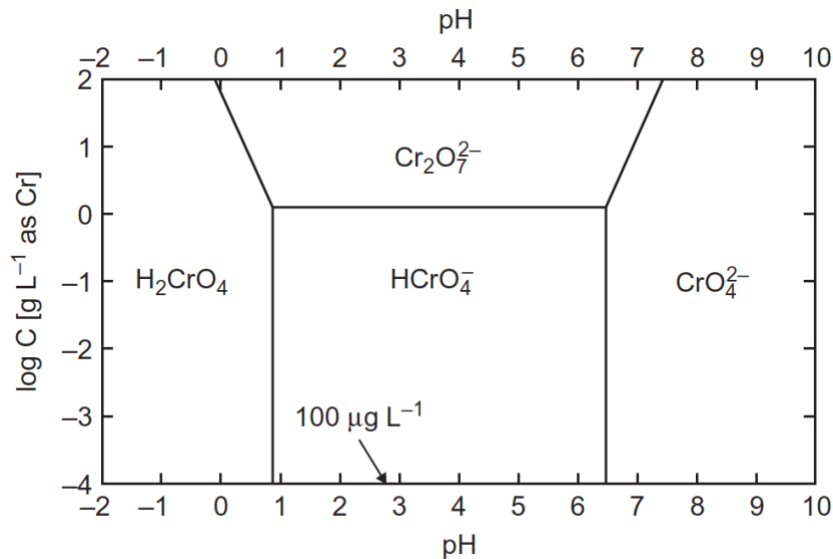


Figure 1. log C–pH diagram showing the speciation of Cr(VI) (Bryjak et al., 2016).

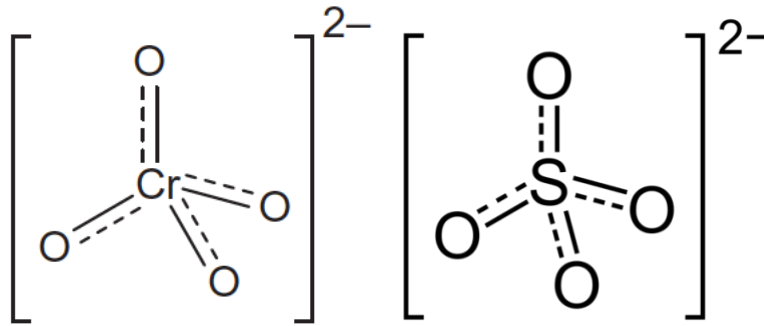


Figure 2. Tetrahedral structure of chromate and sulfate anions (Bryjak et al., 2016).

1.1.1 Toxicity

Cr(III), which is non-toxic at trace levels, is considered an essential micronutrient for humans and is even taken as a dietary supplement (Costa, 2003). Cr(VI), on the other hand, is a human carcinogen. Since chromate mimics the structure of phosphate and sulfate salts as illustrated in **Figure 2**, it is readily taken up into the cells (Sedman et al., 2006). Inhalation of Cr(VI) can lead to elevated lung cancer risk, kidney circulation issues, nerve tissue damage, and death in large doses (Saha et al., 2011; Owlad et al., 2009). By the ingestion route, such as through drinking water, Cr(VI) is also carcinogenic, although less potent than through inhalation (Moffat et al., 2018; Costa, 2003).

1.1.2 Occurrence

Chromium occurs naturally as a mineral in the earth's mantle (Fendorf, 1995). It often exists in the form of Cr(III) within ultramafic- and serpentinite-derived soils and rock, which through natural processes can be oxidized to Cr(VI) in the groundwater, particularly in alkaline, oxic conditions (Oze et al., 2007; Hausladen et al., 2018). Naturally elevated levels of aqueous

Cr(VI) exceeding 50 µg/L in groundwaters have been reported in California, Arizona, Mexico, Brazil, Italy, New Caledonia, Australia, and India (Bryjak et al., 2016). In addition to solely natural processes, Hausladen et al., 2018 found that oxidation of Cr(III) deposits can be accentuated by in situ chemical oxidation (ISCO) of chlorinated solvents where permanganate or persulfate is used, with concentrations of Cr(VI) reported up to 3 mg/L (Hausladen et al., 2018). Groundwater pumping and increase of nutrient content, such as in the Central Valley of California, are also correlated with accelerated Cr(III) oxidation to Cr(VI) (Hausladen et al., 2018).

Cr(VI) may also enter the water supply through industrial processes, such as its uses for paint dyes, rubber, plastic, leather tanning, textiles, copy machine toner, industrial water cooling, petroleum refining, and metal finishing (Owlad et al., 2009; Saha et al., 2011). While industrial discharges tend to lead to more acute Cr(VI) groundwater contamination (typically 300-500 µg/L and in some cases up to 14 mg/L), Hausladen et al., 2018 found that in California, oxidation of naturally occurring Cr(III) affects a much larger area and greater number of water supplies in the state (Hausladen et al., 2018; Bryjak et al., 2016).

According to the USEPA's Second Six-Year Review from 1998-2005, 8623 water supplies in the United States have Cr(VI) above 10 µg/L, with 681 water supply entry points in the state of California. Of the 8623 water supplies, 54% of systems serve populations less than 1000 people and 83% of systems serve populations less than 10,000 people, often through small groundwater-fed pump stations. The highest Cr(VI) occurrences were found in California, Arizona, and Nevada (Seidel & Corwin, 2013). Thus, there is interest in Cr(VI) treatment solutions that are modular and decentralized for these numerous small groundwater-fed systems.

1.1.3 Drinking water regulations

Cr(VI) first entered the public's radar in 1993, when Eric Brockovich famously reported groundwater with 580 µg/L Cr(VI) near Hinkley, California due to wastewater containing Cr(VI) used as a cooling tower corrosion inhibitor that had been stored in unlined ponds (Pellerin & Booker, 2000). As of 1992, the USEPA has regulated total chromium (a measurement of Cr(III) and Cr(VI) combined) at 100 µg/L, and California has had its own MCL of 50 µg/L total chromium, since 1977. The World Health Organization (WHO) has also set a guideline of 50 µg/L on total chromium as of 2003 (McLean et al., 2012). In 2014, California put a drinking water MCL of 10 µg/L Cr(VI) into effect, leaving the state scrambling to invest in research to bring Cr(VI) treatment technologies to full-scale for utilities not in compliance. By 2017, however, the regulation was rescinded due to a lack of economical treatment technologies (*California Manufacturers and Technology Association and Solano County Taxpayers Association v. State Water Resources Control Board.*, 2017). In March 2022, California re-proposed this 10 µg/L Cr(VI) MCL, expected to take effect in early 2024, providing a compliance phasing approach based on number of service connections (California Water Boards, 2023). Thus, this contaminant returns to the forefront of research efforts. Economical technologies for Cr(VI) removal are imperative, especially for California communities that rely on contaminated groundwater for their water supply.

1.2 Conventional Cr(VI) treatment technologies

For Cr(VI) removal, the EPA lists three best available technologies (BATs), which are those technologies found to be effective for bringing Cr(VI) concentrations below 1 µg/L at full-scale. These are reverse osmosis (RO), reduction coagulation and filtration by ferrous sulfate or

ferrous chloride (RCF), and ion exchange (IX) (Dummer, 2021). Ion exchange will be discussed extensively in Section 1.3. A fourth technology still in the research stage is reduction and filtration using stannous chloride. Due to high costs from operation and concentrate disposal, and comparatively lower water recoveries, RO has not proved economical for small-scale groundwater-fed systems seeking to remove trace Cr(VI) from drinking water (Seidel et al., 2013). During the three years of the 10 µg/L MCL for Cr(VI) in California from 2014-2017, utilities installed full-scale regenerable strong base anion exchange (SBA-IX), regenerable weak base anion exchange (WBA-IX), single-use SBA-IX (Carothers & Gorman, 2023), and RCF technologies, some of which continue to operate to the present day. With this reinstated MCL, there is a need for improvement of current technologies.

1.2.1 RCF by ferrous iron

Reduction, coagulation, and filtration systems add ferrous sulfate or ferrous chloride to convert Cr(VI) to Cr(III) in reduction contactors, which take 1-3 minutes for reduction to complete. Next, additional coagulant or an oxidant is added to form flocs that adsorb Cr(III), which is removed in media filters. The filters are backwashed for 4-5 minutes, sending backwash waste to a sewer discharge. This sewer discharge can be an issue for many groundwater well facilities, where such a connection is not available. In addition, backwash solids may prove hazardous, requiring disposal at a hazardous waste site (Qin et al., 2005). A typical process flow is shown in **Figure 3**. An example of an operational full-scale system is Las Lomas Station 305, owned by California Water Service Company, which treated influent water with 20 µg/L Cr(VI), 214 µg/L Fe, and 263 µg/L Mn simultaneously using RCF processes (Huynh & Edjan, 2023). Advantages include simple process, lack of competition with other oxyanions, and the potential

lack of disposal of a hazardous waste brine or resin (Gorman et al., 2023). Disadvantages of this process include backwash waste, which requires sewer discharge or possible hazardous solids disposal, and a larger utility footprint than ion exchange (Marracocco & Kennedy, 2023).

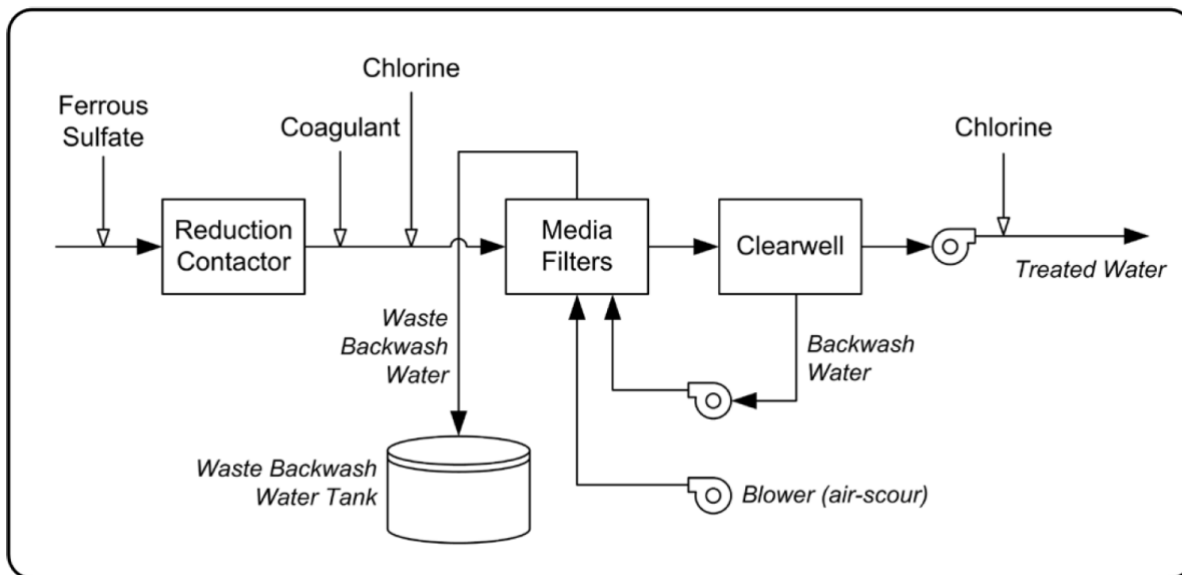
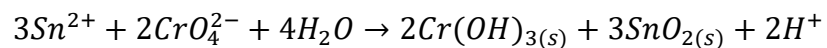


Figure 3. Process flow of RCF Cr(VI) system (Najim et al., 2014).

1.2.2 Stannous chloride

Reduction by stannous chloride, SnCl_2 , is an up-and-coming treatment technology for Cr(VI) in drinking water. This chemical is approved as a corrosion inhibitor for drinking water, but has not yet been widely adopted (Moffat et al., 2018; Henrie et al., 2019). Used similarly to ferrous sulfate, stannous chloride is a chemical reductive treatment using Sn(II) addition according to the following equation (H. Liu & Yu, 2020):



Compared to ferrous RCF, the stannous process has faster reduction kinetics and requires a lower stoichiometric molar ratio, removing the need for coagulation and flocculation in favor of a

simple post-reduction filtration step for removal of particulates (Kennedy et al., 2018). This process has the potential to lower capital and operation and maintenance (O&M) costs (Moffat et al., 2018). Stannous chloride reduction for Cr(VI) removal has been tested at a pilot scale for drinking water applications, but future research is needed to understand distribution system interactions between Cr(III), free chlorine, and pipe corrosion scales (Henrie et al., 2019; H. Liu & Yu, 2020).

1.3 Ion exchange fundamentals

Ion exchange is a technology used to remove dissolved ionic constituents from water. While ion exchange occurs in nature on clays and other minerals, water treatment applications consist of commercially synthesized resin beads with charged functional groups, which can target specific ions from water. The most common ion exchange systems are those used in individual household applications for water softening to remove calcium and magnesium and commercial or laboratory demineralization systems to remove all electrolytes, producing a pure water (Crittenden et al., 2012). Municipal water treatment applications include removal of nitrate, barium, radium, perchlorate, arsenic, and chromium.

1.3.1 Resin properties

Tens of ion exchange resin manufacturers exist worldwide, with hundreds of different resins specifically designed for particular target ions or applications (SenGupta, 2017). There are two categories of ion exchange: cation exchange and anion exchange. Cation exchange resins have negatively charged functional groups, which can exchange cations onto the resin. Anion exchange resins have positively charged function groups, which can exchange anions onto the resin. The difference between weak and strong acid and weak and strong base resins is the

electrolytic strength of the functional groups on the resin, exhibited in their differing pK_a values, as shown in **Table 1**. For instance, a weak base ion exchanger has a pK_a of 6.7-8.3, meaning that their functional groups will not be charged, giving up an OH^- ion, unless the pH is below this range. Strong base ion exchangers, on the other hand, have a pK_a of 13, meaning that they will be charged across all operational water qualities ($pH < 13$). Since Cr(VI) is in the form of CrO_4^{2-} at alkaline pH ranges relevant to groundwater, this work will focus on strong base anion exchange.

Table 1. Types of resin and their pK_a values (Crittenden et al., 2012).

Resin Type	pK_a
Strong acid	< 0
Weak acid	4-5
Weak base	6.7-8.3
Strong base	> 13

Strong base anion exchange (SBA-IX) resin consists of a polymeric skeleton that is crosslinked with divinylbenzene (DVB). The functional groups are covalently bound on the skeleton at regular intervals. SBA-IX resin most often uses quaternary ammonium functional groups for its positive charged groups. To maintain electroneutrality, negatively charged presaturant ions such as Cl^- or OH^- are loosely bound to the functional groups (Benjamin and Lawler, 2013). **Figure 4** shows a visual representation of a SBA-IX resin bead.

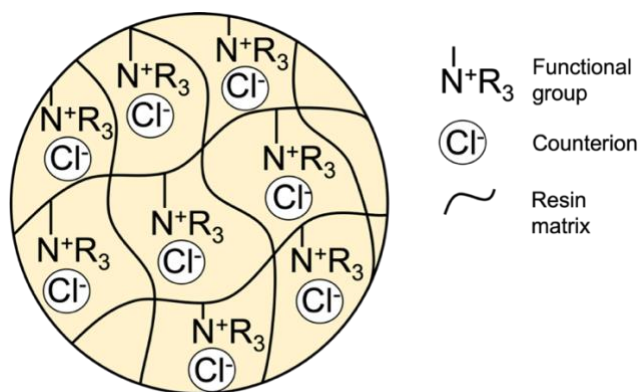


Figure 4. Schematic of SBA-IX resin bead.

There are two types of polymeric matrix structures common to SBA-IX resin: polystyrene and polyacrylate (acrylic), both shown in **Figure 5**. Between the two matrix types, acrylic SBA-IX resin is more hydrophilic, with higher concentration of functional groups, increasing its selectivity for divalent ions like CrO₄²⁻ and SO₄²⁻ and its resistance to organic fouling (de Dardel, 2013a; SenGupta, 2017).

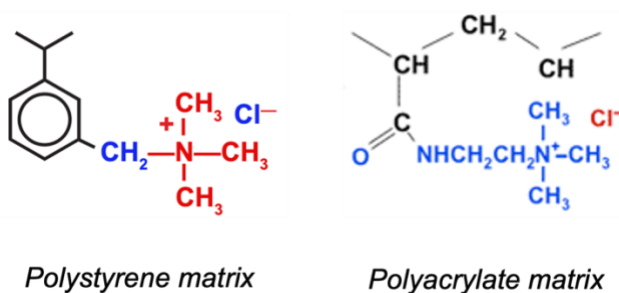


Figure 5. Polymeric matrices of SBA-IX resin (de Dardel, 2013a).

SBA-IX resin functional groups fall into two types. Type 1 quaternary ammonium resin is made up of a trimethylamine, three methyl groups attached to the nitrogen atom. Type 2 quaternary ammonium resin is made up of a dimethylethanolamine, which has an additional ethanol group, decreasing the resin selectivity for ions with respect to OH⁻, but increasing the

resin capacity and regeneration efficiency (de Dardel, 2013a; Crittenden et al., 2012; SenGupta, 2017). **Figure 6** shows the functional groups for each type of resin.

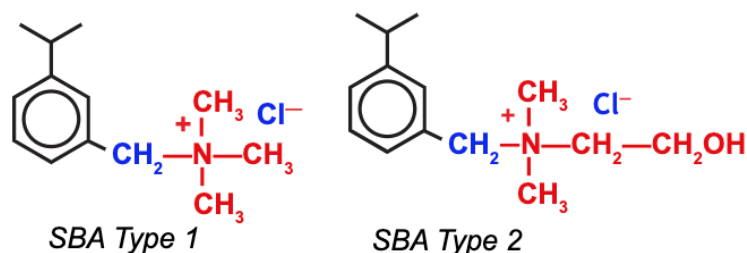


Figure 6. Functional groups of Type 1 and Type 2 SBA-IX resin (de Dardel, 2013a).

SBA-IX resin is also classified as either gel (microreticular) or macroporous (macroreticular), depending upon the synthesis methods. Gel resin is typically 4-10% DVB, is translucent, has high water content, and has a large ability to swell and shrink. Macroporous resin is typically 20-25% DVB, is opaque, has lower water content, and has a limited ability to swell and shrink (Crittenden et al., 2012). Resin swelling and shrinking is caused by ion exchange osmosis. Because the functional groups on the resin are immobile, there is high internal osmotic pressure in the resin (SenGupta, 2017). As water molecules move into the resin to lower this pressure, the resin expands. Lower degrees of DVB crosslinking allow the resin to move more freely, leading to a larger ability to swell and shrink without fracturing the resin. While gel resin is a continuous phase, macroporous resin is composed of smaller microsphere units linked together; therefore, macroporous resin has greater surface area and porosity, allowing exchange of large ions. The two resin morphologies are shown in **Figure 7** and **Figure 8**.

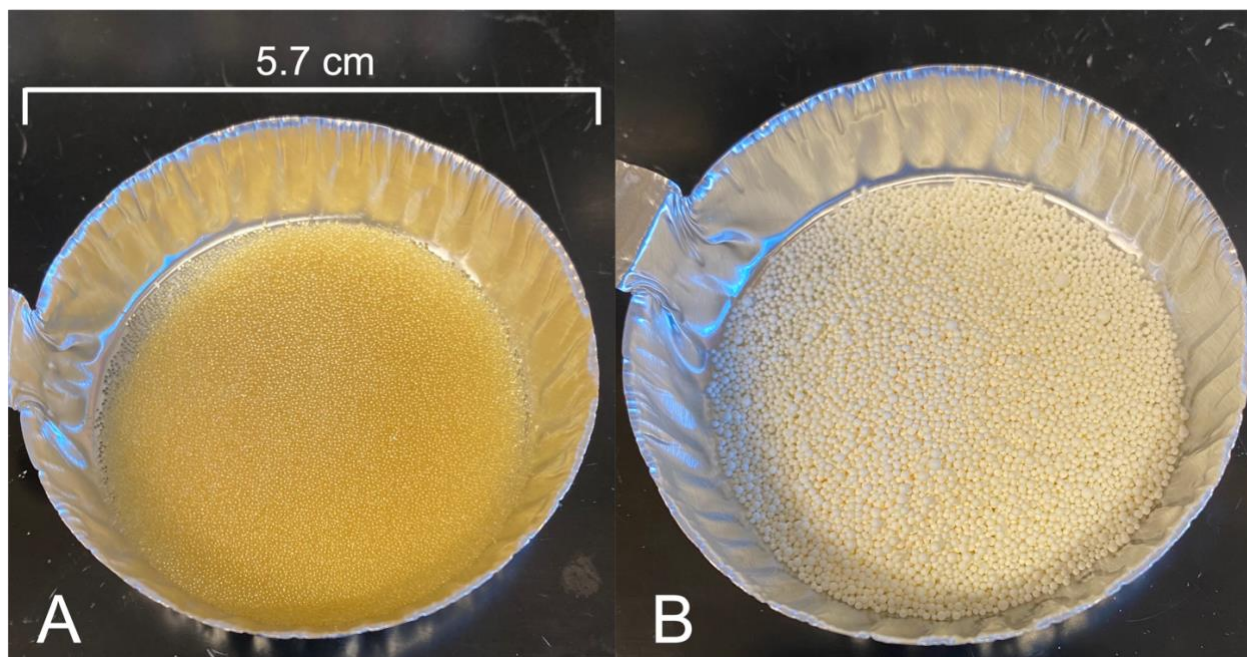


Figure 7. (A) Gel A600E Purolite[®] resin (B) Macroporous TP 107 Lanxess Lewatit[®] resin.

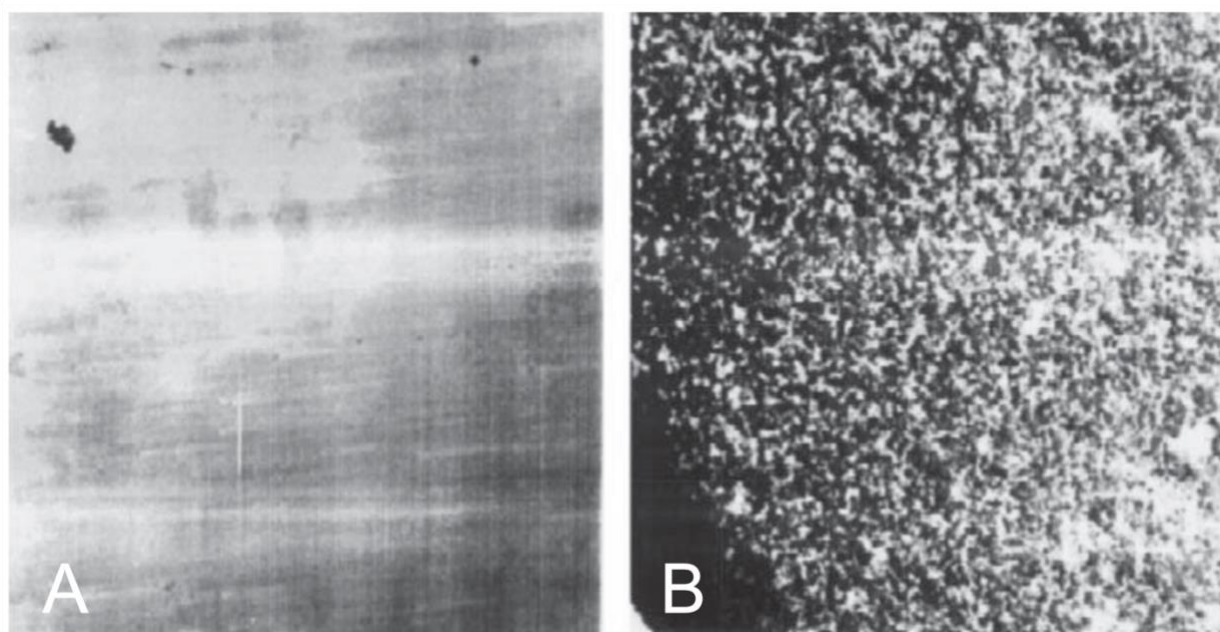


Figure 8. Transmission electron microscopy (TEM) of (A) gel (B) macroporous anion exchange resin (P. Li & SenGupta, 2000).

1.3.2 Capacity

Resin capacity is defined as the number of charged functional groups per dry resin mass or volume. In order to measure resin capacity, a batch test can be performed. To do so, a known mass of resin in its presaturant form is placed in a known volume of solution containing the target ion and any other background ions. The solution is brought to equilibrium by stirring the batch for sufficient time, at which point the solution concentration is measured. Then, mass of target ion that exchanged onto the resin is determined by difference between final and initial solution concentration. For instance, if 1 g of dry anion exchange resin with a wet bead specific gravity of 1.09 can exchange a maximum of 100 mg CrO_4^{2-} onto it, its resin capacity would be as follows:

$$\frac{100 \text{ mg } \text{CrO}_4^{2-}}{\text{g resin}} * \frac{1 \text{ g } \text{CrO}_4^{2-}}{1000 \text{ mg } \text{CrO}_4^{2-}} * \frac{1 \text{ mol } \text{CrO}_4^{2-}}{116 \text{ g } \text{CrO}_4^{2-}} * \frac{2 \text{ eq } \text{CrO}_4^{2-}}{1 \text{ mol } \text{CrO}_4^{2-}} * \frac{1090 \text{ g resin}}{1 \text{ L}} = \frac{1.88 \text{ eq}}{\text{L}}$$

To confirm the resin capacity, a variety of resin masses and solution volumes can be tested and plotted as an isotherm, which shows the equilibrium distribution of ions between a solution and the ion exchanger at a given temperature. The isotherm plots equilibrium concentration of target ion in solution on the x-axis and q , the resin capacity, on the y-axis. An example five-point capacity isotherm is shown in **Figure 9**.

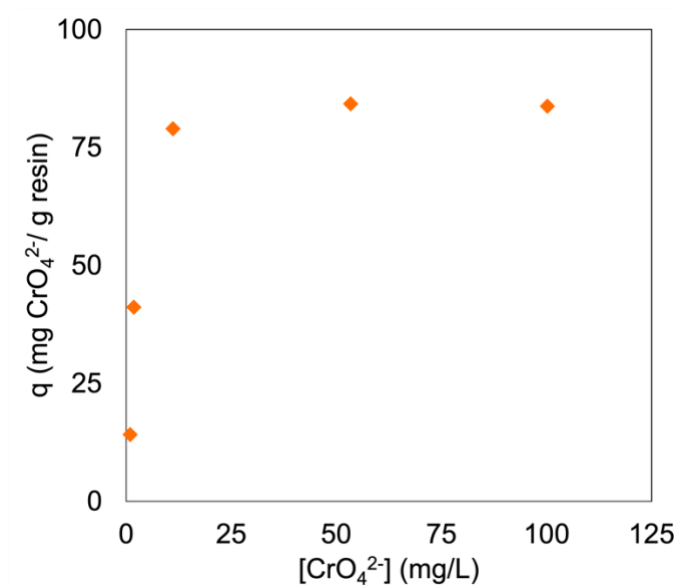
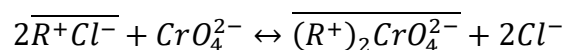


Figure 9. Capacity isotherm for CrO_4^{2-} using a SBA-IX resin.

1.3.3 Selectivity

When background constituents other than the target ion are present in a groundwater, understanding the affinity of a resin for one constituent over another, called selectivity, becomes important. In groundwater contaminated with Cr(VI), relevant ions include CrO_4^{2-} , SO_4^{2-} , NO_3^- , Cl^- , and HCO_3^- . Other co-occurring oxyanionic contaminants can include arsenic, vanadium, and uranium (Flint et al., 2021).

For the exchange equation between CrO_4^{2-} and Cl^- , a selectivity coefficient $K_{\text{CrO}_4/\text{Cl}}$ can be defined, which is the equilibrium constant for CrO_4^{2-} over Cl^- , with the overbar indicating resin phase. For $K_{A/B} > 1$, A is preferred by the ion exchange resin, while for $K_{A/B} < 1$, B is preferred.



$$K_{CrO_4/Cl} = \frac{\overline{C_{CrO_4}}(C_{Cl})^2}{(\overline{C_{Cl}})^2 (C_{CrO_4})}$$

A separation factor can also be defined, which represents the affinity of one ion over another (Benjamin & Lawler, 2013). The separation factor is the same as the selectivity coefficient for homovalent ion exchange, but for heterovalent ion exchange, the values are different. The case of the separation factor $\alpha_{CrO_4/Cl}$ illustrates this.

$$\alpha_{CrO_4/Cl} = \frac{\overline{C_{CrO_4}}(C_{Cl})}{(\overline{C_{Cl}})(C_{CrO_4})}$$

When $\alpha_{A/B} < 1$, A is less preferred in the resin than B. When $\alpha_{A/B} = 1$, A and B are equally preferred. When $\alpha_{A/B} > 1$, A is more preferred than B.

Selectivity is resin- and water chemistry-specific. In dilute aqueous solutions, higher valence anions have a higher selectivity than lower valence anions (Clifford & Weber Jr., 1982; Crittenden et al., 2012). Between same charged anions, such as NO_3^- , Cl^- , and HCO_3^- , ions with greater atomic number, larger ionic radius, and smaller hydrated radius have higher selectivity (Crittenden et al., 2012). Between ions such as CrO_4^{2-} and SO_4^{2-} , resin-specific differences can come into play, such as pore size distribution, crosslinking, and hydrophilicity of the matrix (Crittenden et al., 2012; A. K. Sengupta et al., 1986). For Cr(VI) selective resins, such as the Purolite® polystyrene type 1 A600E resin used in this work, the selectivity factors for relevant ions typically have the following relationship (de Dardel, 2013b).



Like for resin capacity, resin selectivity can be measured by a series of batch tests, which are dosed with a known mass of resin and known concentrations of the constituents of interest. An isotherm can be plotted, as shown in blue in **Figure 10**.

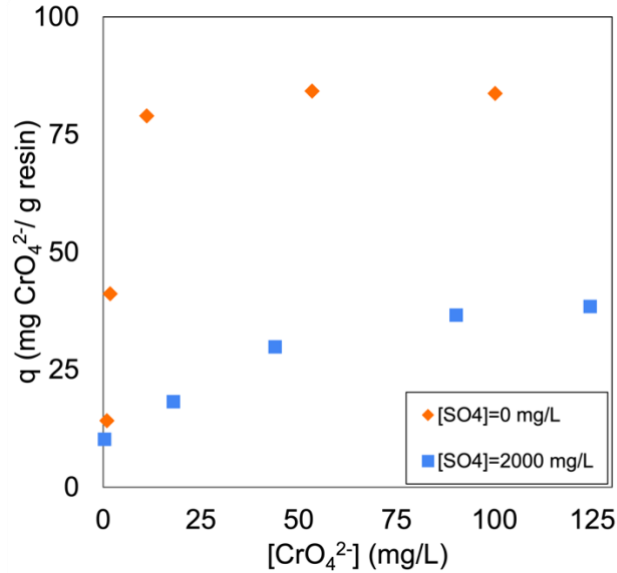


Figure 10. Selectivity isotherm for CrO_4^{2-} over SO_4^{2-} using a SBA-IX resin.

Trace ion exchange is the case where the target ion in the liquid phase exists in much lower concentrations than background constituents (SenGupta, 2017). In these cases, high resin selectivity is especially important for removal of the target ion. For example, in groundwaters, SO_4^{2-} is often at concentrations thousands of times higher than CrO_4^{2-} , causing it to be a competitor for ion exchange functional groups. Thus, SO_4^{2-} is a primary driver of capacity of SBA-IX resin used for trace Cr(VI) removal (Gorman et al., 2016). For trace Cr(VI) removal at alkaline pH, Cr(VI) will take the form of a favorable or linear isotherm (A. K. Sengupta et al., 1986).

1.3.4 Isotherm behavior

Isotherms can be favorable, unfavorable, or linear, shown in **Figure 11**, depending upon conditions.

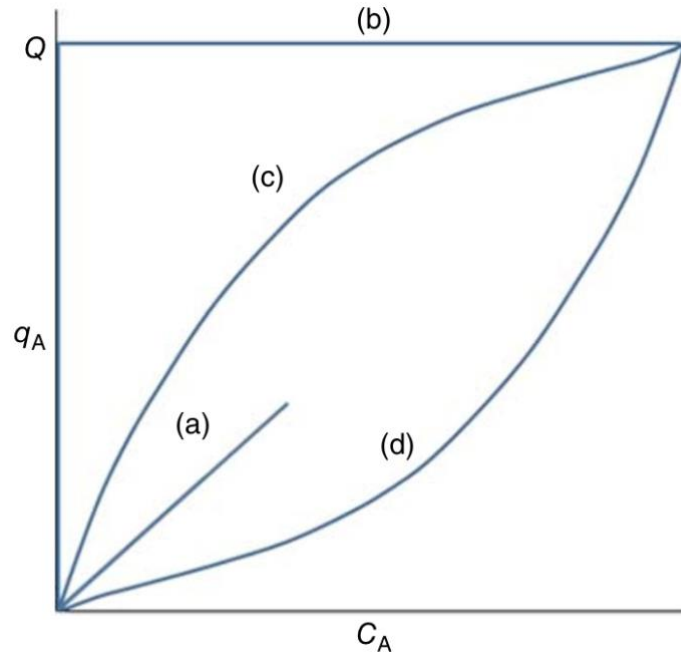


Figure 11. (a) Linear, (b) rectangular, (c) favorable, and (d) unfavorable isotherms (SenGupta, 2017).

In cases of trace concentrations of a constituent, such as when $[\text{CrO}_4^{2-}] \ll [\text{SO}_4^{2-}]$, the CrO_4^{2-} capacity isotherm can be described by a linear isotherm model due to a linear dependence between capacity and equilibrium concentration of the trace constituent. Favorable isotherms, with their characteristic concave downward shape, occur where the selectivity coefficient $K_{A/B} > 1$ for non-trace constituents A and B. Unfavorable isotherms, with their characteristic concave upward shape, occur where $K_{A/B} < 1$.

Similar to granular activated carbon and other adsorption processes, some approaches try to compare isotherms using the empirical Langmuir and Freundlich isotherm models (Benjamin & Lawler, 2013).

$$\text{Langmuir: } q = \frac{q_{\text{max}} K_{\text{Lang}} c}{1 + K_{\text{Lang}} c}$$

$$\text{Freundlich: } q = k_f c^n$$

In these equations, q is the resin-phase concentration, c is the equilibrium liquid-phase concentration, and K_{Lang} , q_{max} , k_f , and n are empirically fitted constants. **Figure 12** shows these models compared to a linear equation. The Langmuir adsorption model aligns better with the finite number of exchange sites, with q_{max} equal to the resin capacity. The use of the Langmuir model is discouraged for modeling pure ion exchange, because it is not constrained by laws of mass action or exchange on a charge equivalent basis (Hauptert et al., 2021). However, a Langmuir or Freundlich model may be more representative of hybrid anion exchangers with heterogeneous removal mechanisms such as ion exchange, adsorption, and reduction and precipitation.

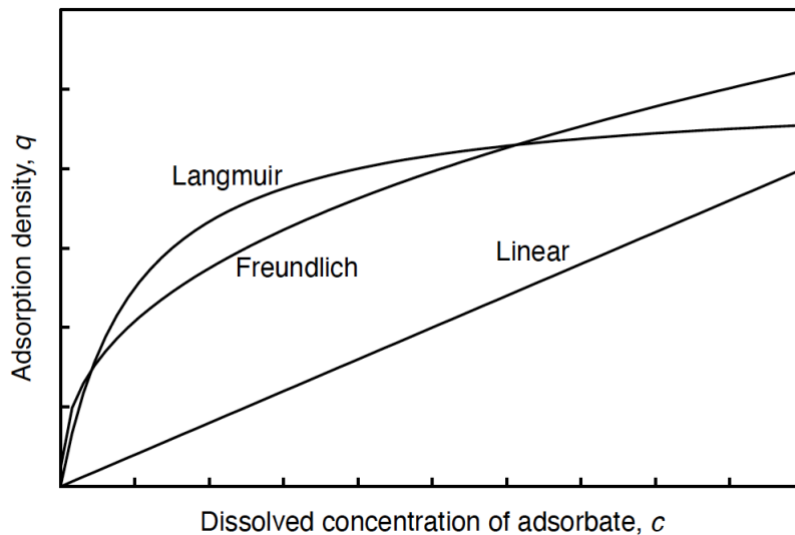


Figure 12. Langmuir, Freundlich, and Linear equations (Benjamin & Lawler, 2013).

1.3.5 Mass transfer

The kinetics of ion exchange can be thought of in terms of six individual steps, which are illustrated in **Figure 13** for cation exchange (SenGupta, 2017). Ions first move from bulk

solution to the resin liquid film; second, diffuse across the liquid film; third, diffuse within the resin particle; and fourth, exchange onto a functional group, which removes a presaturant ion. Fifth, the presaturant ion on the functional group diffuses out of the particle to the film layer. Sixth and lastly, it diffuses across the film layer into the bulk solution. To maintain a charge balance, the rate of mass transfer of the both ions must be equal but opposite in direction.

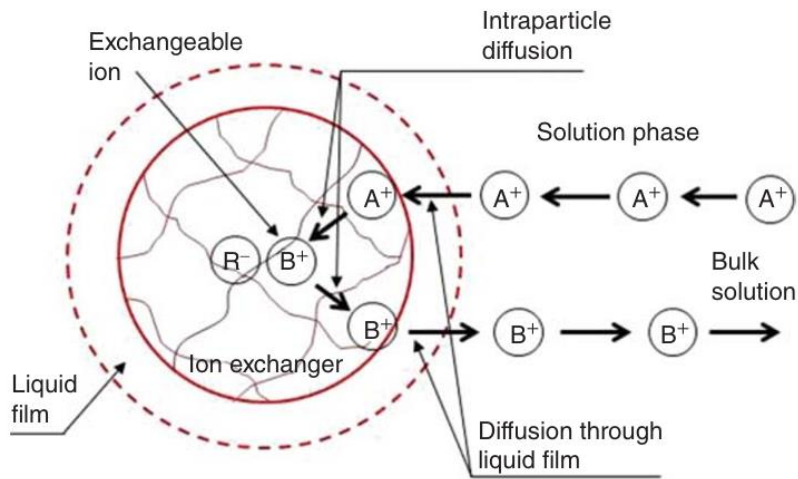
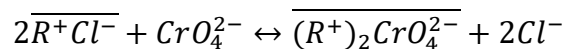


Figure 13. Mass transfer into a cation exchange resin (SenGupta, 2017).

The chemical reaction describing exchange of CrO_4^{2-} onto a SBA-IX resin with Cl^- as the presaturant ion is described as follows, with the overbar indicating the resin phase (SenGupta, 2017).



Since CrO_4^{2-} is a divalent ion, when one ion exchanges onto the resin, it releases two monovalent presaturant ions. This chemical reaction is a fast step compared to the overall rate of ion exchange. The kinetics of ions moving from a solution into an ion exchange resin can have two potential rate-controlling steps: liquid film mass transfer and intraparticle mass transfer. Most often, since the film layer is small compared to the radius of the resin, intraparticle diffusion is

rate-controlling. There are, however, circumstances in which film diffusion is dominant. These include when the liquid phase concentration is low, resin capacity is high, resin particle size is small, crosslinking is low, or advection of the bulk solution is low and therefore the stagnant film layer is large (Helfferich & Plesset, 2004; Crittenden et al., 2012). A Helfferich number can be defined for a given ion and resin to calculate whether liquid film or intraparticle diffusion is the rate-controlling step, where q_T is the total resin phase concentration (eq/L), D_p is the resin phase diffusion coefficient (m^2/s), δ is film layer thickness, which varies for liquids from 10-100 μm (m), C is the liquid phase concentration (eq/L), D_l is the liquid phase diffusion coefficient (m^2/s), r_0 is resin bead radius (m), and α_j^i is the separation factor of the ion exchanging in over the ion exchanging out of the resin (Crittenden et al., 2012).

$$He = \frac{q_T D_p \delta}{C D_l r_0} (5 + 2\alpha_j^i)$$

For $He \ll 1$, intraparticle diffusion is rate controlling. For $He \approx 1$, both film layer and intraparticle diffusion are important to the ion exchange mass transfer rate. For $He \gg 1$, film layer diffusion is rate controlling (Bunzl, 1995). Therefore, to ensure an ion exchange processes reaches equilibrium, maintaining high enough advection velocity through fluidized bed columns or mixing batch experiments is necessary to ensure film layer diffusion does not control the ion exchange kinetics.

1.3.6 Operation

Ion exchange water treatment processes contact influent water with a fixed or fluidized bed of ion exchange resin. A flow rate and wet volume of resin are set based on a predetermined empty bed contact time (EBCT). Empty bed contact time, usually measured in minutes, is defined as follows.

$$EBCT = \frac{\text{Wet resin volume}}{\text{Flow rate}}$$

Operation of IX processes is cyclical, consisting of loading and regeneration phases. During loading, the target constituents exchange onto the resin, sending the presaturant ions, often Cl^- in the case of SBA-IX resins, into the effluent water. As the column becomes loaded with highly selective target ions such as CrO_4^{2-} , the mass transfer zone moves down the column, resembling plug flow with dispersion behavior. This mass transfer zone (MTZ) is shown in

Figure 14.

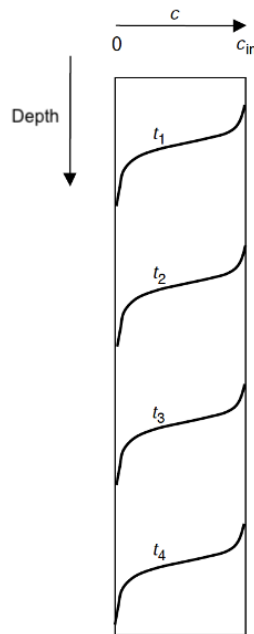


Figure 14. Mass transfer zone over time for a highly selective target ion such as CrO_4^{2-} in a downflow fixed-bed column IX system (Benjamin & Lawler, 2013).

Instead of tracking volume of influent solution to breakthrough, the number of bed volumes of water treated is used. Bed volumes (BV) treated are defined as follows.

$$BVs\ treated = \frac{Total\ solution\ volume}{Resin\ volume}$$

When all the charged functional groups, also called active sites, are at equilibrium with the target constituent, the target constituent is said to breakthrough to the effluent water. This phenomenon can be understood through **Figure 15**.

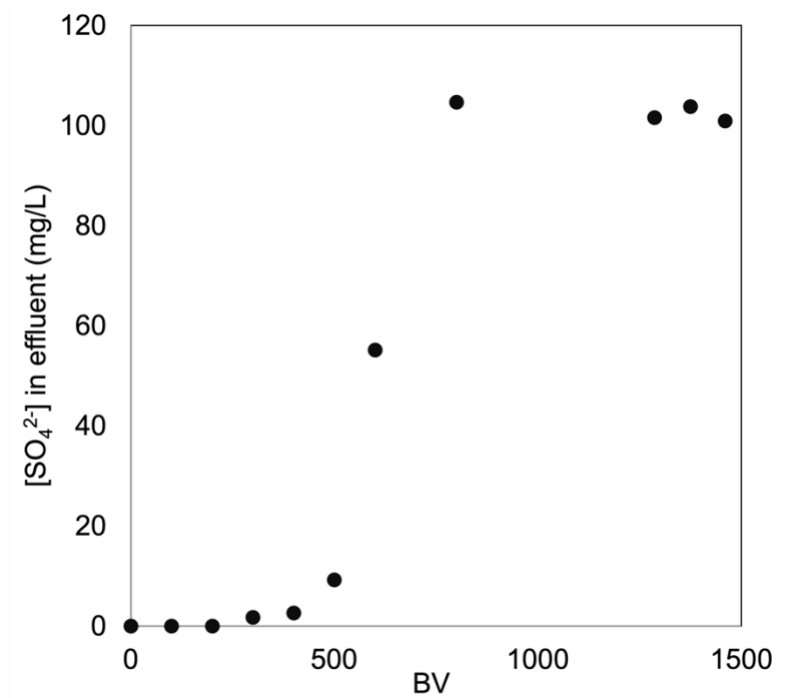


Figure 15. Breakthrough curve of SO_4^{2-} in an anion exchange column.

When or before an IX vessel reaches breakthrough (based on the regulations surrounding the target constituent), loading ceases or is transferred to another vessel in series. Regeneration, the second phase of operation, then occurs. During regeneration, the resin is returned to its original state by sending through the bed a concentration salt solution, also known as a brine, which exchanges presaturant ions back onto the resin and sends the target constituents into the concentrated waste brine for disposal. A regeneration curve is shown in **Figure 16**. Using 4-5

BV of a 10-14% w/w NaCl solution is standard for regeneration of SBA-IX resins used for CrO_4^{2-} removal (Korak et al., 2023).

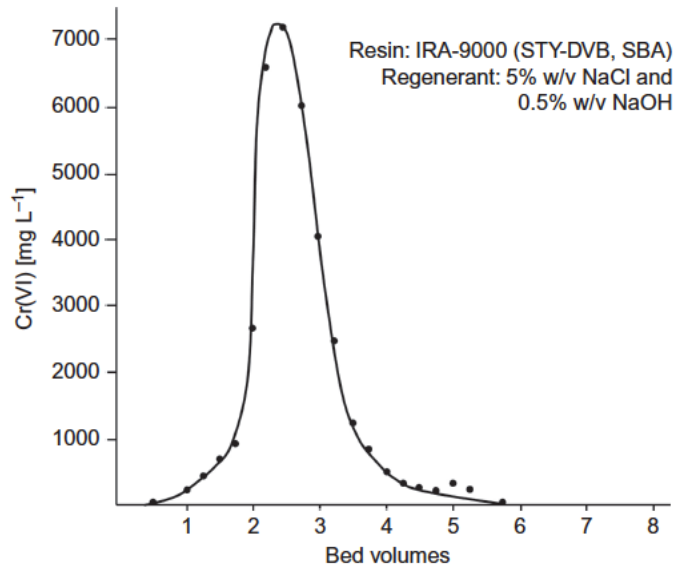


Figure 16. Regeneration curve of SBA-IX for Cr(VI) removal at alkaline pH (Bryjak et al., 2016).

Disposal of ion exchange waste brine is one of the greatest challenges for IX processes, which are often operated at remote groundwater pump sites without access to a wastewater discharge. In addition, when the target constituent, such as CrO_4^{2-} , is hazardous, the brine coming off the resin can have high concentrations of hazardous material, with concentrations of CrO_4^{2-} ranging from 12-320 mg/L (Korak et al., 2023). These hazardous brines must not only be hauled offsite, but disposed of at special hazardous waste facilities, which is costly (Korak et al., 2023).

Various configurations of ion exchange contactors exist. A fixed bed contactor with a water hold-down system is kept in place by filling the entire column with liquid to keep resin in place. The UPCORE system runs countercurrent, meaning that the influent service flow is in the

downward direction, while the regeneration flow is in the upward direction. The Bayer-Lewatit upflow fluidized bed system sends the service flow in the upward direction and the regeneration flow in the downward direction. In this system, there is enough freeboard for resin to expand in its fluidized state. Advantages of upflow operation include less resin clumping and less mechanical stress on the resin (Crittenden et al., 2012). However, since the fluidized bed has increased porosity compared to a packed bed, throughput usually decreases.

1.3.7 Cr(VI) operation

Ion exchange is the most widely used technology for Cr(VI) treatment in drinking water. SBA-IX systems feed influent water through packed-bed contact vessels full of resin, which remove CrO_4^{2-} from water. Both regenerable and non-regenerable SBA-IX resins exist. Multiple-use resins can be regenerated when beads reach their maximum capacity by sending a high salt regenerant solution, typically 10-14% (w/w) NaCl, through the contact vessels and collecting the waste brine (Najim et al., 2014). A typical process flow is shown below in **Figure 17**.

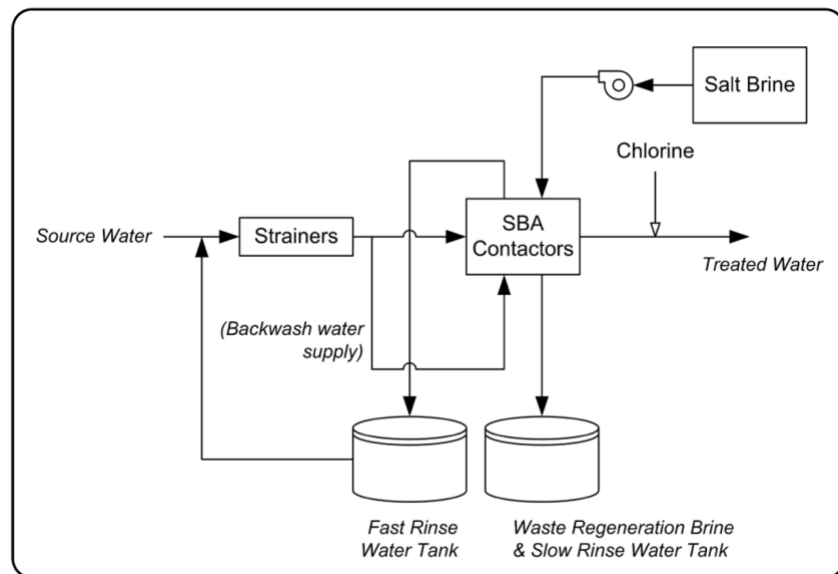


Figure 17. Process flow of regenerable SBA-IX system (Najim et al., 2014).

Single-use resins also exist, which run similarly to regenerable SBA-IX systems, except resin is disposed of when it reaches capacity, instead of being regenerated. In groundwaters with low SO_4^{2-} , which drives SBA-IX resin capacity, single-use systems can have very long run times and be especially advantageous for groundwater wells that only run a few hours a day. Operation is very simple without the need for regeneration. In addition, spent resins can be characterized to ensure they are non-hazardous, allowing simple landfill disposal (Carothers & Gorman, 2023).

Weak base anion exchange (WBA-IX) is another type of ion exchange treatment technology for Cr(VI). When influent water is lowered to a pH of about 6, these WBA-IX resins benefit from very high capacity, potentially saving costs of resin regeneration or disposal. However, in order to modify pH, HCl or CO_2 must be added to influent water to lower its pH, and then NaOH must be used to bring pH back up after contactor vessel treatment. Thus, despite long run times, due to management of liquid acids and chemical addition requirement, WBA-IX is rarely selected by utilities.

Overall, ion exchange is a best available technology for Cr(VI) removal, with many full-scale applications in place. Its advantages include simple process flow, high selectivity for Cr(VI) and lack of sludge production. Disadvantages include operational challenges including monitoring for breakthrough, constant need for changing bag filters to prevent sanding of the resins, and resin and brine disposal.

1.4 Hybrid ion exchange

Hybrid ion exchange (HIX) is an up-and-coming class of ion exchange that disperses metal or metal oxide nanoparticles within ion exchange resin (SenGupta, 2017). There are a number of advantages to synthesizing nanoparticles on ion exchange resin, rather than using

these nanoparticles by themselves. On their own, metal nanoparticles can lack durability and demonstrate high pressure drops when operated in fixed-beds (G. Liu et al., 2022; SenGupta, 2017). Impregnating these nanoparticles on ion exchange resin provides a stable substrate and the possibility of a regenerable process. According to the Donnan Membrane Principle, the immobile charged functional groups within resin give rise to semipermeable membrane behavior of the resin to prevent like-charged ions from entering the resin and concentrate opposite-charged ions within the resin (Sarkar et al., 2010; SenGupta, 2017). Since, resin with ion-permeable solid-liquid interfaces can retain high concentrations of trace water contaminants, in solutions with trace levels of target ions, the HIX resin can exhibit faster kinetics than metal nanoparticles on their own. HIX also promises higher sorption capacity, exploiting the sorption capacity of both the metal adsorbent and the ion exchange capacity of the resin.

A variety of HIX resins have been researched, including magnetically active polymeric particles (MAPPs) (Leun & SenGupta, 2000); and nanoparticles of Fe^0 , Zn^0 (Zhang et al., 2008), Pd^0 (D. Sengupta et al., 2014), and Cu^0 (Pande et al., 2008); zirconium oxide (M. Li et al., 2020); and hydrated ferric oxide (HFO). HFO nanoparticles dispersed within SBA-IX have become commercially available for arsenic removal from drinking water under the name ArsenX^{np} (currently sold as FerrIXTMA33E), shown in **Figure 18**.



Figure 18. Purolite ArsenX^{np} HIX resin.

This ArsenX^{np} resin has been demonstrated at full-scale in Connecticut, South Dakota, Oregon, and Arizona for trace arsenic removal from groundwater sites (Chen et al., 2011; Kabay et al., 2010). It has also been successfully operated at field-scale in remote villages in West Bengal, India, where the process has been shown to load for 20,000 BV to removal arsenic below the MCL of 50 $\mu\text{g/L}$ and regenerate without significant loss of resin capacity (Sarkar et al., 2007). This case study shows the promise of HIX technology for the future.

1.4.1 Nanoscale zero valent iron

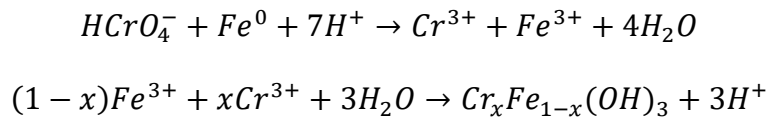
Nanoscale zero valent iron (NZVI) is elemental iron (Fe^0) synthesized as nanoparticles, which significantly increases surface area for adsorption as opposed to powder or granular iron (Cross et al., 2009). Elemental iron is abundant, inexpensive, and non-toxic, although an iron

secondary MCL of 0.3 mg/L exists in drinking water due to the reddish color and metallic taste of the element. NZVI has proven to be an excellent reactive sorbent for groundwater remediation. It has been used for pilot and full-scale remediation at over 50 sites worldwide to treat halogenated solvents and a number of inorganic contaminants including nitrate, perchlorate, selenate, arsenate, arsenite, and chromate (Han et al., 2015; Mueller et al., 2012). However, when used on its own, NZVI has a number of drawbacks. Because of its high reactivity, NZVI can lose its capacity before its particles come into contact with a target species (Cross et al., 2009). Due to magnetic and Van de Waals forces, NZVI is also prone to aggregation, which reduces its surface area (Ravikumar et al., 2016). Thus, impregnation of NZVI on substrates such as polymers and porous carbon has been found to be a more effective use of the metal.

HIX impregnation of NZVI has been researched for various contaminants, including nitrate (Jiang et al., 2011; Park et al., 2009), 2,4,6-trichlorophenol (Tai et al., 2016), phosphorous (G. Liu et al., 2022), Pb(II) (Chanthon et al., 2018; Shi et al., 2013), As(III) (Du et al., 2013), and Cr(VI) (Fu et al., 2013; Gao et al., 2022; Toli et al., 2016; Toli, Mystrioti, Avgoustidis, et al., 2021; Toli, Mystrioti, Xenidis, et al., 2021). Applications span both industrial wastewater treatment and remediation of polluted groundwater.

1.4.2 *Cr(VI) removal mechanism*

The following mechanism of Cr(VI) removal by NZVI impregnated on resin has been proposed for water at an acidic pH, where HCrO_4^- is the dominant species of Cr(VI):



NZVI is proposed to reduce Cr(VI) to Cr(III) while oxidizing Fe⁰ to Fe(III). Then, the Cr(III) and Fe(III) are proposed to co-precipitate on the resin (Fu et al., 2013). For an anionic exchange resin D201, this process is illustrated in **Figure 19**.

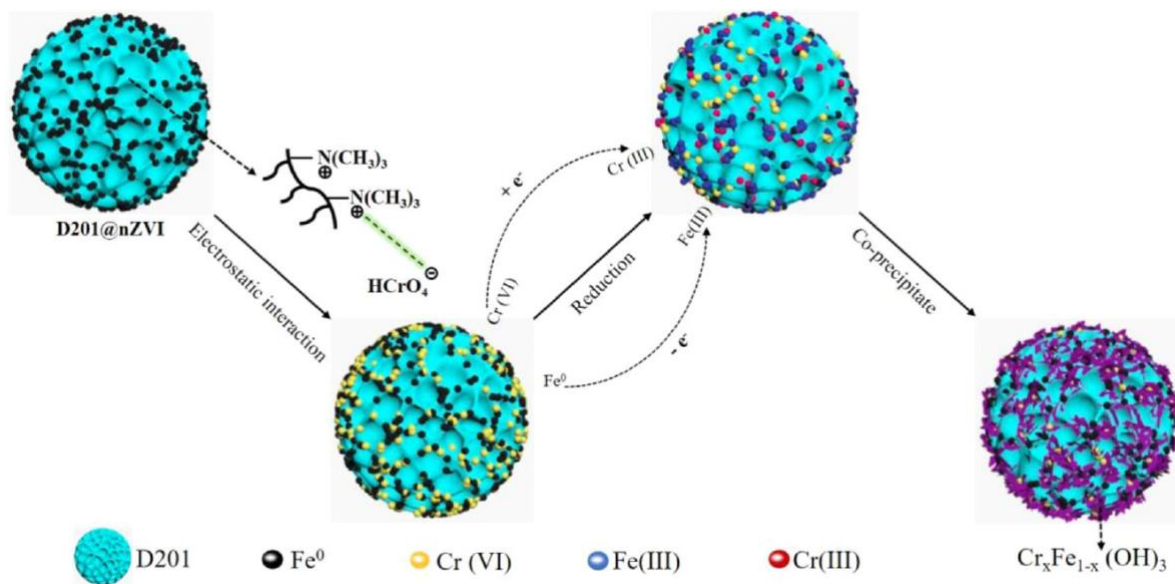


Figure 19. Removal of HCrO_4^- using SBA-IX resin impregnated with NZVI (Gao et al., 2022).

At higher pH values such as those relevant to groundwater, Gao et al., 2020 suggests that Cr(VI) removal by NZVI decreases because Cr(III) and Fe(III) hydroxides are more likely to form, preventing adsorption and reduction of Cr(VI) (Gao et al., 2022). However, an exact mechanism of CrO_4^{2-} removal by NZVI-impregnated SBA-IX resin has not been proposed.

1.4.3 Summary of previous findings

Three studies have investigated NZVI HIX using batch Cr(VI) removal experiments. Fu et al., 2013 synthesized NZVI on a cationic exchange resin, focusing on batch testing for wastewater treatment applications at pH 3-9 with 20-40 mg/L Cr(VI) (Fu et al., 2013). NZVI dose, resin dose, pH, and initial concentration of Cr(VI) were all found to be important

parameters in batch removal of Cr(VI) (Fu et al., 2013). When used resin was re-treated with ferrous iron and borohydride solution, it exhibited 80% removal efficiency in batch tests over 4 reuse cycles for Cr(VI) removal (Fu et al., 2013). Toli et al., 2016 synthesized NZVI on a cationic exchange resin, focusing on batch testing at pH 2.7-8.5 with 5-25 mg/L Cr(VI) (Fu et al., 2013). Kinetics were found to follow a first order rate law (Toli et al., 2016). When resin was regenerated using a solution of 2 N HCl, 1 N NaCl, and 1 N NaOH, over 87% Cr(VI) removal efficiency was demonstrated over three cycles (Toli et al., 2016). Gao et al., 2020 synthesized NZVI on a macroporous SBA-IX resin, focusing on batch removal of 20-150 mg/L Cr(VI) from water with pH 3-10 for industrial wastewater treatment applications (Gao et al., 2022). The study reported a resin capacity of 123.14 mg Cr(VI)/g NZVI-impregnated resin using D201, a SBA-IX resin; however, no comparison was made to unmodified ion exchange resin (Gao et al., 2022). The resin was regenerated with 0.1 M NaOH, finding close to 100% Cr(VI) removal efficiency in batch tests over 6 cycles (Gao et al., 2022).

Only a couple studies have performed column experiments for Cr(VI) removal, both using cation exchange resin with NZVI dispersed in it. Toli et al., 2021 synthesized NZVI on a cationic exchange resin, examined column removal of 5 mg/L Cr(VI) from water with pH 4.9 (Toli, Mystrioti, Xenidis, et al., 2021). Running the column to a breakthrough at Cr(VI) concentration of 10 µg/L with EBCT of 2.8 minutes found that the column treated less than 10 BV of influent water (Toli, Mystrioti, Xenidis, et al., 2021). Another study by the same author performed column removal of 0.5-5.2 mg/L Cr(VI) from wastewater effluent with pH 3-7.5. Using an influent water quality of 500 µg/L Cr(VI) and other background constituents including 85 mg/L SO₄²⁻, 347 mg/L Cl⁻, and 192.5 mg/L Na⁺, breakthrough to 100 µg/L Cr(VI) was reached at approximately 300 BV (Toli, Mystrioti, Avgoustidis, et al., 2021).

1.4.4 Research gap

HIX has been demonstrated at full-scale for arsenic removal and several bench-scale studies have examined hybrid ion exchange for removal of Cr(VI) from wastewater. Relevant Cr(VI) studies and their scope are summarized in **Table 2**. At pH ranges and trace levels of Cr(VI) relevant to drinking water, studies are lacking. In addition, no other studies have yet examined column removal of relevant Cr(VI) concentrations by NZVI HIX using anion exchange resin.

Table 2. Previous studies using NZVI HIX for Cr(VI) removal.

Study	Resin	Experiment	[Cr(VI)] (mg/L)	pH	Application
(Fu et al., 2013)	Cationic	Batch	20 – 40	3 – 9	Industrial wastewater treatment
(Toli et al., 2016)	Cationic	Batch	5-25	2.7-8.5	Contaminated water
(Gao et al., 2022)	Anionic	Batch	20 – 150	3 – 10	Industrial wastewater treatment
(Toli, Mystrioti, Xenidis, et al., 2021)	Cationic	Column	5	4.9	Industrial wastewater treatment
(Toli, Mystrioti, Avgoustidis, et al., 2021)	Cationic	Column	0.5 – 5.2	2-7.5	Industrial wastewater treatment
Our work	Anionic	Batch Column	175 0.1	8	Groundwater-sourced drinking water treatment

According to Dr. Sudipta Sarkar, a professor of Civil Engineering at Indian Institute of Technology and expert on Cr(VI) ion exchange, “A considerable amount of work has been done on the use of ion exchange for selective removal of trace Cr from industrial and hazardous wastewaters. However, due to the absence of a low MCL value for the presence of Cr(VI) in drinking water until now, not much work has been done on the removal of trace concentration of Cr(VI) from contaminated drinking water” (Bryjak et al., 2016). Given the 2022 newly proposed California MCL of 10 $\mu\text{g/L}$ Cr(VI), our work aims to disperse NZVI within SBA-IX resin for trace Cr(VI) removal from drinking water. We have synthesized, characterized, and verified performance of NZVI on SBA-IX resin in batch and fluidized bed experiments. In addition, we have critically considered the viability and practicality of this HIX technology, including selectivity over background constituents, durability, and impact on pH and water chemistry of influent water.

2 CHAPTER 2: METHODS

2.1 Chemicals and reagents

All chemicals were analytical reagent grade. Solids used included ferric chloride ($\text{FeCl}_3 \cdot 6\text{H}_2\text{O}$), sodium borohydride (NaBH_4), 1,5-diphenylcarbazide ($\text{C}_{13}\text{H}_{14}\text{N}_4\text{O}$), sodium sulfate (Na_2SO_4), sodium chloride (NaCl), sodium nitrate (NaNO_3), and sodium bicarbonate (NaHCO_3). Solutions used included absolute ethanol ($\text{C}_2\text{H}_6\text{O}$), acetone, hydrochloric acid (HCl), sulfuric acid (H_2SO_4), nitric acid (HNO_3), 1000 mg/L sodium chromate (Na_2CrO_4), and 5% w/v sodium chromate tetrahydrate ($\text{Na}_2\text{CrO}_4 \cdot 4\text{H}_2\text{O}$). N_2 gas was used for deoxygenating solutions. Ultrapure type 1 water (Milli-Q[®]) was used for all experiments, except for column experiments, which used type 2 water (ion exchange and granular activated carbon treated) for influent water. Alconox Citranox[®] was used to clean plasticware and Liquinox[®] was used to clean glassware, followed by rinsing with ultrapure type 1 Milli-Q[®] water.

2.2 Resins

Purolite[®] A600E, A500Plus, and S106 resins and LANXESS Lewatit[®] TP 107 resin were selected as NZVI synthesis substrates. These four resins were chosen based on their variety of resin properties shown in **Table 3**, including strong base, weak base, gel, macroporous, polystyrene, and polyacrylate. A600E, TP 107, and S106 resins are used specifically for Cr(VI) treatment, with both A600E and TP 107 tested in pilot- and field-scale applications (Gorman et al., 2016; Flint et al., 2021). A500Plus is typically used for demineralization and removal of silica (Purolite, n.d.). After initial synthesis experiments detailed in Section 3.1, A600E was selected as the primary resin for batch and column testing.

Table 3. Properties of selected resins as reported by manufacturers.

Resin	A600E	A500Plus	TP 107	S106
Manufacturer	Purolite®	Purolite®	LANXESS Lewatit®	Purolite®
Strong or Weak Base	SBA	SBA	SBA	WBA
Gel or Macroporous	Gel	Macro	Macro	Macro
Matrix	Polystyrene	Polystyrene	Polyacrylate (acrylic)	Epoxy Polyamine
Functional Group	Type I Quaternary Ammonium	Type I Quaternary Ammonium	Quaternary Ammonium	Polyamine
Ionic Form	Chloride	Chloride	Chloride	Free Amine
Manufacturer Reported Capacity (eq/L)	1.6	1.15	2.4	2
Particle Size Range (µm)	570 ± 50	300 - 1200	450 - 650	300 - 2000

2.3 Analytical methods

Inductively coupled plasma mass spectrometry (ICP-MS) was used to quantify final reported total chromium and iron concentrations, using an EPA 6020B method with collision cell gases (helium or hydrogen) to decrease molecular ion interferences. All samples analyzed by ICP-MS were diluted to between 5 and 500 µg/L as Cr and acidified to 1% HNO₃ with trace metal grade HNO₃. Ion Chromatography (IC) was used to quantify sulfate, chloride, and nitrate concentrations, using the EPA 300.1 method. Analysis used an AS18-Fast-4µm (Dionex IonPac) column and potassium hydroxide eluent. Analytes were detected using either suppressed conductivity or absorbance at 215 nm. For ICP-MS and IC, quality control included daily calibration, independent calibration verification, spectral interference checks (ICP-MS only), sample replicates, and matrix spikes.

The pH of samples was determined using a Mettler Toledo InLab® Expert Go-ISM pH sensor, calibrated daily with pH 4, 7, and 10 buffer solutions. Electrical conductivity was

determined using a Mettler Toledo InLab® 710 conductivity sensor, calibrated daily with a 1413 $\mu\text{S}/\text{cm}$ standard solution.

For preliminary screening experiments, a variety of colorimetric methods were used to measure Cr(VI) and iron concentrations, using a Hach DR6000 UV-VIS Spectrophotometer. For concentrations from 1.95 $\mu\text{g}/\text{L}$ to 250 $\mu\text{g}/\text{L}$ Cr(VI), a modified EPA 7196A method was developed to minimize sample volume and hazardous Cr(VI) waste based on the Standard Method for the Examination of Water and Wastewater 3500-Cr D and Lace et al., 2019 (Lace et al., 2019). The method reacts Cr(VI) with 1,5-diphenylcarbazide (DPC) in acidic conditions to form a pink-colored complex that absorbs at 540 nm. First, an acetone solution of 0.4 M H_2SO_4 with 0.5% 1,5-diphenylcarbazide was created. Then, 2 mL of this solution was added to 10 mL of sample. Absorbance was measured on the spectrophotometer at 540 nm using a 50 mm glass cuvette that held 5 mL of sample. Each day sampling occurred, a fresh DPC solution was created, as the solution became discolored after several hours. The 50 mm path length was selected to increase absorbance values, as following the Beer-Lambert Law:

$$A = cl\varepsilon(\lambda)$$

Where A is absorbance, c is concentration of sample (mol/L), l is length of the light path (cm), and ε is the molar absorptivity of the solution (L/mol-cm) as a function of wavelength, λ . Thus, by increasing pathlength, absorbance readings was increased to be in a measurable range from 0.01 to 0.9. A calibration curve, shown in **Figure 20**, was made using a 1000 $\mu\text{g}/\text{L}$ Cr(VI) stock to create standards from 1.95 $\mu\text{g}/\text{L}$ to 250 $\mu\text{g}/\text{L}$ Cr(VI).

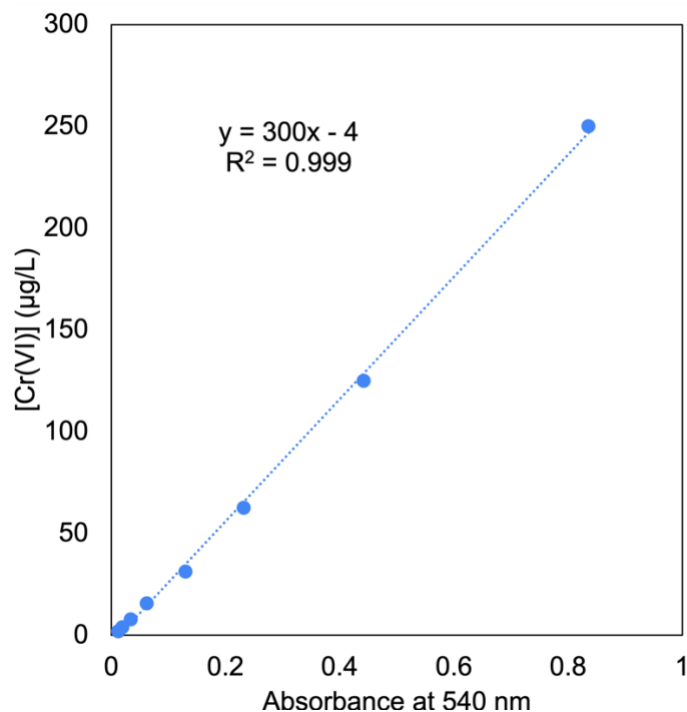


Figure 20. 1,5-Diphenylcarbazide method calibration curve for measuring Cr(VI) concentrations in water with a 50 mm path length.

For concentrations from 195 µg/L to 25 mg/L, Cr(VI) samples were measured directly at 373 nm using a 10 mm pathlength, using the absorbance of chromate at this wavelength (Arias-Paić & Korak, 2020; Haupt, 1952). The calibration curve is shown in **Figure 21**, which was made using a 1000 µg/L Cr(VI) stock to create standards from 195 µg/L to 25 mg/L Cr(VI). All samples with Cr(VI) above 25 mg/L were diluted before absorbance was measured.

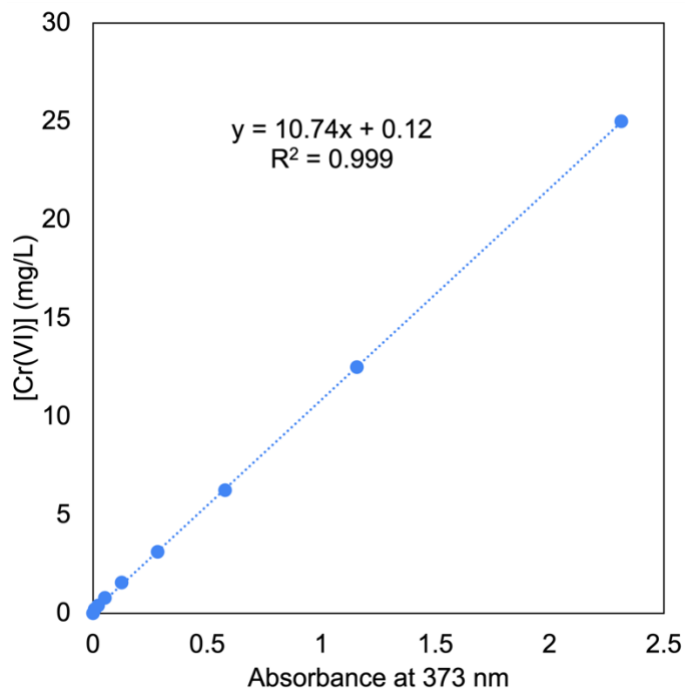


Figure 21. Calibration curve for measuring Cr(VI) concentrations in water.

To measure concentrations of iron in preliminary experiments, Fe^{3+} was also measured by a colorimetric method. All iron samples were diluted in a 0.2 M HCl absolute ethanol solution. In this high chloride-ethanol solution, FeCl_4^- becomes the dominant iron species, with peaks shown in **Figure 22** (Nomura et al., 2022).

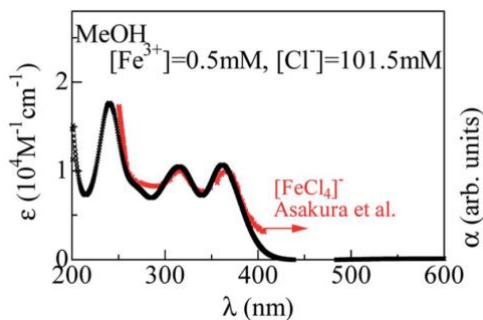


Figure 22. Molar absorptivity of FeCl_4^- in an excess-chloride methanol solution (Nomura et al., 2022).

To confirm this, ferric chloride (FeCl_3) was used to create standards with Fe^{3+} concentrations of $50 \mu\text{g/L}$ to 25 mg/L in 0.2 M HCl in ethanol solution. The following peaks, shown in **Figure 23**, were found by performing a full UV-VIS scan.

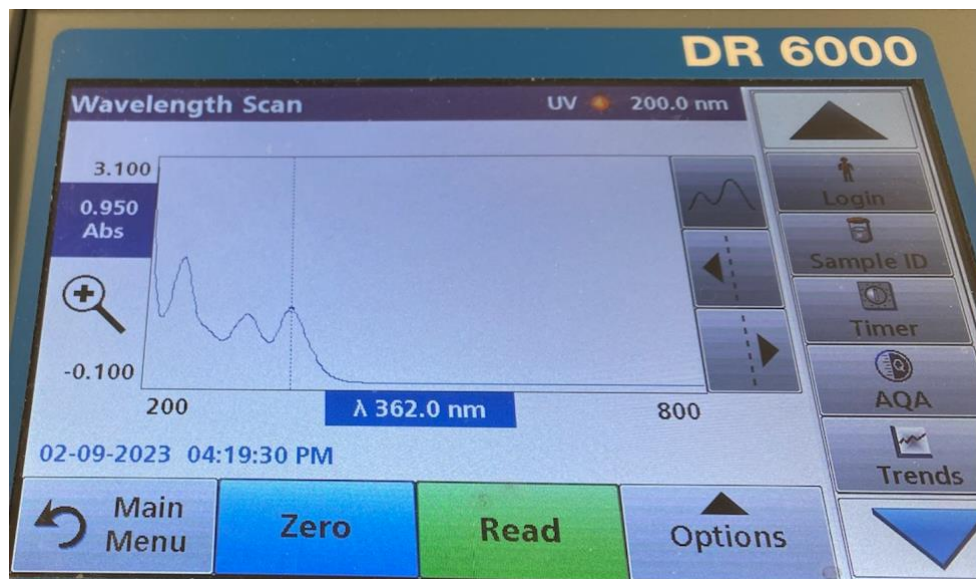


Figure 23. Full scan of 5.5 mg/L Fe^{3+} in an excess-chloride ethanol solution.

Thus, a calibration curve, shown in **Figure 24**, based on known iron concentrations was created and measured at 362 nm using a 10 mm path length. Iron samples were diluted with 0.2 M HCl in ethanol solution to fall within the calibration range.

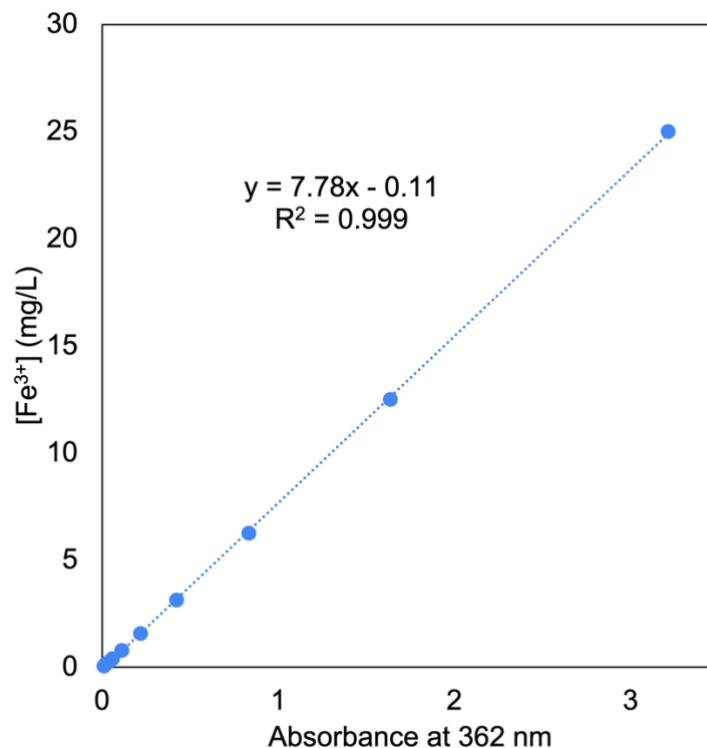
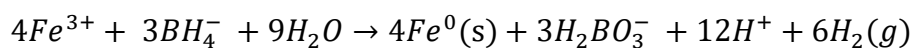
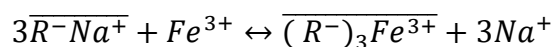


Figure 24. Calibration curve of Fe³⁺ in an excess-chloride ethanol solution at 362 nm.

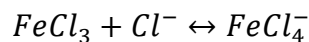
2.4 Synthesis

Synthesis of NZVI particles has been studied extensively. The most common approach is through borohydride reduction of ferric or ferrous iron to Fe⁰. Synthesizing NZVI on a cation exchange resin substrate, the technique is fairly straightforward: Fe³⁺ or Fe²⁺ is exchanged onto the resin and borohydride reaction is performed to reduce the iron:

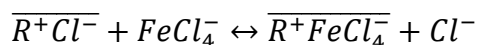


For SBA-IX, exchanging cationic Fe³⁺ onto the positive functional groups is not possible due to the Donnan Membrane Principle. Therefore, a tetrachloroferrate (FeCl₄⁻) solution must first be created, using FeCl₃•6H₂O and HCl, NaCl, and/or ethanol to convert FeCl₃ into the anionic form

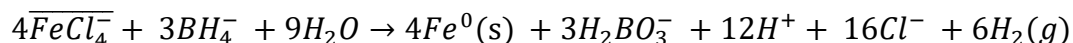
(Jiang et al., 2011). In excess-chloride alcohol solutions, $FeCl_4^-$ becomes the dominant ferric iron species, according to the following equation (Nomura et al., 2022):



Next, the $FeCl_4^-$ species is exchanged onto the anion exchange resin.



The ferric iron is then reduced to Fe^0 , similar to the cation exchange method:



This reaction produces solid NZVI, in addition to dihydrogenborate ($H_2BO_3^-$), H^+ , Cl^- , and hydrogen gas. An illustration of NZVI synthesized on anion exchange resin is shown in **Figure 25**.

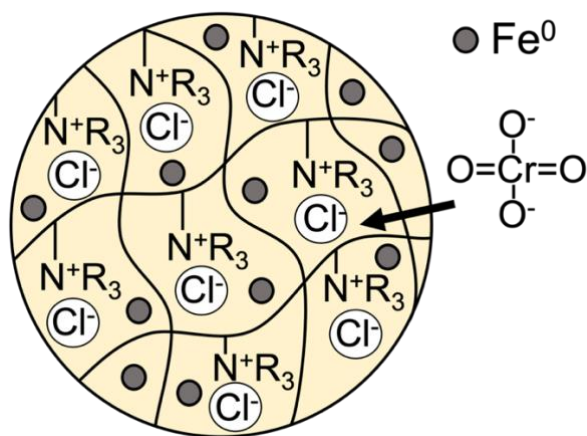


Figure 25. NZVI-impregnated SBA-IX resin for CrO_4^{2-} removal.

A handful of prior studies detail their methodologies, shown in **Table 4**, for synthesizing NZVI on strong base anion exchange resin. The majority of the studies began with a $FeCl_3 \cdot 6H_2O$ solution. In order to exchange Fe^{3+} onto the anion exchange resin, the $FeCl_3$ is converted into $FeCl_4^-$ form using HCl, NaCl, and/or ethanol. One work used 0.5 M $FeCl_3$ with 1 M HCl, with a resin-solution ratio of 1:10 using Purolite A500Plus resin (Pan et al., 2015). Another work

created a 500 mL solution of 2 M FeCl₃ and 2 M HCl with 10 g of polystyrene anion exchange resin with quaternary ammonium functional groups (Jiang et al., 2011). A third study used an ethanol solution with 0.005 M FeCl₃ and 0.01 M HCl at 70°C for 10 g IRA-402 resin (G. Liu et al., 2022). A fourth work used 100 mL of solution of 1 M HCl with 10% ethanol, ample NaCl, and 1 M FeCl₃ to exchange onto 1 g macroporous polystyrene anion exchange resin (Song et al., 2022).

Two other studies proposed different methods for impregnating iron on SBA-IX resin. Tai et al., 2016 used a 40 mL solution of FeCl₂•4H₂O to stir 5 g anion exchange resin, according their procedure to exchange Fe²⁺ (Tai et al., 2016). It is uncertain how effectively the Fe²⁺ entered their anion exchange resin, however, due to the Donnan Membrane Principle. Gao et al., 2020 used a 100 mL solution with 0.09 M FeCl₃ to stir 1 g D201 resin, without mention of how Fe³⁺ was exchanged onto the anion exchange resin (Gao et al., 2022).

After stir times ranging from 30 minutes-12 hours (Gao et al., 2022; G. Liu et al., 2022), procedures included generic rinsing of FeCl₄⁻-resin (Pan et al., 2015), 5 times rinsing in alcohol (Jiang et al., 2011), and rinsing with DI water until filtrate pH 7 was reached (G. Liu et al., 2022).

Next, either NaBH₄ or KBH₄ were used as reducing agents for the iron, ranging from 2 M (Pan et al., 2015), ultrasonic shaking in 1% NaBH₄ (Jiang et al., 2011), varying NaBH₄ or KBH₄ concentration from 0.9-7.2% (Jiang et al., 2012; Song et al., 2021; Song et al., 2022), titration of 20 mL 10% (m/v) KBH₄ (Tai et al., 2016), and titration of 100 mL 0.36 M NaBH₄ (Gao et al., 2022).

After reduction, common treatments included centrifugation (Gao et al., 2022), resin rinsing (Tai et al., 2016) with deoxygenated water (Jiang et al., 2011; Pan et al., 2015) or

absolute ethanol (Gao et al., 2022; Pan et al., 2015; Song et al., 2021), vacuum drying (Pan et al., 2015; Jiang et al., 2011; Gao et al., 2022), or drying at room temperature (G. Liu et al., 2022).

Table 4. Prior methodology for NZVI synthesis on SBA-IX resin.

Study	Resin mass (g)	Fe (M)	Addition to convert to FeCl_4^-	Fe stir (h)	Fe rinse	BH_4^- (M)	NZVI Rinse	Drying	Other
(Pan et al., 2015)	–	0.5	1 M HCl	4	–	2	DI water and alcohol	Vacuum at 30°C	–
(Jiang et al., 2011)	10	2	2 M HCl	10	Alcohol	0.26	Deoxy water	Vacuum	Ultrasonic shaking in BH_4^-
(Tai et al., 2016)	5	0.25	–	2	DI water	1.9	DI water	–	Used Fe^{2+} , BH_4^- titrated
(Gao et al., 2022)	1	0.089	–	0.5	–	0.36	Absolute ethanol	Vacuum	BH_4^- titrated, Centrifuged
(Song et al., 2021)	1	–	HCl	4	Absolute ethanol	0.17 -1.3	Ethanol	Vacuum at 40°C	–
(G. Liu et al., 2022)	10	0.005	0.01 M HCl in ethanol at 70°C	12	DI water until pH = 7	0.02	NaCl soak	Room temp for 48 h	–
(Song et al., 2022)	1	1	1 M HCl NaCl 10% ethanol	4	–	1.3	NaCl, NaOH, HCl, and ethanol	45°C	–
Our work	10	0.05	0.1 M in ethanol at 70°C	12	Absolute ethanol	0.1	Absolute ethanol	Vacuum	BH_4^- stir at 50°C

For our work, a variety of conditions were tested over the course of 28 screening experiments. Based on comparison between previous studies, we modified concentration and volume of FeCl_3 and NaBH_4 , concentration of reagents (i.e., HCl and ethanol) that convert FeCl_3

to FeCl_4^- , stir time, order of reduction (i.e., NaBH_4 before FeCl_3), resin mass and type (i.e., A600E, TP 107, A500Plus, and S106), temperature of reaction, method of NaBH_4 addition (i.e., titration of NaBH_4 into resin solution versus dropping FeCl_4^- -resin into NaBH_4 solution), FeCl_4^- -resin rinsing reagent (i.e., DI water versus ethanol), and FeCl_4^- -resin and NZVI-resin drying.

2.4.1 FeCl_4^- -A600E optimization

Once initial screening experiments were complete and a NZVI-resin could be synthesized reproducibly, targeted experiments were run to determine the FeCl_4^- loading on the resin. Concentration and volume of FeCl_4^- solution were varied to create an isotherm. Assuming the manufacturer-reported resin capacity and specific gravity, the theoretical mass of iron loaded on 1 g of A600E resin is as follows:

$$\begin{aligned} & \frac{1.6 \text{ eq A600E}}{\text{L}} * \frac{1 \text{ L}}{1090 \text{ g A600E}} * \frac{1 \text{ eq FeCl}_4^-}{1 \text{ eq A600E}} * \frac{1 \text{ mol FeCl}_4^-}{1 \text{ eq FeCl}_4^-} * \frac{55.845 \text{ g Fe}}{1 \text{ mol FeCl}_4^-} * \frac{1000 \text{ mg}}{\text{g}} \\ & = 82.0 \frac{\text{mg Fe}}{\text{g A600E}} \end{aligned}$$

Thus, based on the theoretical loading of 82 mg Fe/g A600E, iron concentration and volume conditions were tested that spanned the expected iron loading range using a face-centered central composite design, as shown in **Figure 26**.

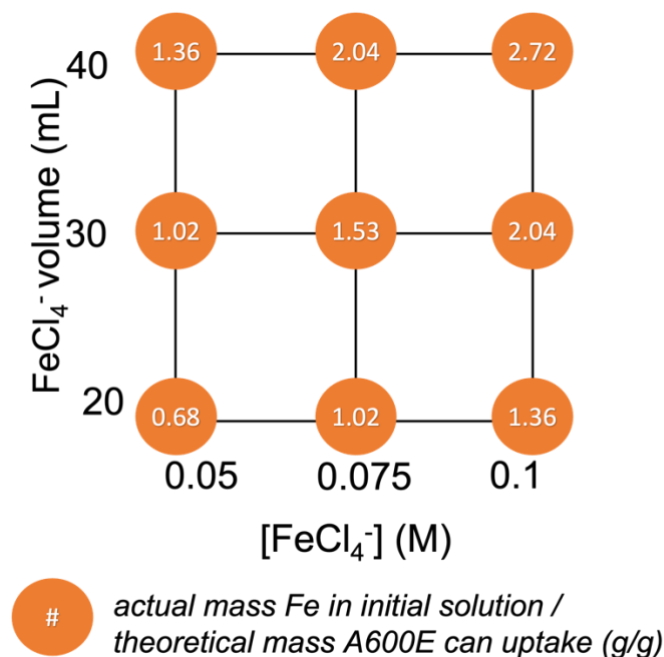


Figure 26. Iron loading test matrix for FeCl₄⁻-A600E.

The ratio of the mass Fe in the initial FeCl₄⁻ solution to the theoretical mass of iron A600E can uptake is calculated in **Figure 26** is exemplified for the 40 mL 0.05 M condition as follows:

$$\frac{0.05 \text{ mol FeCl}_4^-}{L} * \frac{55.845 \text{ g Fe}}{1 \text{ mol FeCl}_4^-} * \frac{1 L}{1000 \text{ mL}} * \frac{40 \text{ mL}}{1 \text{ g A600E}} * \frac{1 \text{ g A600E}}{82 \text{ mg Fe}} * \frac{1000 \text{ mg Fe}}{\text{g Fe}}$$

$$= \frac{1.36 \text{ g Fe in solution}}{\text{g Fe on A600E resin}}$$

A ratio below 1 indicates that not enough iron was in solution to fully load the ion exchange sites, while a ratio above 1 indicates that iron was expected to be in excess and remain in the solution at equilibrium.

To test each of the nine conditions, 1 g of dry A600E resin was stirred at 100 RPM in a small beaker with 20-40 mL containing 0.05-0.1 M Fe³⁺ and 0.1-0.2 M HCl in ethanol solution on a hotplate set at 70°C for 12 hours. HCl concentration was always maintained at twice the iron

concentration to ensure excess chloride conditions. After the equilibrium was attained, the resin was removed from the beaker and vacuum filtered with 5 rinses of 5 mL absolute ethanol to remove impurities and excess iron on the resin. After ethanol rinsing, the resin was air dried for 24 hours. All nine conditions were tested in replicate.

Iron loading onto the FeCl_4^- -A600E was analyzed by acid digestion. To do so, 0.1 g of dry FeCl_4^- -A600E was digested in 50 mL of 2% HNO_3 solution for 24 hours. The resin visibly leached iron, returning to its original dull yellow color. The iron concentration in solution was then quantified to calculate mass of iron that had been exchanged onto the resin.

2.4.2 *NZVI-A600E optimization*

After iron loading on FeCl_4^- -A600E was established, the next step was to determine the optimal concentration and volume of NaBH_4 needed for the reduction reaction. Enough NaBH_4 was needed to reduce all Fe^{3+} to Fe^0 ; however, too much NaBH_4 on the resin can have negative practical implications, discussed further in Section 3.5. Theoretically, a 3:4 NaBH_4 :Fe molar ratio is required for NZVI to form. Practically, however, NaBH_4 is added in a 3:1 or 4:1 NaBH_4 :Fe molar ratio (Barreto-Rodrigues et al., 2017; G. Liu et al., 2022; Gao et al., 2022; Pan et al., 2015). Thus, based on literature, NaBH_4 : FeCl_4^- molar ratios from 2.7 to 10.9 were tested using the face-centered central composite design shown in **Figure 27**.

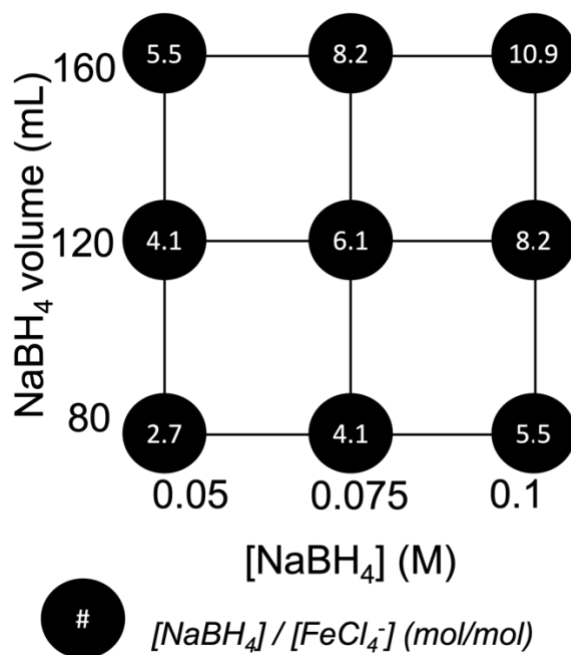


Figure 27. Sodium borohydride loading test matrix for NZVI-A600E.

To test each of the nine conditions, 80-160 mL of water was purged of O₂(g) using a N₂(g) balloon in a round-bottom three-neck flask on a hotplate set at 50°C for 30 minutes. Sodium borohydride (NaBH₄) was added to create the 0.05-0.1 M NaBH₄ solution. 1 g of dry FeCl₄⁻-A600E was dropped directly into the NaBH₄ solution and stirred at 200 RPM for 15 minutes. The iron immediately reacted with the borohydride, forming H₂(g) and NZVI on the resin. After the reaction had completed, the solution cleared. The solution was decanted and the resin, now black and magnetic, was vacuum filtered and rinsed with 150 mL of deoxygenated water and 5 mL absolute ethanol. Resin was vacuum dried for 48 hours prior to characterization and experimentation. All nine conditions were tested in replicate.

After the NZVI-A600E had dried, four tests were performed on each of the nine resin conditions in replicate to determine gas production, iron loading, and performance in batch testing. To visually observe gas production, 0.2 g dry NZVI-A600E was placed in 10 mL of

deoxygenated water for 24 h. To visually observe cracking, dissecting microscopy was used to quantify breakage by counting approximately 150 resin beads and recording the number of cracked or broken beads. To determine iron loading, 0.1 g of dry NZVI-A600E was digested in 50 mL of 2% HNO₃ solution for 24 hours. The resin visibly leached iron, returning to its original light yellow color. The iron concentration in solution was then quantified to calculate the mass of iron on the resin. To determine Cr(VI) removal and impact on pH during 24 h batch experimentation, NZVI-A600E was soaked in 2 N NaCl in deoxygenated water for 30 minutes after synthesis to load exchange sites with chloride. NZVI-A600E was rinsed with DI water and vacuum dried for 48 hours. 100 mg of dry NZVI-A600E resin was weighed out and placed in a 25 mL solution of 175 mg/L Cr(VI) and 2000 mg/L SO₄²⁻ in a 125 mL plastic bottles. Initial pH of the solution was measured. The bottles were shaken at room temperature on a shaker table for 24 hours and sampled to quantify chromium. The mass of Cr(VI) removed was calculated as a subtraction of final mass from initial mass based on concentration of each ion in solution. All batches were performed in duplicate for each of the nine conditions. The pH after 24 h was also measured, and pH change over the course of the experiment was calculated.

2.5 Resin density change

To study the impact of FeCl₄⁻-A600E and NZVI-A600E synthesis on resin density, 1 g dry A600E in Cl⁻ form was stirred in FeCl₄⁻ according to the final synthesis conditions in replicate. Each batch of dry FeCl₄⁻-A600E resin was weighed. Then, 1 g of the dry FeCl₄⁻-A600E resin was reduced to NZVI-A600E according to the final synthesis conditions in replicate. Each batch of dry NZVI-A600E resin was weighed. In order to determine impact of moisture content

on resin weight, 1 g of dry Cl⁻ form A600E, FeCl₄⁻-A600E, and NZVI-A600E (all in replicate) were also placed in the oven at 100°C overnight and then re-weighed.

2.6 Characterization

Several types of characterization were performed. A visual inspection of the NZVI-A600E was performed to verify color change of resin. Resin was also attracted with a stirbar to ensure magnetic properties of NZVI. A Nikon SMZ800 dissecting microscope was used to evaluate resin shape and breakage. To quantify breakage, approximately 150 resin beads were counted and the number of cracked or broken beads was noted. Scanning electron microscopy–energy-dispersive X-ray spectroscopy (SEM-EDS) were used to evaluate resin shape and map elemental iron composition on the resin (Hitachi SU8010). Prior to analysis, platinum was sputtered onto the resin beads until a thickness of 3 nm was reached on the surface. X-ray photoelectron spectroscopy (XPS) were applied with a Kratos Supra x-ray photoelectron spectrometer to verify presence of Fe⁰ on the first 10 nm of the resin surface. Survey spectra were used to calculate the atomic % of the surface while the high-resolution spectra provided information on elemental chemical state. Scan sweeps and dwell time were increased to increase signal to noise ratio. Charge neutralization parameters were optimized with continuous scans on the carbon 1s peak. The Al K alpha x-ray source was operated at 1486.69 keV and 15.00 mA current emission. Survey spectra were acquired from 0-1200 eV with a resolution of 160, while high resolution scan ranges were based off the element being analyzed and a resolution of 20. A Shirley background was used and a Gaussian-Lorentzian mixture (25:75) functions were used. All spectra were calibrated using a C-C/C-H peak position of 284.8 eV.

2.7 Batch experimentation

Both resin capacity and selectivity equilibrium batch experiments were performed. A600E came from the manufacturer in chloride form. NZVI-A600E was soaked in 2 N NaCl in deoxygenated water for 30 minutes after synthesis to load exchange sites with chloride, followed by rinsing with DI water. A600E was air-dried and NZVI-A600E was vacuum dried for 48 hours. Masses ranging from 50 to 400 mg of dry resin were weighed, with the difference in density of A600E and NZVI-A600E resin corrected for later. For the capacity batch experiment, a solution of 175 mg/L Cr(VI) was created from $\text{Na}_2\text{CrO}_4 \cdot 4\text{H}_2\text{O}$ stock solution. For the selectivity batch experiment, a solution of 175 mg/L Cr(VI) and 2000 mg/L SO_4^{2-} was created from $\text{Na}_2\text{CrO}_4 \cdot 4\text{H}_2\text{O}$ stock solution and $\text{Na}_2\text{SO}_4(\text{s})$, respectively. Volumes from 25 to 100 mL of solution were poured into 125 mL plastic bottles along with the masses of dry resin. pH was approximately 8.5 for all solutions. The bottles were shaken at room temperature on a shaker table for 24 hours and sampled to quantify chromium, sulfate, and chloride. The mass of Cr(VI) and SO_4^{2-} removed by the resin was calculated as a subtraction of final mass from initial mass based on concentration of each ion in solution. All batches were performed in duplicate.

2.8 Fluidized bed column experimentation

To test water matrices representative of groundwater, flow-through, fluidized bed column experiments were performed. An upflow fluidized bed was selected over a downflow fixed bed column to prevent $\text{H}_2(\text{g})$ bubble accumulation in the bed from NZVI, discussed further in Section 3.5. Column details are shown in **Table 5**.

Table 5. Column engineering parameters.

Inner Diameter (mm)	Wet resin volume (mL)	EBCT (min)	Volumetric flow rate (mL/min)
10.74	18	3	6

The influent water quality was selected to simulate a high sulfate, Cr(VI)-contaminated groundwater, shown in **Table 6**.

Table 6. Column influent water quality.

Parameter	Value
Cr(VI)	91 ± 2 µg/L
SO ₄ ²⁻	100 mg/L
Cl ⁻	10 mg/L
NO ₃ -N	5 mg/L
HCO ₃ ⁻	292 mg/L
pH	8

In order to perform the column experiment, a laboratory setup was first configured with influent water passing from a 25 gallon barrel by a Masterflex[®] L/S[®] pump upflow through the column and into an effluent water composite waste bin. Pressure gauges were placed before and after the column to measure pressure in the system. 18 mL of wet A600E or NZVI-A600E resin was placed into the column with Fluval[®] FX5 polyester pad placed in the top and bottom of the column to prevent resin loss. After resin was loaded, the column was flushed with type 2 water to remove air bubbles from the system. Next, 5 BV (90 mL) of 2 N NaCl was passed upflow through the column to ensure all Cl⁻ was exchanged on all ion exchange sites. Following this regeneration, type 2 water was sent through the column until the effluent conductivity was below 200 µS/cm. The influent solution with the composition in **Table 12** upflowed continuously to load the column. An effluent sample was taken every 200 BV until 10 µg/L Cr(VI) breakthrough was reached, according to the anticipated Cr(VI) MCL in the State of California. Composite

effluent water was also collected in a tub and weighed every 400 BV to ensure volumetric flow rate was maintained. The upflow fluidized bed column setup is shown in **Figure 28**. After the NZVI-A600E column experiment, the post-column resin was harvested in four cross-sections and dried for characterization.

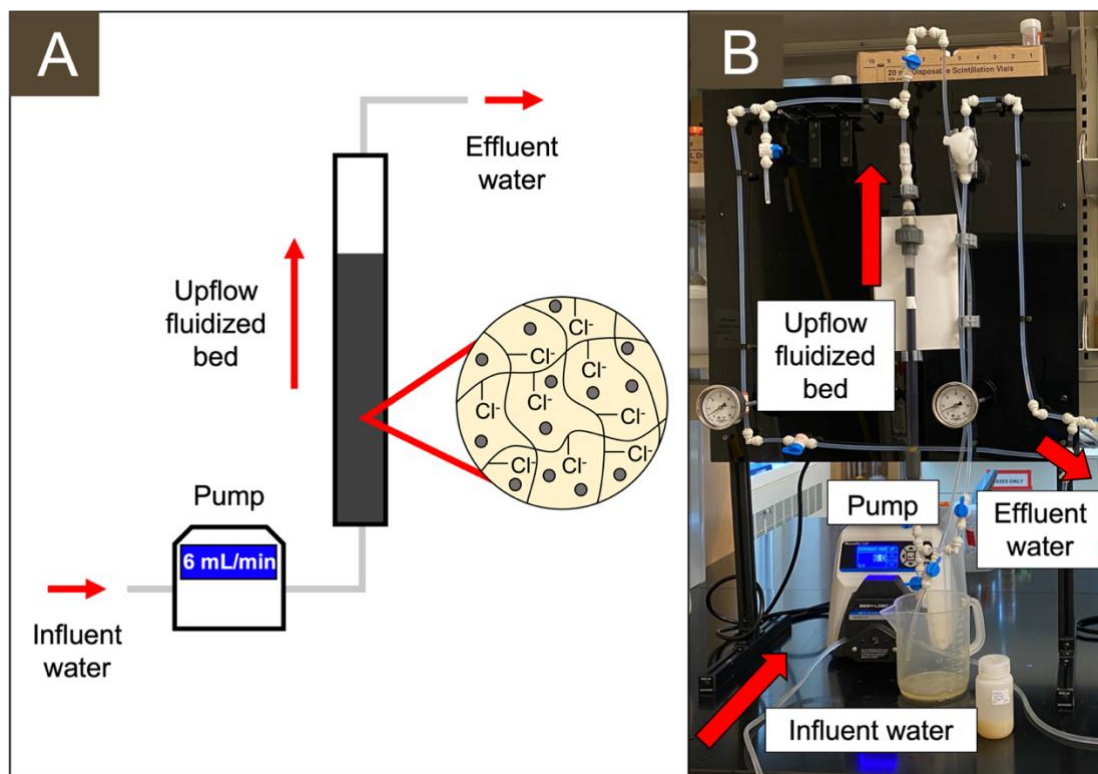


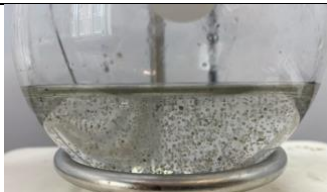
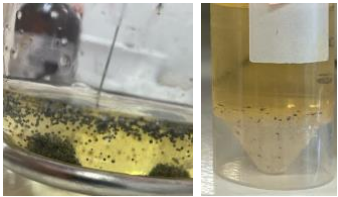
Figure 28. (A) Schematic and (B) photo of upflow fluidized bed column setup.

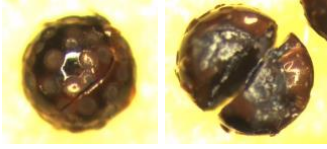
3 CHAPTER 3: RESULTS

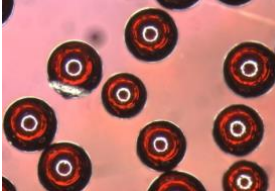
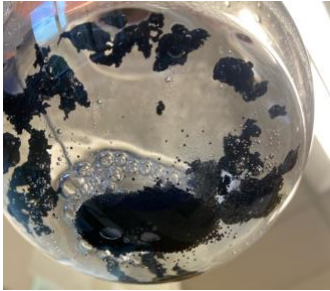
3.1 Synthesis

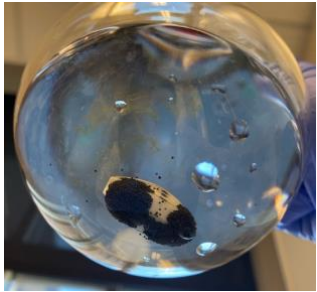
In order to synthesize NZVI-A600E resin, a variety of conditions were tested over the course of 28 experiments, shown in **Table 7**. Success of experiments for this initial screening phase was determined by color, dissecting microscopy, and attraction to the stir bar, since NZVI was expected to be completely black and magnetic.

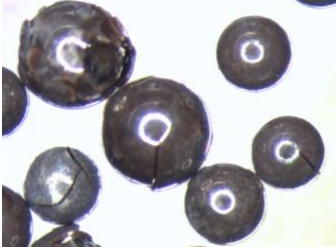
Table 7. Synthesis of NZVI screening experiments using anion exchange resin, with each row documenting the incremental change in approach.

Experiment	Approach	Outcome	Images
1	Stirred A600E resin in FeCl ₃ solution for 0.5 h, titrated NaBH ₄ directly into FeCl ₃ solution	NaBH ₄ reacted with aqueous Fe ³⁺ instead of resin and could not be separated out from aqueous NZVI.	
2	Drained FeCl ₃ solution after 0.5 h stir, rinsed resin 3x with water, titrated NaBH ₄ onto resin	Resin floated in NaBH ₄ but did not react, which shows that SBA-IX resin cannot exchange Fe ³⁺ directly.	
3	Stirred for 16 h in FeCl ₃ solution	No reaction again, since SBA-IX resin cannot exchange Fe ³⁺ directly.	—
4	Used FeSO ₄ solution instead of FeCl ₃ solution	SBA-IX resin cannot exchange Fe ²⁺ directly either.	
5	Soaked resin in NaBH ₄ and then titrated in FeCl ₃	Resin initially turned a grey-black and was magnetic after titration of FeCl ₃ , but the reaction reversed within 0.5 h, turning the resin white.	

6	Stirred resin in 0.2 M FeCl ₃ with 0.4 M HCl in ethanol (FeCl ₄ ⁻ solution)	Resin turned partially magnetic black, indicating formation of NZVI, but also partially orange-red.	
7	Pre-soaked resin in Cl ⁻ prior to stir in FeCl ₄ ⁻ solution	Same result as experiment 6 indicates that Cl ⁻ pre-soak was not important.	
8	Soaked resin in NaBH ₄ and then titrated in FeCl ₃ , this time removing resin from reaction after 5 minutes before the reaction could reverse	Resin turned a grey-black color, but was not deep black. NaBH ₄ -first method was terminated.	
10	Stirred resin in FeCl ₄ ⁻ solution at 70°C, rinsed FeCl ₄ ⁻ resin in 2.5 L DI water until pH = 6	FeCl ₄ ⁻ resin turned deep red due to formation of Fe(OH) ₃ (s). Resin remained predominantly red after NaBH ₄ reduction.	
11	Decreased concentration to 0.005 M FeCl ₃ and 0.01 M HCl in ethanol and reduced with 0.02 M NaBH ₄	No reaction occurred.	—
12	Increased concentration to 1 M FeCl ₃ and 2 M HCl in ethanol and reduced with 4 M NaBH ₄	Using a dissecting microscope, resin cracked and had red-brown color with white crystals, which may be excess NaBH ₄ on the resin.	

13	Used TP 107 resin	Resin appeared to react with NaBH_4 , but upon closer inspection was yellow-grey.	
14	Used A500Plus resin	Resin decomposed into a powder after the FeCl_4^- loading step. No reaction with the NaBH_4 occurred.	
15	Used S106 resin	Resin appeared to react with NaBH_4 . Upon closer inspection, resin was dark red. Future tests focus on A600E.	
16	Stirred A600E resin in FeCl_4^- solution at 70°C , rinsed FeCl_4^- resin in NaHCO_3 until $\text{pH} = 8.3$	FeCl_4^- resin turned deep red due to formation of $\text{Fe}(\text{OH})_3(\text{s})$. Resin remained deep red after reaction with NaBH_4 .	
17	Rinsed FeCl_4^- resin in NaOH until $\text{pH} = 8.3$, dissolved NaBH_4 titration solution in absolute ethanol instead of DI water, and performed NaBH_4 reduction in ice bath	FeCl_4^- resin turned deep red due to formation of $\text{Fe}(\text{OH})_3(\text{s})$.	
18	Rinsed FeCl_4^- resin 1x with absolute ethanol instead of DI water, performed reduction reaction at 70°C	Since the DI water rinsing appeared to cause $\text{Fe}(\text{OH})_3(\text{s})$ formation, rinsing with ethanol formed black, magnetic resin. However, NZVI also formed in the bulk solution and stuck to the resin.	

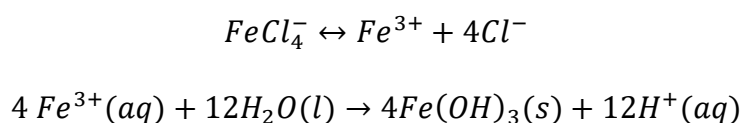
19	Scaled up from 1 g resin to 10 g and rinsed FeCl_4^- resin 5x with absolute ethanol, tried to separate aggregate NZVI from resin in sieve	Separation of bulk aggregated NZVI from resin using sieve was unsuccessful.	
20	To reduce ethanol use, stirred resin in 0.1 M FeCl_3 0.2 M HCl in 20% ethanol instead of absolute ethanol	Absolute ethanol was found to be important to exchange FeCl_4^- onto the resin (see image of FeCl_4^- resin stirred in absolute ethanol on left compared to 20% ethanol on right).	
21	Rinsed 0.5 g FeCl_4^- resin 11x with absolute ethanol	Black magnetic NZVI formed on the resin and no aggregate formed, however an excessive amount of absolute ethanol was used to achieve this result which is not practical for upscaling.	
22	Rinsed 20 g FeCl_4^- resin 10x with absolute ethanol	Black magnetic NZVI formed on the resin but aggregate NZVI also formed in solution and stuck to the resin as in experiments 18-19.	—

23	Rinsed 4 g FeCl_4^- resin 5x with absolute ethanol and then air dried for 24 h, then added dried FeCl_4^- resin directly into NaBH_4 solution	Black magnetic NZVI formed on the resin and no aggregate formed. However, dissecting microscopy revealed resin had small cracks and NZVI-resin bubbled when placed in DI water.	 
24	Soaked NZVI-A600E in 0.005 M HCl to attempt to quench bubbling	HCl soak caused NZVI-resin to oxidize quickly, turning a yellow-brown color.	
25	Performed reduction reaction at 25°C	No visual differences from 70°C.	—
26	Performed reduction reaction at 50°C	No visual differences from 70°C, so moved forward with reaction at 50°C.	—
27	Used conditions that were optimized for A600E on A500Plus resin	While A500Plus did not decompose like in experiment 14 this time, resin was yellow and grey instead of black.	
28	Used conditions that were optimized for A600E on TP 107 resin	Black magnetic NZVI formed on the resin and no aggregate formed. However, dissecting microscopy revealed resin was cracked, and NZVI-resin bubbled when placed in DI water.	

The screening experiments identified important experimental variables, including selection of rinse solutions, order of reduction steps, method of NaBH_4 addition, stir time, temperature, and mass of resin used relative to reaction volumes. In order to load FeCl_4^- on the

resin, absolute ethanol was required and could not be diluted, and excess HCl at twice the molar concentration of iron was required. A temperature of 70°C encouraged exchange of FeCl₄⁻ onto the resin, as opposed to a room temperature stir. A visual indicator of successful resin loading with FeCl₄⁻ was a bright orange color.

To prepare the FeCl₄⁻-resin for the reduction reaction, rinsing 5x in absolute ethanol was best for removal of impurities and excess iron. Deionized (DI) water was not used for rinsing to prevent formation of Fe(OH)₃(s) on the resin, according to the following reactions.



While exchange of BH₄⁻ onto the resin and reduction of titrated FeCl₃ was possible, the reaction was not stable and had the potential of reversing itself, as shown in experiment 5 in **Table 7**. The best method of NaBH₄ addition was to first air dry the FeCl₄⁻-resin for 24 h prior to the NaBH₄ reaction to prevent aggregate iron from forming in solution. A N₂(g)-purged NaBH₄ solution was created and the dry FeCl₄⁻-resin was introduced directly into the solution. Titration of NaBH₄ solution into DI water with the FeCl₄⁻-resin led to hydrolysis of the pre-loaded FeCl₄⁻. Titrating NaBH₄ into DI water caused a reaction between NaBH₄ and Fe³⁺ in solution rather than on the resin, as shown in experiments 18, 19, and 22 in **Table 7**. The reaction was performed on a hot plate set at 50°C to increase the reaction speed. The reaction was substantially complete after 15 minutes as indicated by reduced bubbling. A mass of 10 g FeCl₄⁻-resin was determined to be the maximum amount of resin that could be reduced in one 2000 mL beaker with 1200 mL of solution.

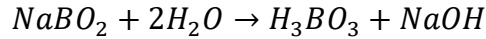
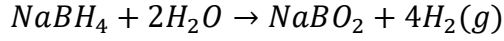
After the reduction reaction was complete, selection of rinse solution was also important. The most successful approach rinsed NZVI-resin with absolute ethanol and deoxygenated DI

water. Rinsing with either oxygenated DI water or HCl oxidized the iron on the resin more quickly as indicated by a color change from black to red. The resin was dried in a vacuum desiccator for 24 h to prevent oxidation by $O_2(g)$. Oxidation of Fe^0 on the resin will be discussed further in Section 3.3.4.

Of the four resins tested (i.e., A600E, TP 107, A500Plus, and S106), A600E and TP 107 produced the best NZVI-resin products based on upon initial screening, as exemplified in experiments 23 and 28. A500Plus and S106, on the other hand, did not turn completely black nor magnetic during experiments, as shown in experiments 14, 15, and 27. Because A600E is a common resin for Cr(VI) treatment, this resin was selected for further synthesis optimization and characterization through batch and column testing. Synthesis optimization, characterization, and performance testing of NZVI immobilized on TP 107, A500Plus, and S106 resins is suggested for future work.

3.1.1 $FeCl_4^-$ -A600E optimization

Once NZVI-A600E was successfully synthesized, the concentration and volume of reagents were optimized to determine impact on cracking of the NZVI on the resin, gas formation when NZVI-A600E when was placed in solutions, and increases of solution pH. It was postulated that these issues arose from excess $NaBH_4$ used in the experiments. Concentration and volume of $FeCl_4^-$ and $NaBH_4$ solutions were varied to minimize resin cracking, maximize batch Cr(VI) removal, and minimize increase in batch pH. Resin cracking was monitored as a surrogate for Fe leaching from resin and pH increase was monitored as a surrogate for presence of excess $NaBH_4$, since $NaBH_4$ produces a solution of sodium metaborate ($NaBO_2$), which is strongly alkaline when hydrated (Brack et al., 2015; PubChem, n.d.).



To determine the optimal concentration of FeCl_4^- to load onto the resin, the isotherm in **Figure 29** was created. The error bars represent the standard error on four of the isotherm points, which were run in replicate. Since all the points fit the same isotherm regardless of the FeCl_4^- concentration and volume combination, it was found that the mass of iron in the initial solution was more important to determination of loading than concentration and volume individually.

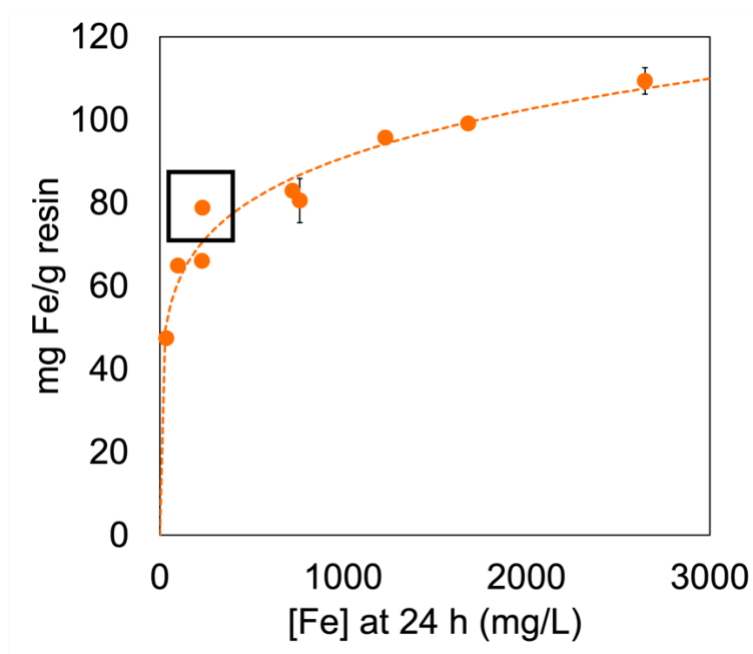


Figure 29. Isotherm of iron loading onto A600E resin.

The Freundlich adsorption isotherm model is defined by the following equation:

$$q = k_f c^n$$

where k_f and n are empirical constants (Benjamin & Lawler, 2013). To fit the constants to the data, the nonlinear specialized modeling tool in JMP Pro 15 was used. Fitted parameters are shown in **Table 8**.

Table 8. Freundlich fitted parameters for the A600E iron loading isotherm.

Parameter	Value
k_f	28 ± 3
n	0.173 ± 0.017

In order to select an iron concentration and volume point on the isotherm for NaBH_4 reduction experiments, a condition in the middle of the isotherm was chosen. The highest iron conditions on the isotherm were avoided to prevent overloading the resin with FeCl_4^- , which could have been the cause of iron leaching into solution and formation of aqueous NZVI instead of NZVI formation on the resin during synthesis screening. Thus, the 0.05 M Fe with 40 mL Fe solution/g A600E was selected for further experimentation, highlighted with a box in **Figure 29**. Relevant parameters of this point are highlighted in **Table 9**. The calculated iron loading rate of 78.8 ± 0.6 mg Fe/g resin matched well with the expected theoretical iron loading of 82 mg Fe/g resin discussed in Section 3.1.1.

Table 9. Selected iron loading condition.

Parameter	Value
Initial Fe concentration (M)	0.05
mL Fe solution/g A600E	40
mg Fe/g resin	78.8 ± 0.6
Equilibrium Fe concentration (mg/L)	232

3.1.2 NZVI-A600E optimization

Once the iron loading condition was selected, the NaBH_4 concentration and volume for the reduction reaction were varied systematically to determine the optimal dose of NaBH_4 to reduce all Fe^{3+} without overloading the resin.

Gas production was observed from all nine NaBH_4 concentration and volume conditions, as shown in **Figure 30**.

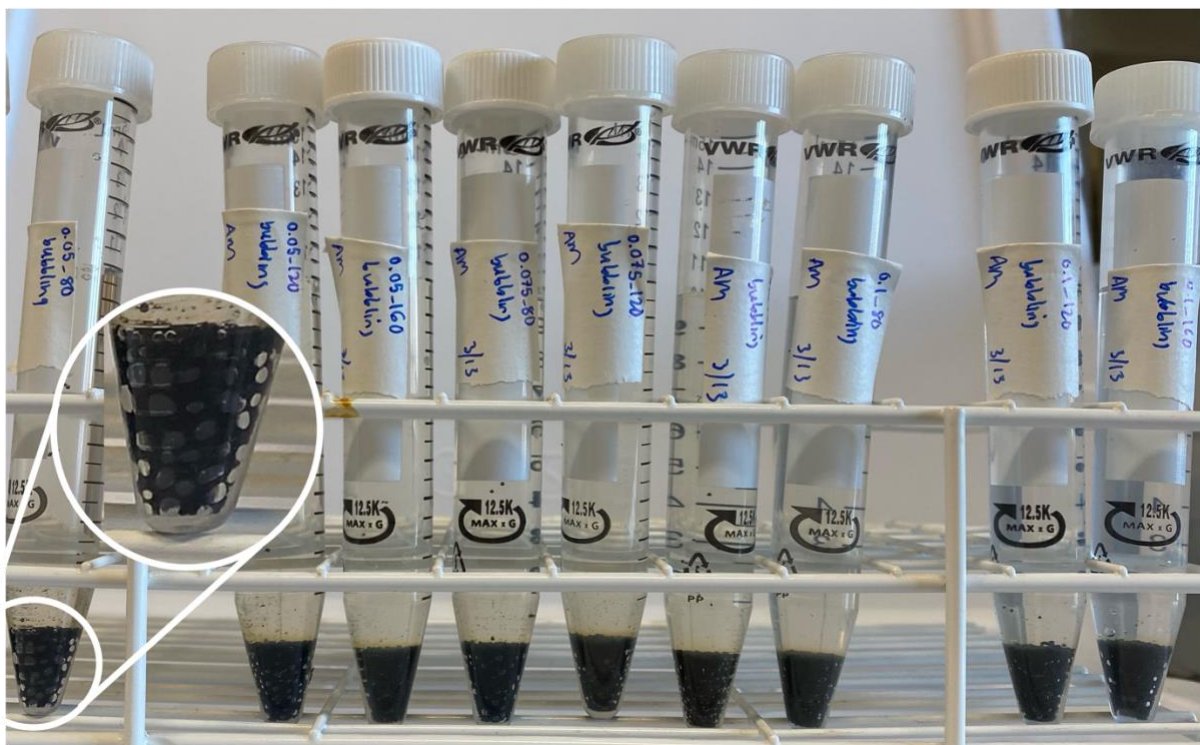
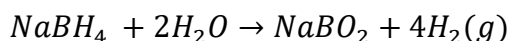
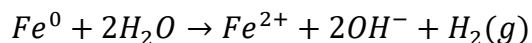


Figure 30. NZVI-A600E produced gas bubbles at all 9 conditions tested.

Initially, gas was expected only at conditions with excess NaBH_4 , according to the following reaction between NaBH_4 and water:



However, gas production occurred at all conditions, including those with less NaBH_4 than stoichiometrically required. This was likely due to the simultaneous reaction that occurs between Fe^0 and H_2O to produce $\text{H}_2(g)$, shown in the following equation:

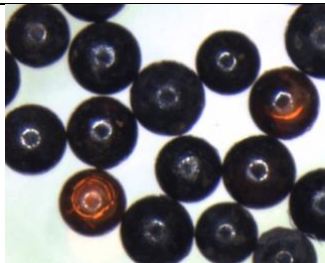
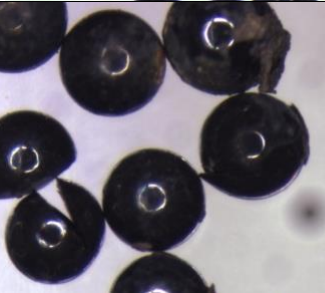


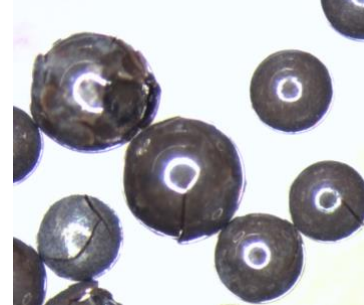
Thus, no conclusions about optimal NaBH_4 dose were drawn based off of the visual gas production test. In order to draw conclusions based on this variable, future work could measure the quantity of gas produced determine if more gas was produced from higher NaBH_4 conditions.

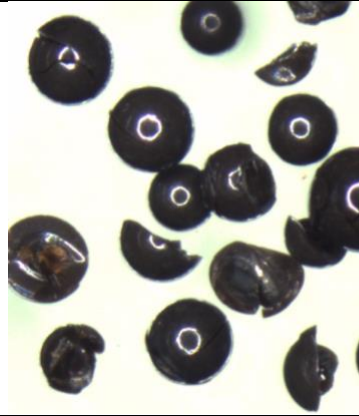
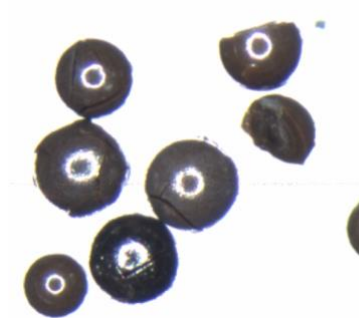
Since Fe^0 produces gas regardless of the reductant used to synthesize it, the use of NZVI in packed bed systems, which require purging of air bubbles in order to maintain plug flow conditions, may be limited.

Resin cracking was found to be correlated with NaBH_4 dose (molar ratio of NaBH_4 to FeCl_4^-). The higher the reductant dose, the more the resin was cracked and even broken. **Table 10** shows images of each resin condition.

Table 10. Dissecting microscopy images of NZVI-A600E over varied NaBH_4 conditions.

$[\text{NaBH}_4]$ (M)	NaBH_4 volume (mL)	$[\text{NaBH}_4]/$ $[\text{FeCl}_4^-]$ (mol/mol)	Resin cracked (%)	Results and discussion	Dissecting microscope image
0.05	80	2.7	1	While no resin was cracked, some resin beads remained in FeCl_4^- and had not been reduced.	
0.05	120	4.1	16	Some resin were cracked and some aggregate NZVI was oxidizing on the resin.	
0.05	160	5.5	19	Some resin were cracked and some aggregate NZVI was oxidizing on the resin.	

0.075	80	4.1	42	Resin beads were chipped slightly.	
0.075	120	6.1	63	Resin beads were chipped slightly.	
0.075	160	8.2	67	Resin beads were chipped slightly.	
0.1	80	5.5	58	Resin beads were chipped slightly.	

0.1	120	8.2	89	Many resin beads were broken into pieces.	
0.1	160	10.9	80	Many resin beads were broken into pieces.	

To quantitatively investigate the dependence of cracking upon both NaBH_4 concentration and volume, a two-way ANOVA analysis was run in JMP Pro 15. Concentration ($p = 7 \times 10^{-5}$), volume ($p = 0.005$), concentration \cdot concentration ($p = 0.015$), and volume \cdot volume ($p = 0.025$) were found to be significant effects for the response variable of % resin cracking. Volume was a surrogate for increased molar ratio of $\text{NaBH}_4:\text{FeCl}_4^-$. Concentration had the greatest impact on resin cracking. **Figure 31** shows a contour plot of the impact of NaBH_4 concentration and volume on cracking.

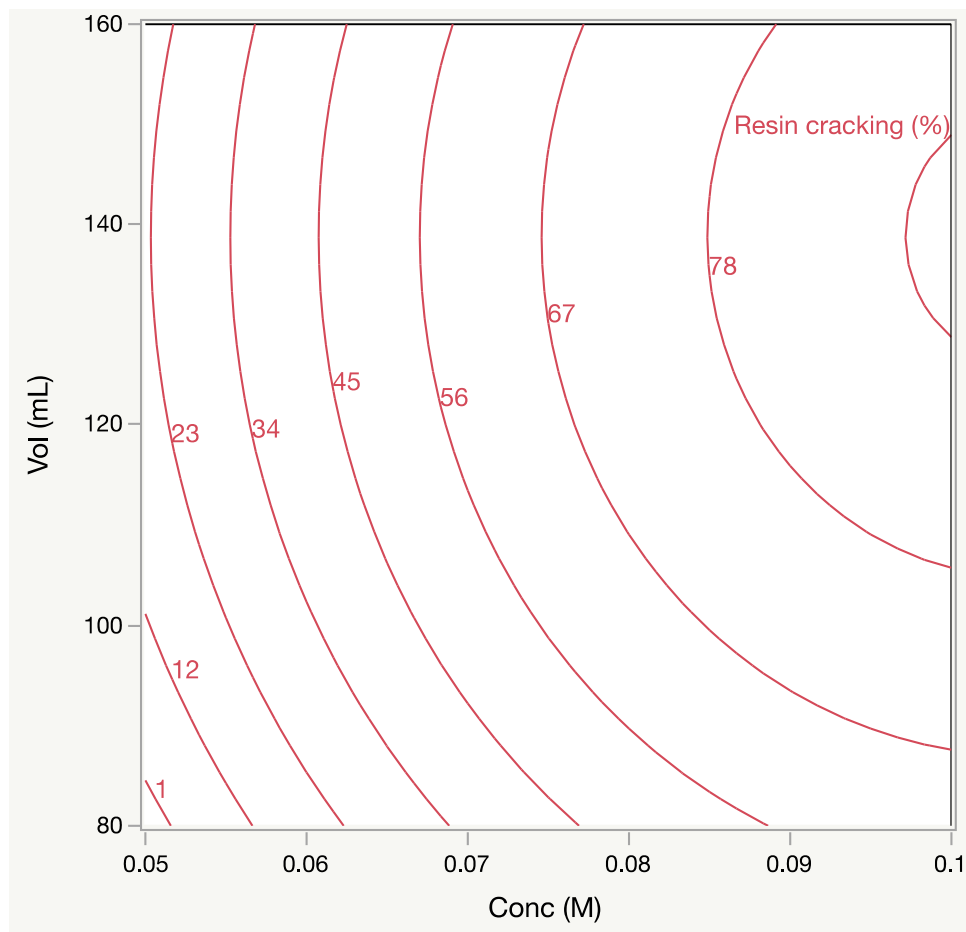


Figure 31. Contour plot of dependence of resin cracking (%) on NaBH₄ conditions.

Batch Cr(VI) removal and pH change results are shown in **Table 11**. The goal of the central composite design was to minimize cracking and pH increase and maximize Cr(VI) uptake. While the results pointed to one condition as optimal (i.e., the 0.05 M NaBH₄ and 80 mL solution/g resin), there are several reasons this condition was not selected. First, when observed visually and under the dissecting microscope, about 20% of the resin beads were still orange, indicating that not enough NaBH₄ had been added to react with all the iron, as shown in **Table 10**.

Table 11. Resin cracking, Cr(VI) removal, and pH change from varying NaBH₄ parameters in replicate.

[NaBH ₄] (M)	mL NaBH ₄ /g FeCl ₄ ⁻ -A600E	[NaBH ₄]/[FeCl ₄ ⁻] (mol/mol)	Resin cracked (%)	Cr(VI) uptake (mg Cr(VI)/g resin) ¹	pH increase ¹
0.05	80	2.7	1	30.8 ± 0.5	0.3 ± 0.2
0.05	120	4.1	16	29.9 ± 0.6	0.8 ± 0.1
0.05	160	5.5	19	29.60 ± 0.02	0.79 ± 0.01
0.075	80	4.1	42	28.1 ± 0.2	0.92 ± 0.1
0.075	120	6.1	63	29.6 ± 0.2	0.76 ± 0.07
0.075	160	8.2	67	29.8 ± 0.2	0.72 ± 0.01
0.1	80	5.5	58	29.8 ± 0.6	0.78 ± 0.01
0.1	120	8.2	89	30.5 ± 0.2	0.87 ± 0.01
0.1	160	10.9	80	30.2 ± 0.2	0.77 ± 0.01
Pristine A600E			0	27.43 ± 0.08	0.41 ± 0.03

¹Uncertainties listed are standard errors for experiments with n=2.

In addition, the standard error of 0.5 between replicates on the Cr(VI) uptake for this condition was slightly higher than many of the other points, decreasing confidence in its accuracy. Therefore, the condition with the next highest Cr(VI) removal, 0.1 M NaBH₄ and 120 mL solution/g resin, was selected for batch and column experimentation. Unfortunately, this condition suffered from high cracking as shown in **Table 10**, and pH increase, both likely due to excess of NaBH₄. The central composite design approach was expected to find a NaBH₄ condition with complete NZVI formation but without the downsides of using excess NaBH₄. However, no such condition was found. Future studies could screen other variables to determine what about the NaBH₄ solution was causing the resin beads to crack. Our hypothesis was that since air dried FeCl₄⁻-A600E resin was dropped directly into the NaBH₄ solution, the shock of simultaneous resin re-hydration and Fe³⁺ reduction to Fe⁰ led to the resin to expand while the NZVI formed. This was accentuated at high NaBH₄ doses, which cause the Fe³⁺ reduction to occur faster. However, when hydrated FeCl₄⁻-A600E resin was used (instead of air dried resin) or

NaBH₄ solution or solid was titrated in, suspended NZVI formed in the bulk solution and was challenging to separate out and oxidized on the resin quickly, as discussed in Section 3.1.

Therefore, optimizing the procedure to simultaneously prevent aggregate NZVI and uncracked resin would require further screening experiments. For the purpose of this work, the 0.1 M NaBH₄ and 120 mL NaBH₄ solution/g resin condition was selected as the optimal condition.

3.1.3 Final synthesis procedure

After optimization of all synthesis variables was complete, the following methodology was used for characterization, batch, and column experiments. First, 10 g of dry A600E resin was stirred at 200 RPM in a round bottom flask with 400 mL 0.05 M Fe³⁺ and 0.1 M HCl in ethanol solution on a hotplate set at 70°C for 12 hours. This allowed Fe³⁺ to exchange onto the strong base anion exchange resin as FeCl₄⁻. **Figure 32** shows a picture of the FeCl₄⁻ solution.

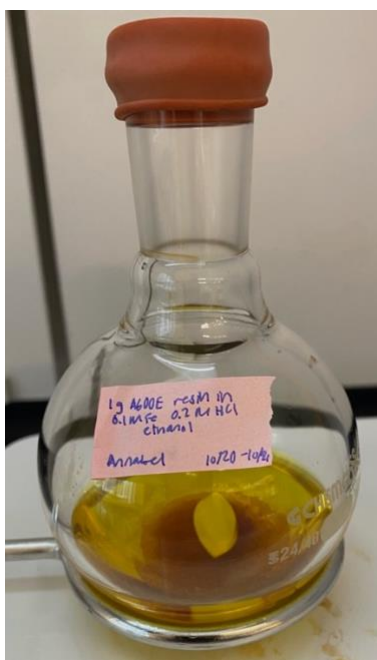


Figure 32. FeCl₄⁻ exchange onto A600E resin.

After the exchange step was complete, the resin was removed from the flask and vacuum filtered with 5 rinses of 50 mL absolute ethanol to remove impurities and excess iron on resin.

After ethanol rinsing, the resin was air dried for 24 hours. Next, 1200 mL water was purged of O₂(g) using a N₂(g) balloon in a covered 2000 mL beaker on a hotplate set at 50°C for 30 minutes. Air purging was performed to prevent fast oxidation of NZVI. Solid sodium borohydride (NaBH₄) was added to create a 0.1 M NaBH₄ solution. Then, 10 g of dry FeCl₄⁻ exchanged A600E was dropped directly into the NaBH₄ solution and stirred at 200 RPM for 15 minutes. The iron immediately reacted with the borohydride, forming H₂(g) and NZVI on the resin, as shown in the following equation and **Figure 33**.

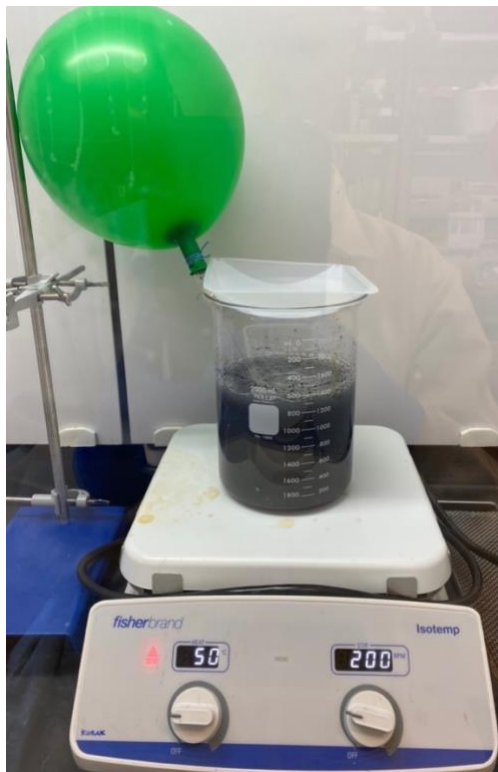
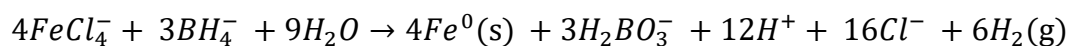


Figure 33. Reduction of Fe³⁺ to Fe⁰ by NaBH₄ on A600E resin.

After the reaction had completed, the solution cleared. The solution was decanted and the resin, now black and magnetic, was vacuum filtered and rinsed with 300 mL of deoxygenated water and 50 mL absolute ethanol. Resin was either vacuum dried prior to characterization and batch experiments or stored in deoxygenated water prior to column experiments. A summary of the visual impact on the resin is shown in **Figure 34**. The pristine A600E resin was dull yellow, the FeCl_4^- -A600E was bright orange, and the NZVI-A600E was black in color.



Figure 34. (A) Pristine A600E (B) FeCl_4^- -A600E (C) NZVI-A600E.

3.2 Resin density change

The impact of resin form on its density has not been previously presented in the literature. Resin density is important because resin capacity in batch experimentation is measured per mass of dried resin. When the density is different between the same type of resin in two different forms, such as pristine A600E and NZVI-A600E, this difference can bias performance comparisons. The NZVI-A600E resin was approximately 13% heavier than the A600E resin in Cl^- form, as shown in **Table 12**. In order to ensure the NZVI-A600E mass gain was not simply due to differences in moisture retention on the resin during air drying, the two air dried samples were both put in the oven at 100°C overnight. When removed from the oven, A600E lost 8.8%

mass and NZVI-A600E lost 7.9% mass. A t-test comparing two samples assuming equal variances was performed to show that the average percent mass lost in the oven between the A600E and NZVI-A600E trials could not be concluded to be different (p=0.18). Thus, since both forms of the resin lost a similar mass percentage when oven dried, it was concluded that the NZVI-A600E resin was not merely holding more moisture than A600E when air dried, but was more dense due to the NZVI formation in the particle. Density of the NZVI-A600E resin impacted batch isotherm results and upflow column bed expansion (and therefore Cr(VI) removal).

Table 12. Resin mass change for 1 g of each resin in replicate.

Parameter	A600E	FeCl₄-A600E	NZVI-A600E
Mass increase from A600E (air dried) (%)	-	26.21 ± 0.09	13 ± 2
Mass loss in oven (%)	8.8 ± 0.4	4.3 ± 0.1	7.9 ± 0.2

To account for the resin density difference for batch experiments, the following equation was used.

$$\text{mass NZVI A600E} * \frac{1 \text{ g A600E}}{1.13 \text{ g NZVI A600E}} = \text{density corrected mass NZVI A600E}$$

For a mass of 0.05 g NZVI-A600E used in a batch experiment, a density corrected mass of 0.044 g was used in isotherms to compare to unmodified A600E resin.

$$0.05 \text{ g NZVI A600E} * \frac{1 \text{ g A600E}}{1.13 \text{ g NZVI A600E}} = 0.044 \text{ g NZVI A600E (density corrected)}$$

3.3 Characterization

After optimization of iron loading (0.05 M Fe and 40 mL solution/g resin) and borohydride reduction (0.1 M NaBH₄ and 120 mL solution/g resin), the NZVI-A600E resin was characterized. Freshly synthesized NZVI-A600E resin was characterized in addition to post-column experimentation NZVI-A600E resin.

3.3.1 Visual inspection

Resin was first visually inspected. It was black, as shown in **Figure 35** and magnetic, since it was attracted to the metal stir bar, as shown in **Figure 36**.



Figure 35. Freshly synthesized NZVI-A600E.



Figure 36. NZVI-A600E attracted to a metal stir bar in a round bottom flask.

3.3.2 *Dissecting microscopy*

Dissecting microscope images are shown in **Figure 37**. The A600E resin was light yellow and uniformly shaped. The fresh NZVI-A600E was black and uniformly shaped; however, some resin beads were cracked. The post-column NZVI-A600E was orange-brown.

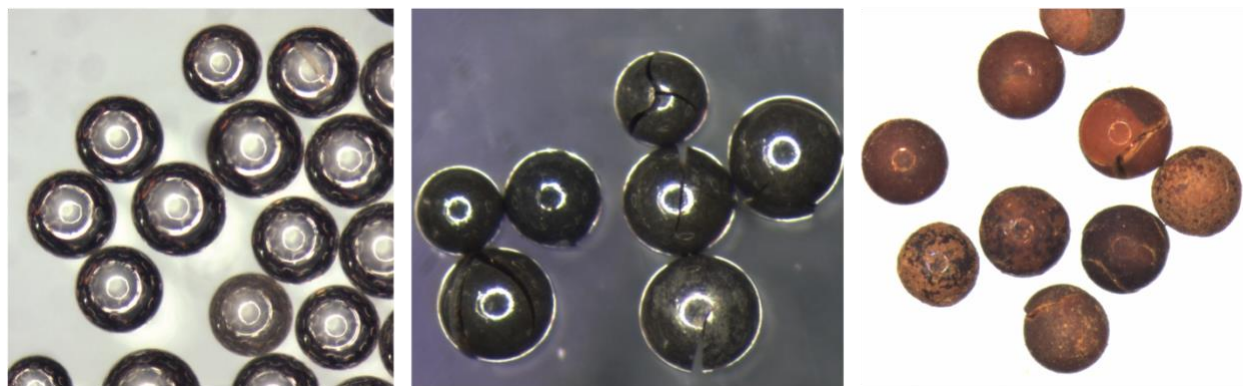


Figure 37. Dissecting microscope images of (A) A600E (B) fresh NZVI-A600E (C) post-column NZVI-A600E.

3.3.3 SEM-EDS

SEM-EDS in **Figure 38** shows that the NZVI-A600E resin beads were indeed cracked. The EDS recorded 25% Fe on the NZVI-A600E and 49% Fe on the post-column NZVI-A600E, as shown in **Figure 39**. EDS data showed a trend where carbon and oxygen were consistent through the EDS but chlorine decreased after synthesis and disappeared after column experimentation. On the post-column resin, there was a fine layer of reddish-orange powder on the outside of the resin beads shown in **Figure 38c**. EDS analysis of the post-column resin also showed a significant increase of iron on the surface of the resin which supports the hypothesis that the iron was oxidizing on the resin surface.

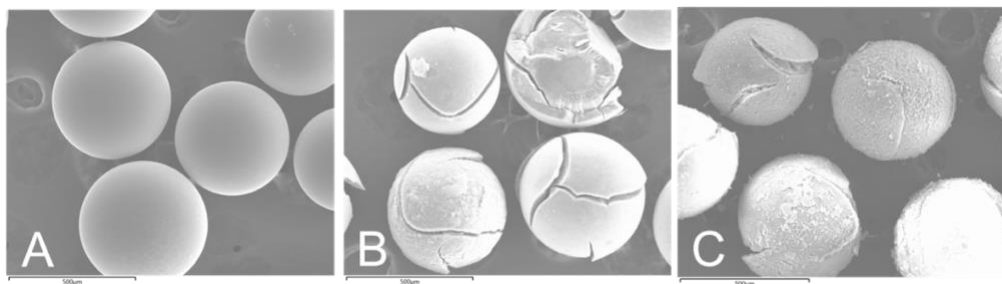


Figure 38. SEM-EDS image of (A) A600E (B) fresh NZVI-A600E (C) post-column NZVI-A600E.

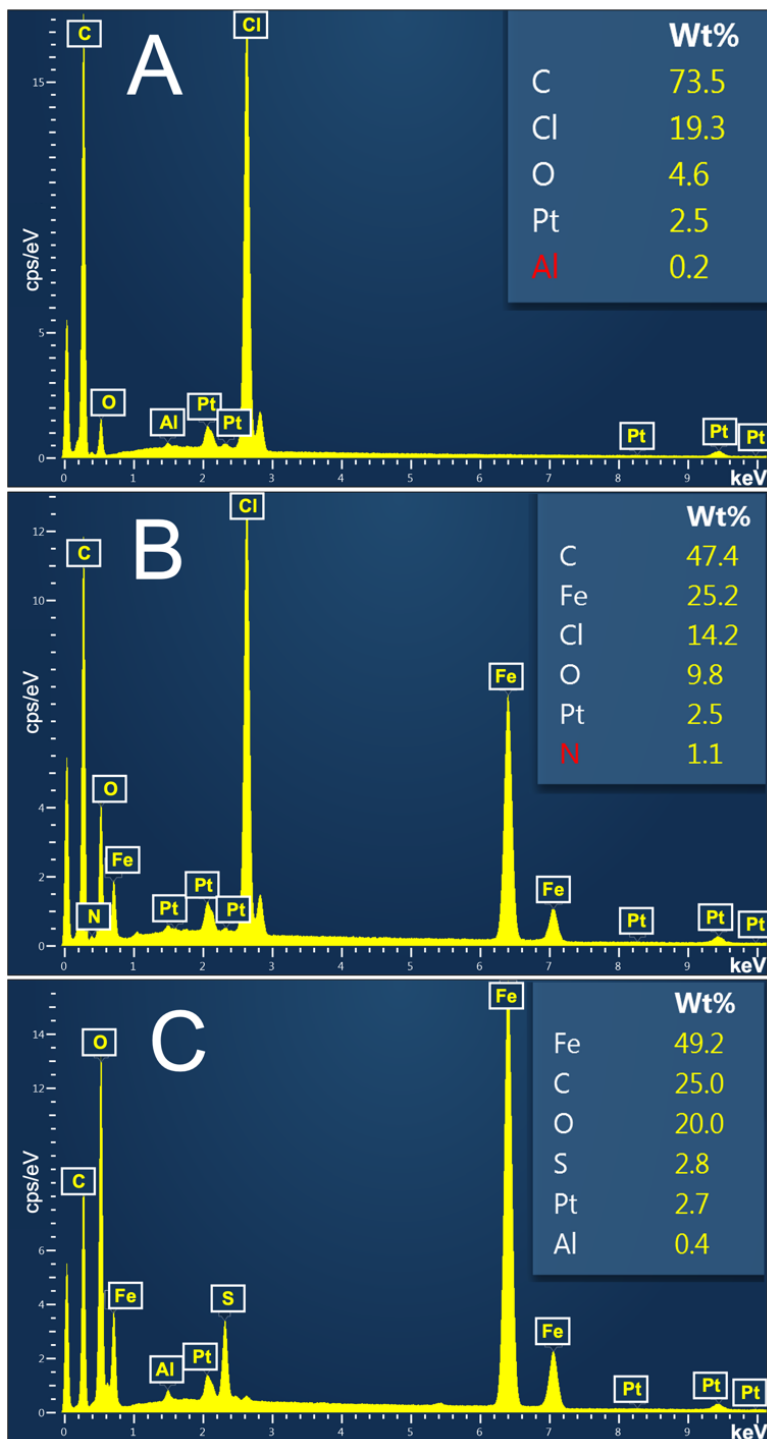


Figure 39. Elemental composition of (A) A600E (B) fresh NZVI-A600E (C) post-column NZVI-A600E.

3.3.4 XPS

The XPS full scan binding energy peaks at 700 eV in **Figure 40** indicate the presence of iron on the NZVI-A600E resins. The freshly synthesized (not yet run in an experiment) A600E resin showed peaks for C 1s at 285 eV, O 1s at 531 eV, Cl 2p at 197eV, N 1s at 400 eV and Si 2p at 101 eV. There was also an Fe 2p peak at 711eV. After column experimentation, the C 1s and O 1s peaks persisted but the Cl 2p peak became nonexistent, likely due to displacement of Cl⁻ in the resin by other ions in solution.

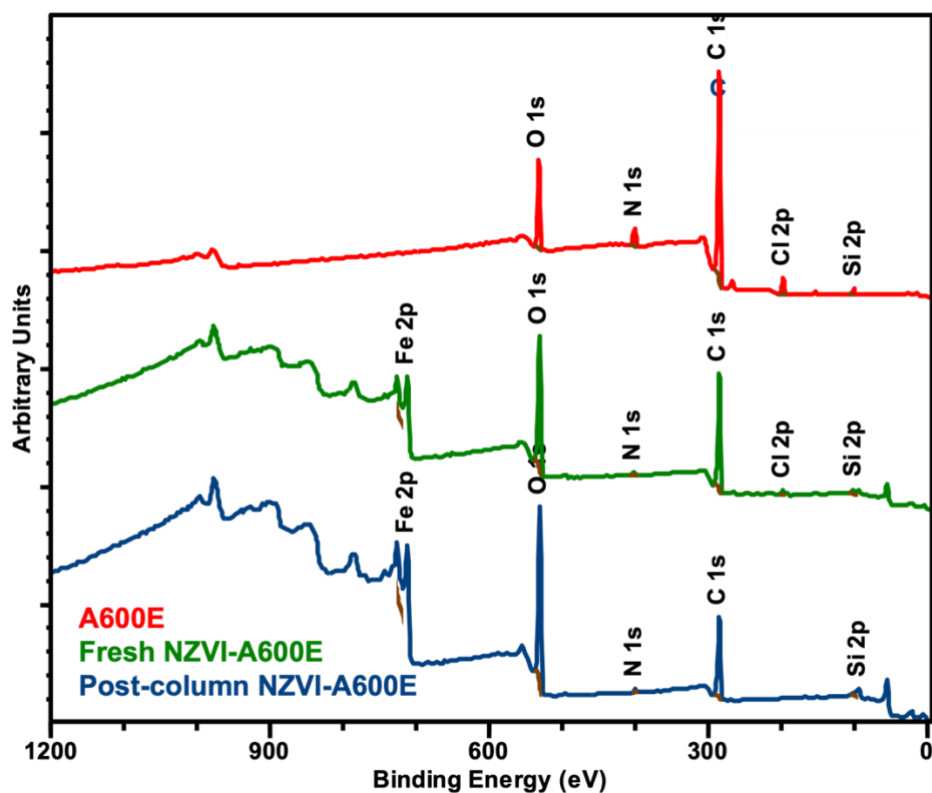


Figure 40. XPS spectrum of A600E, fresh NZVI-A600E, and post-column NZVI-A600E.

According to literature (Du et al., 2013; Shi et al., 2013), 707 and 720 eV peaks correspond to Fe^0 , while 710 and 724 eV peaks correspond to oxidized iron valence states (i.e., Fe^{2+} and Fe^{3+}). The NZVI-A600E resin was run twice: the day it was synthesized and 30 days after synthesis. As shown in the high-resolution Fe scan for the NZVI-A600E resin in **Figure 41a**, there is presence of a small shoulder at 707 eV, which can be attributed to Fe^0 . The 707 eV shoulder is stronger on the day of synthesis sample compared to the sample run 30 days after synthesis. Since the sample run 30 days after synthesis shows a decrease in Fe^0 signal, we can conclude that the surface of the resin was oxidized by $\text{O}_2(\text{g})$ in air over time. This indicates that the surface exposed to air of NZVI-resin is not stable in air. The lack of 707 eV Fe^0 peak in the post-column NZVI-A600E resin in **Figure 41b** is hypothesized to be the reaction of the Fe^0 with $\text{Cr}(\text{VI})$, converting all iron back to oxidized iron.

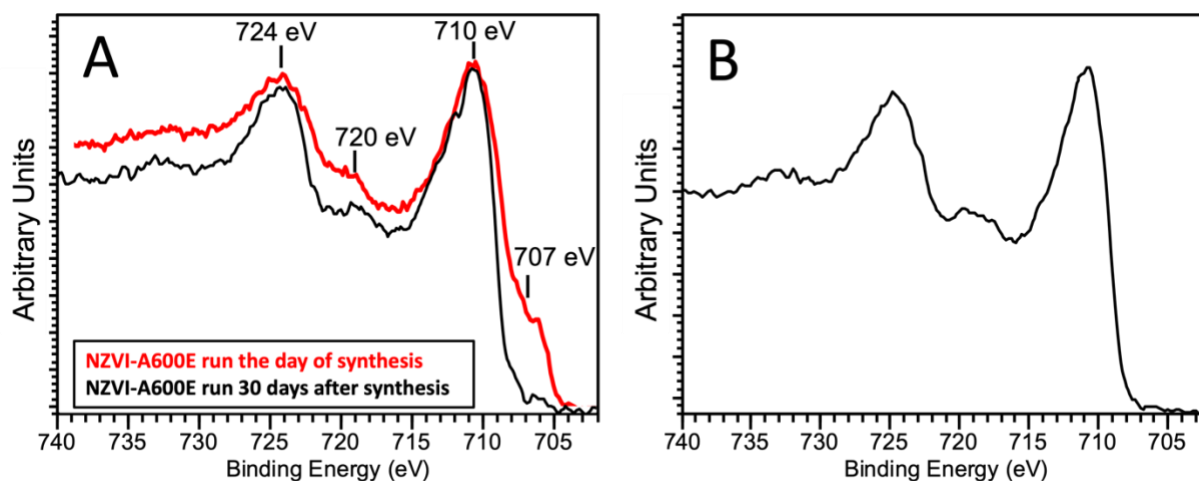


Figure 41. XPS scan from 705-740 eV of (A) fresh NZVI-A600E (B) post-column NZVI-A600E.

We expected to see an even stronger Fe⁰ signal; however, XPS analysis with spherical samples will typically lead to a reduction in peak intensities due to shadowing effects (Shard, 2020) (Easton et al., 2020). Intensity of the Fe⁰ may be due to a “core-shell structure” where iron may form a core of zero valent iron with a shell of iron oxides which has been suggested by multiple researchers that have synthesized Fe nanoparticles. To further confirm the presence of zero valent iron in the resin, x-ray diffraction could provide additional information on the iron crystalline structure where zero valent iron has characteristic reflection based off its diffraction plane (Xi et al., 2010; Noubactep, 2009; Sun et al., 2006; Y. Liu et al., 2005; Nurmi et al., 2005; X. Li & Zhang, 2007).

3.4 Batch experiments

Batch experiments were performed to understanding isotherm behavior of the ion exchange resin. Capacity was compared using resin that was initially in chloride form in a solution containing only sodium chromate. Differences in selectivity were assessed using resin initially in Cl⁻ form in a solution containing both sodium chromate and sodium sulfate. While equilibrium batch experiments are simple and easier to perform than flow through column experiments, this study revealed their drawbacks.

3.4.1 Capacity

The capacity experiments did not reveal improvement of resin sorption capacity by NZVI-A600E compared to A600E. The resulting isotherm is graphed in **Figure 42**. Without resin density correction, there was not a clear difference in resin capacity between the A600E and NZVI-A600E resin. When accounting for the 13% resin density increase from A600E to NZVI-A600E in the isotherm, the NZVI-A600E was found to have the same Cr(VI) sorption

capacity than A600E, using the second to last point on the isotherm. **Table 13** shows these results.

Table 13. Resin capacities (with resin density correction).

Resin	Capacity (mg Cr(VI)/g resin)
A600E	78 ± 5
NZVI-A600E	78 ± 4

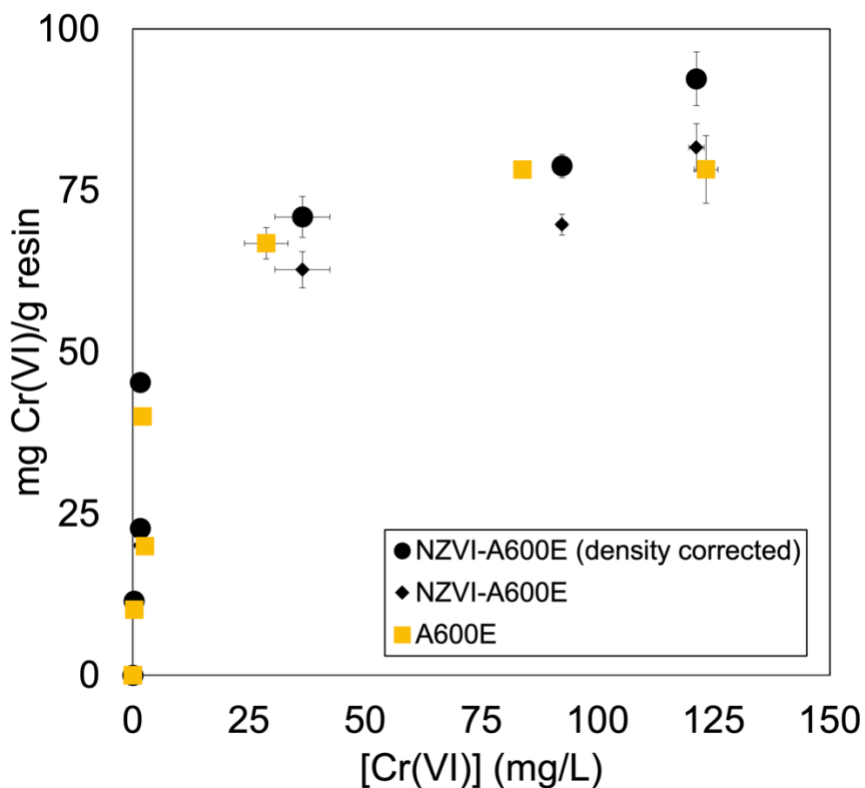


Figure 42. Equilibrium isotherms of A600E and NZVI-A600E (with resin density correction).

The A600E isotherm followed a Langmuir-like trend with capacity leveling off for tests with high solution volume and low resin mass. As seen in **Figure 42**, the isotherm point on the NZVI-A600E (mass corrected) curve with maximum capacity appeared to be an outlier. Therefore, the capacity numbers in **Table 13** may not be the best measure of resin performance.

Visually, **Figure 43** shows the batch bottles after reaching equilibrium in 24 hours. The characteristic green-yellow color of chromate disappears from solution as solution volume decreases and more chromate exchanges onto the resin. The grey-black color of the NZVI-A600E solutions may have come from the dark color of the iron. However, no iron was detected in the batch experiments solutions (samples were not filtered), indicating that the dark color of the iron may have been in particulate form rather than dissolved in the batches.

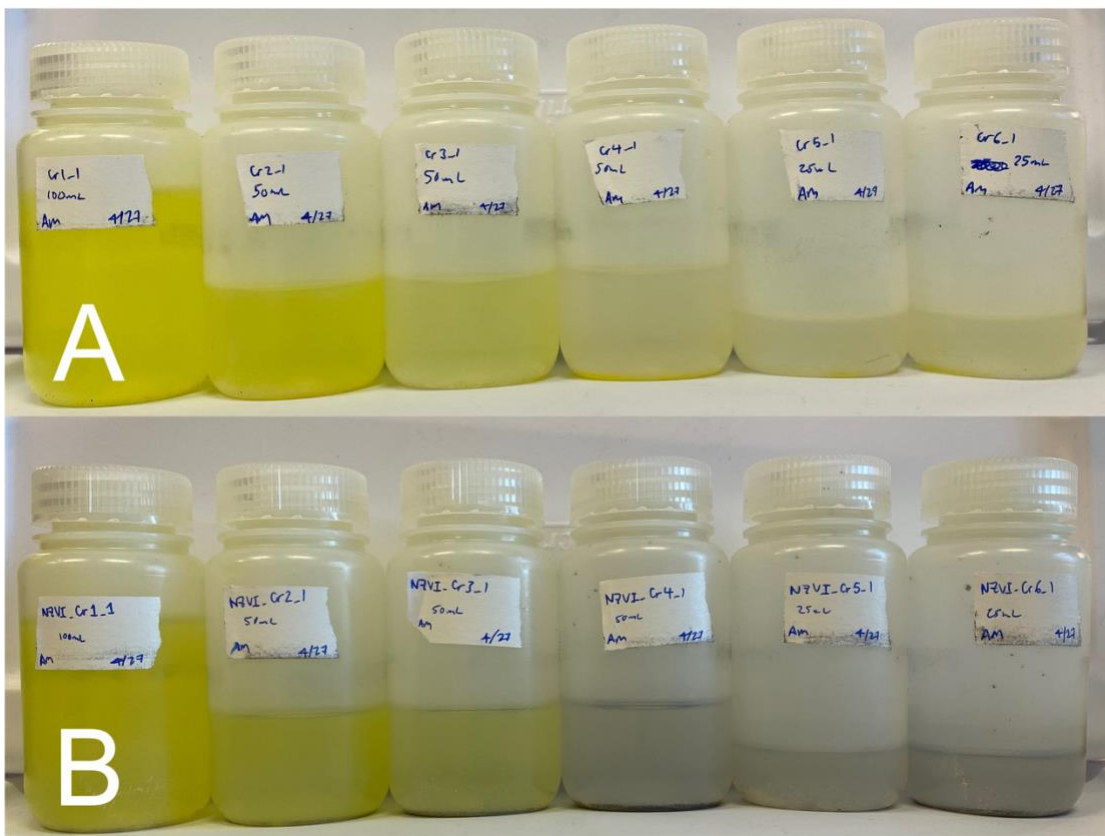


Figure 43. (A) A600E and (B) NZVI-A600E batches after 24 hours.

3.4.2 Selectivity experiments

The selectivity experiments showed that NZVI-A600E had higher affinity for CrO_4^{2-} over SO_4^{2-} than A600E. The separation factors (equal to the selectivity coefficients, since the two ions

are homovalent) are plotted in **Figure 44**. NZVI-A600E showed higher affinity for Cr(VI) than A600E for all points, with NZVI-A600E separation factors $\alpha_{\text{CrO}_4/\text{SO}_4}$ ranging from 13-27, while A600E separation factors ranged from 9-14. This indicates that selectivity for Cr(VI) increased using NZVI-A600E compared to A600E, showing that the new material is promising for selective Cr(VI) removal.

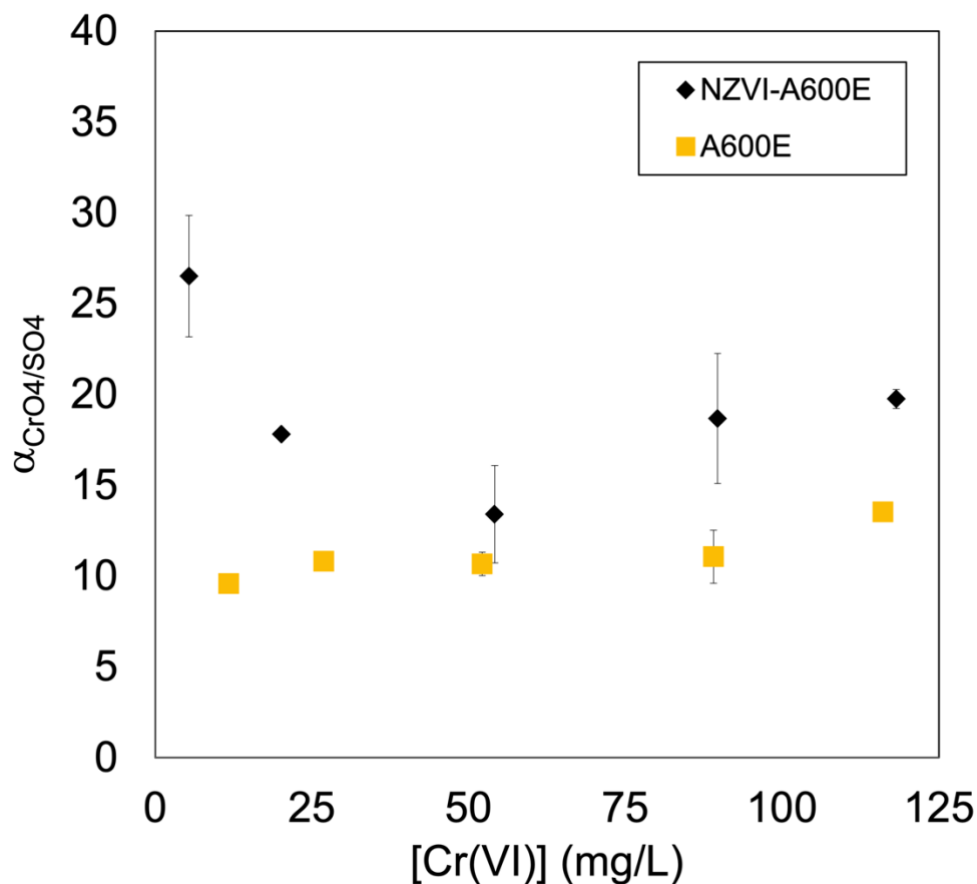


Figure 44. Separation factors $\alpha_{\text{CrO}_4/\text{SO}_4}$ of A600E and NZVI-A600E in 175 mg/L Cr(VI) and 2000 mg/L SO_4^{2-} solution.

When accounting for the 13% resin density increase from A600E to NZVI-A600E in the isotherm, the NZVI-A600E had similar uptake of Cr(VI) to A600E. The trace isotherm for

Cr(VI) is plotted in **Figure 45**. Both NZVI-A600E and A600E Cr(VI) isotherms follow a favorable isotherm shape.

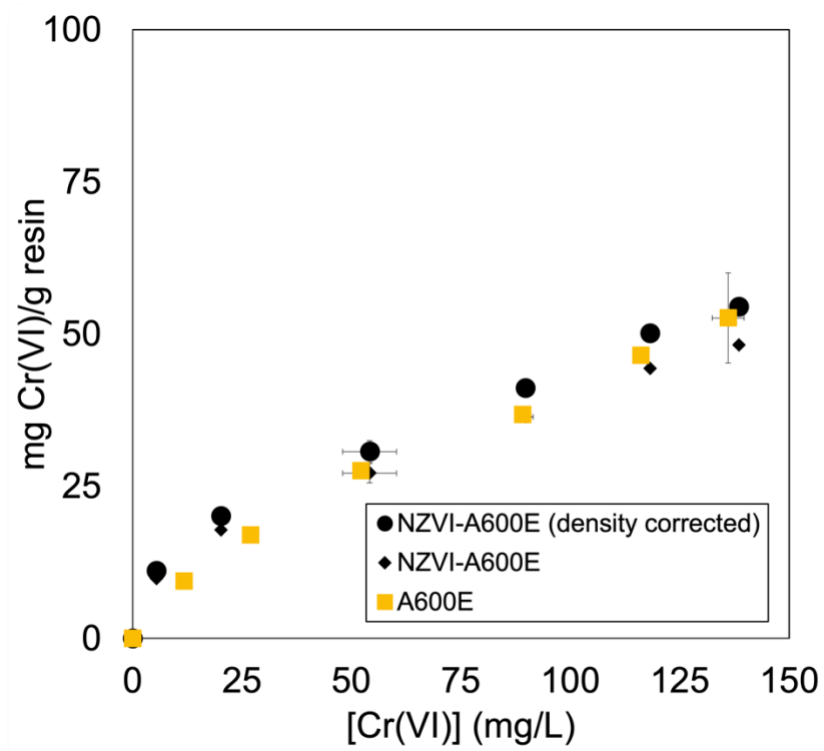


Figure 45. Equilibrium isotherms with 2000 mg/L SO_4^{2-} of A600E and NZVI-A600E (with resin density correction).

The batch tests show that the capacity and selectivity for Cr(VI) is higher for the NZVI-resin, but the difference is relatively small. However, batch testing has experimental constraints that introduce important limitations. The batch tests measured removal of Cr(VI) at 3 orders of magnitude higher concentrations (i.e., 175 mg/L instead of 100 $\mu\text{g/L}$) that expected in groundwater. It is possible that NZVI reacts with high concentrations of Cr(VI) differently than in trace levels. In addition, the test for selectivity over SO_4^{2-} was not a true representation of trace conditions, since SO_4^{2-} is often 3 orders of magnitude higher concentration than Cr(VI) in

groundwater (i.e., 100 mg/L SO_4^{2-} and 100 $\mu\text{g/L}$ Cr(VI)) , as opposed to the 1 order of magnitude higher concentrations in the batch test (i.e., 2000 mg/L SO_4^{2-} and 175 mg/L Cr(VI)). Thus, due to the differences in water quality, redox potential, the batch experiments were only a starting point for further column experimentation.

3.5 Fluidized bed column experimentation

Column experiments are better suited than batch experiments for predicting resin performance for drinking water treatment, because a representative water quality with $\mu\text{g/L}$ instead of mg/L levels of Cr(VI) can be tested over a longer time scale. While batch experiments were beneficial for synthesis screening and for an initial prediction of resin capacity and separation factors for Cr(VI) over SO_4^{2-} , the column experiments are more relevant to practical applications.

The NZVI-A600E resin ran 360% longer to Cr(VI) breakthrough than the A600E resin in the column, as shown in **Table 14** and **Figure 46**. Raw water with 91 $\mu\text{g/L}$ Cr(VI) was fed into the column and effectively treated for the effluent water to non-detect for the first 500 BV for A600E and 1900 BV for NZVI-A600E. Then, Cr(VI) removal by both A600E and NZVI-A600E breakthrough followed an S-shaped curve, which is characteristic of breakthrough curves for favorable isotherms. A comparison endpoint of 10 $\mu\text{g/L}$ Cr(VI) was chosen in **Table 14** because of the anticipated 10 $\mu\text{g/L}$ MCL in California expected to take effect next year in 2024, with A600E treating 800 BV and NZVI-A600E 2880 BV.

Table 14. Column performance between resins.

Resin	Breakthrough to 10 $\mu\text{g/L}$ Cr(VI) (BV)
A600E	800
NZVI-A600E	2880

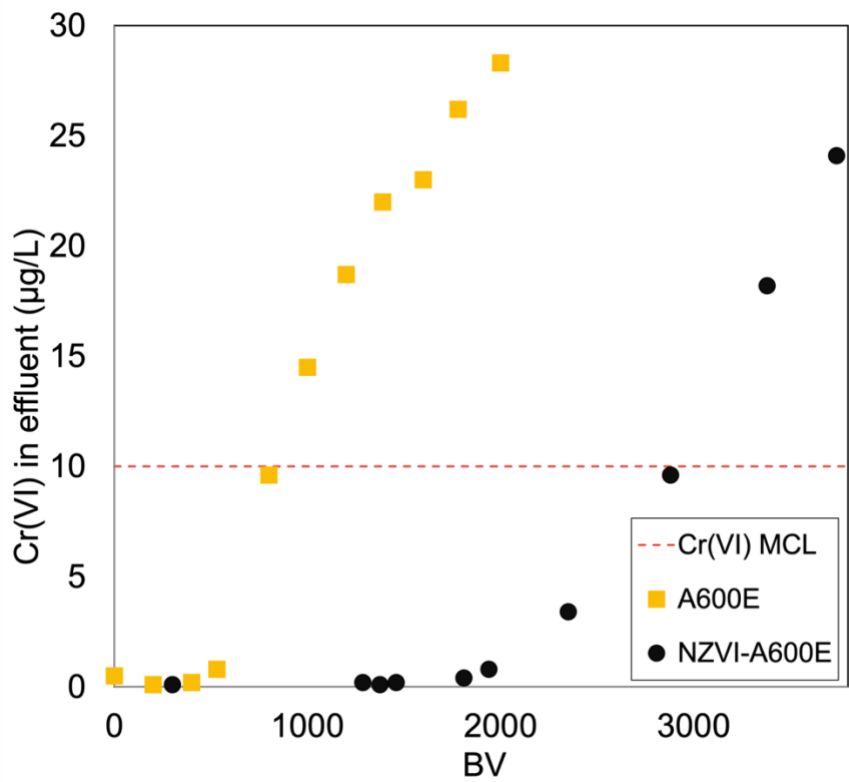


Figure 46. Breakthrough curve for trace Cr(VI) in upflow column experiments.

In contrast to Cr(VI) breakthrough, both A600E and NZVI-A600E demonstrated the same throughput to the influent SO_4^{2-} concentration at 800 BV, as shown in **Figure 47**. Since SO_4^{2-} showed similar breakthrough for both resins, this indicates that the resin capacity for SO_4^{2-} did not change but the capacity for Cr(VI) did increase. It can also be concluded that the NZVI on the resin did not block ion exchange sites when synthesized on the resin, as shown in **Figure 25**. Alongside the resulting 3.6 times as long Cr(VI) throughput, we find that NZVI is effective at selectively removing Cr(VI), without increasing removal of background constituents such as sulfate. This result indicates that the NZVI-resin works well for selective trace Cr(VI) water treatment in high SO_4^{2-} conditions.

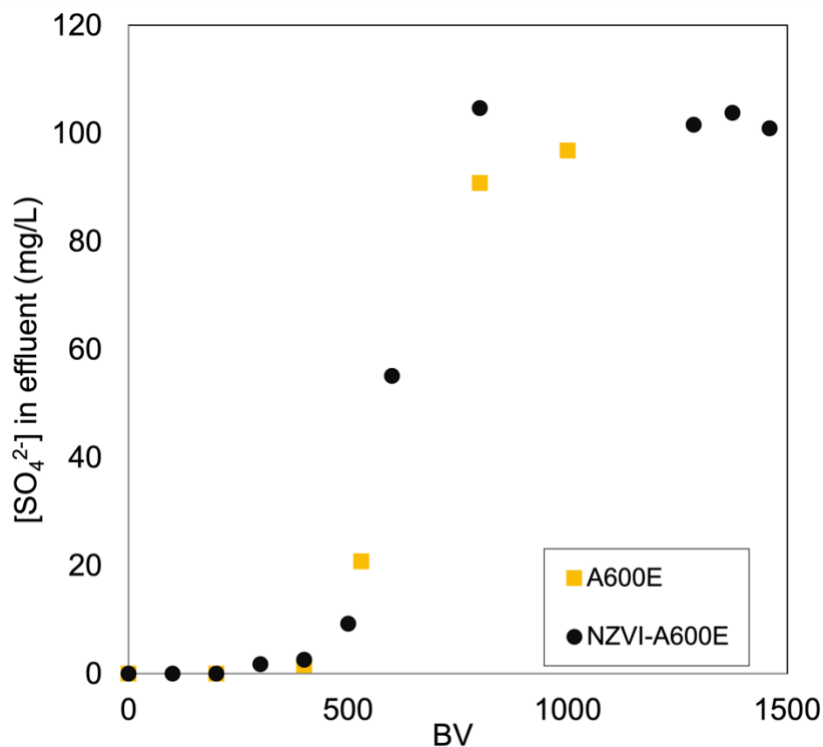


Figure 47. Breakthrough curve for SO_4^{2-} in upflow column experiments.

While the NZVI-A600E resin outperformed the A600E in the column experiment for selective Cr(VI) removal, there were a number of factors to take into account that would have practical implications for full-scale processes. First, since both columns were run upflow, despite using the same wet volume of resin, volumetric flow rate, and column, the heavier NZVI-A600E had a smaller expanded bed height than the A600E. There was an 21% difference in bed height between the resins, as listed in **Table 15**, with A600E resin expanding more due its lower density.

Table 15. Expanded heights of A600E and NZVI-A600E in upflow column experiments.

Resin	Expanded Bed Height (inch)
A600E	13
NZVI-A600E	11.25

To account for this difference in resin density, which may have biased the data in favor of NZVI-A600E performance, the following calculations were performed, shown in **Table 16**.

Table 16. Fluidized bed parameters.

Parameter	A600E	NZVI-A600E
Fixed bed height (m)	0.217	0.217
Expanded bed height (m)	0.330	0.286
Fixed bed resin porosity	0.375	0.326
Expanded bed resin porosity	0.588	0.524
Bed expansion (%)	52	31

Fixed bed resin porosity for both A600E and NZVI-A600E resin were estimated to be 0.375 based on medium (0.30-0.80 mm) spherical particles (Ouchiyama & Tanaka, 1984). Expanded bed resin porosity was calculated according to the following equation (Crittenden et al., 2012):

$$\frac{L_{Expanded}}{L_{Fixed}} = \frac{1 - \varepsilon_{Fixed}}{1 - \varepsilon_{Expanded}}$$

where L is bed height in meters and ε is bed porosity, which is dimensionless. Thus, for the expanded bed porosities:

$$\begin{aligned} \varepsilon_{Expanded,A600E} &= 1 - \left[(1 - \varepsilon_{Fixed,A600E}) * \frac{L_{Fixed,A600E}}{L_{Expanded,A600E}} \right] = 1 - \left[(1 - 0.375) * \frac{0.217}{0.330} \right] \\ &= 0.588 \end{aligned}$$

$$\begin{aligned} \varepsilon_{Expanded,NZVI-A600E} &= 1 - \left[(1 - \varepsilon_{Fixed,NZVI-A600E}) * \frac{L_{Fixed,NZVI-A600E}}{L_{Expanded,NZVI-A600E}} \right] \\ &= 1 - \left[(1 - 0.375) * \frac{0.217}{0.286} \right] = 0.524 \end{aligned}$$

Since the expanded bed porosities between A600E and NZVI-A600E were similar (0.588 compared to 0.524), the resin density difference likely had minimal biased on breakthrough. However, to remove the uncertainty due to differences in porosity between NZVI-A600E and

A600E, a packed bed column experiment would be a better way to compare breakthrough for future experiments.

There were four other factors with potential practical implications, observed during the first 800 BV of the NZVI-A600E resin column experiment: iron leaching, boron leaching, pH increase, and gas bubbling. First, iron leached off the resin into the effluent column water.

Figure 48 shows a plot of iron in the effluent over the course of the run, which was below 25 $\mu\text{g/L}$ by 800 BV. The U.S. EPA has a secondary drinking water standard MCL for iron of 0.3 mg/L, so during the first 800 BV of the run, the iron concentration was above regulatory limits.

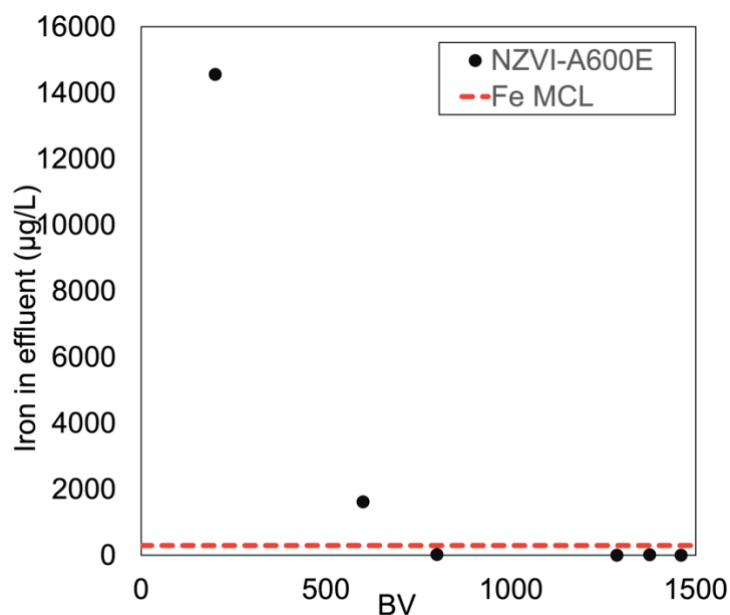


Figure 48. Effluent iron during NZVI-A600E column experiment.

Second, preliminary quick scan results from the ICP-MS indicated that boron was also detected in the effluent, due to residual boron synthesis reagents (e.g., NaBH_4 , NaBO_2 , and H_3BO_3) leaching off the resin. While boron is not federally regulated in drinking water and has not been linked to carcinogenicity, various states (CA, FL, ME, MN, NH, WI) have set drinking

water guidelines ranging from 0.6-1 mg B/L (U.S. Environmental Protection Agency, 2008).

Figure 49 shows approximate boron concentrations detected over the course of the column experiment, with boron concentrations exceeding the state drinking water guidelines early in the run and then going below detectable levels after 800 BV.

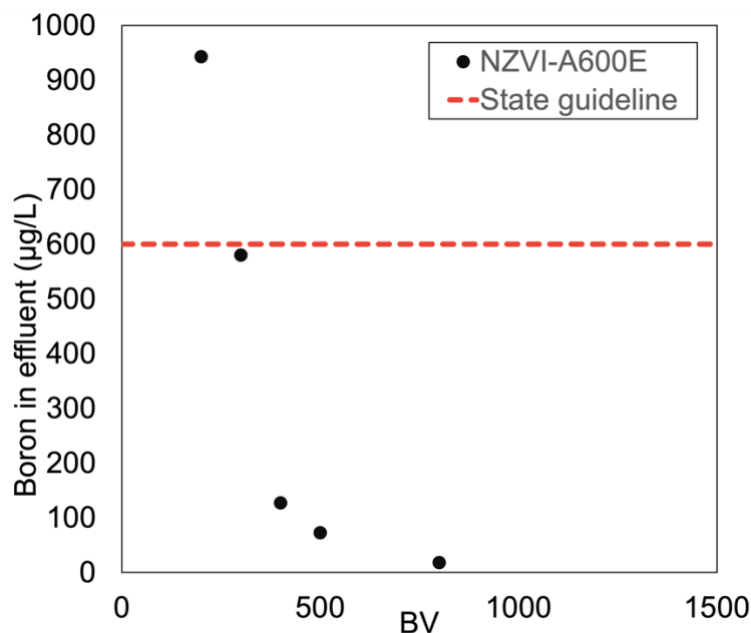


Figure 49. Approximate effluent boron concentrations during NZVI-A600E column experiment.

Third, pH increased during after start-up. By 800 BV, pH had stabilized to the influent pH value, as shown in **Figure 50**. The initial increase in pH is likely due to the NaBH_4 , which forms an alkaline solution. This is opposite from the trend that occurs in SBIX processes: pH usually drops after start-up due to bicarbonate exchanging onto the resin, which can release a H^+ due to the resin favoring CO_3^{2-} (Chen et al., 2020).

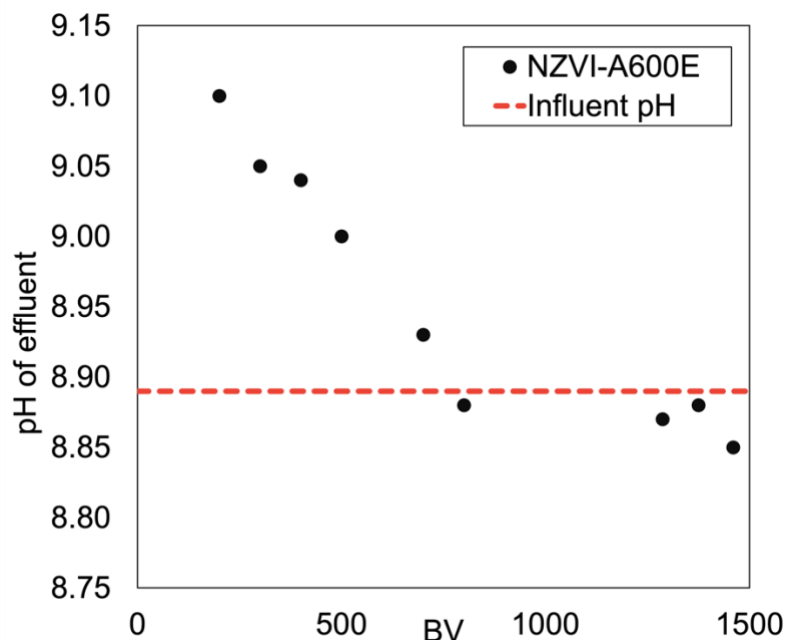


Figure 50. Effluent pH during NZVI-A600E column experiment.

Fourth, hydrogen gas was produced by the NZVI-A600E. It was due to this challenge that the column was run upflow instead of the standard downflow, because gas bubbles in a downflow packed column bed create side channels for influent water to bypass the packed bed, compromising its plug flow behavior. Hydrogen gas production is hypothesized to have occurred due to the combination of both the reaction of excess NaBH_4 with water and the reaction of NZVI with water. By 800 BV, the resin had stopped bubbling and had turned from black to red.

The four cross-sections of the column were examined with the dissecting microscope as shown in **Figure 51**. The resin at the very top of the column, denoted as fluff, was bright orange and appeared to be broken pieces of resin that had risen to the top of the column due to their lighter mass. The top, middle, and bottom section of resin were also no longer black but a rusty orange-brown color. This indicates that the Fe^0 was oxidized over the course of the experiment.

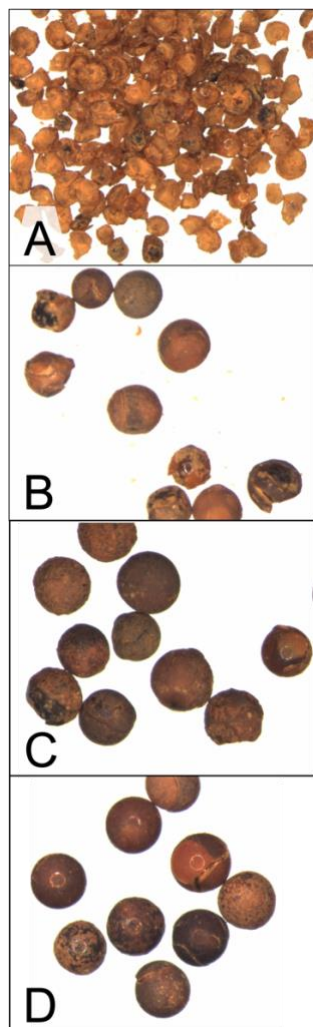


Figure 51. Images of post-column NZVI-A600E (A) fluff, (B) top, (C) middle, and (D) bottom sections.

4 CHAPTER 4: CONCLUSION

4.1 Summary

This work successfully dispersed NZVI on Purolite® A600E strong base ion exchange resin. The field of hybrid ion exchange was advanced through a detailed table of screened synthesis conditions, building upon work in previous studies. For NZVI impregnation on anion exchange resin, the first step was FeCl_4^- exchange, followed by resin rinsing in absolute ethanol and air drying. FeCl_4^- was reduced by dropping the dry resin into a NaBH_4 solution under $\text{N}_2(\text{g})$ conditions, followed by vacuum desiccation. Optimization of NaBH_4 dose to minimize gas production, solution pH increase, and resin cracking was challenging and may require future work.

Resin density increased 13% between unmodified A600E resin and NZVI-A600E resin due to the synthesized iron coating. As this impacts mass-based experiments, it represents a new finding in the field that should be considered in future hybrid ion exchange work.

Batch studies showed improved selectivity for Cr(VI) over SO_4^{2-} , with separation factors reaching 27 using NZVI-A600E as opposed to 14 using unmodified resin in 175 mg/L Cr(VI) 2000 mg/L SO_4^{2-} solution. Batch capacity studies did not provide strong evidence that NZVI-A600E has higher Cr(VI) capacity than the unmodified resin; however, column testing is better suited for testing of representative water qualities for drinking water treatment.

In an upflow fluidized column, NZVI-A600E outperformed unmodified resin by 360%. A breakthrough curve of SO_4^{2-} showed unchanged throughput between the unmodified and modified resin, indicating the improved selectivity of NZVI-A600E for Cr(VI) over SO_4^{2-} . However, column studies also revealed challenges with NZVI-A600E that will need to be

addressed including iron and boron leaching, increased pH, and gas production within the column.

4.2 Practical implications

A600E is used as a regenerable resin for Cr(VI) treatment. To understand regeneration and reuse of NZVI-A600E, batch and column regeneration experiments need to be performed. A regenerant chemical and concentration must be determined that can restore capacity to ion exchange functional groups for Cr(VI) removal without damaging the iron nanoparticles used for Cr(VI) adsorption and reduction. Past work has considered in situ regeneration of NZVI by introducing synthesis reagents into the column (Chanthapon et al., 2018). In addition, experiments understanding mechanism of Cr(VI) removal on NZVI and reuse potential are key for moving forward with this new material.

To solve the challenges of iron and boron leaching, increased pH, and gas production in the column study, synthesis screening experiments and further characterization of resin for NaBH₄ can be considered to understand its role in causing these complications. Since these complications all occurred during the first 800 BV of water treatment, a pre-soak of the resin could also be considered to prevent impact on effluent water quality. The role of resin cracking on iron leaching also ought to be examined in more detail.

4.3 Future horizons

Since hybrid resins have already been put on the market, collaboration with these researchers and resin manufacturers that have already forged the way in up-scaling hybrid ion exchange technology is key. For instance, learning from the challenges of regenerating and up-scaling ArsenX^{np}, a hybrid resin used for arsenic removal, research can be furthered in

transferring laboratory scale synthesis and column experimentation to pilot and full-scale of NZVI-resin (Kabay et al., 2010). This work is a starting point that can be built upon to improve ion exchange as a treatment solution for remediating Cr(VI) contamination in drinking water.

References

- Arias-Paić, M. S., & Korak, J. A. (2020). Forward Osmosis for Ion Exchange Waste Brine Management. *Environmental Science & Technology Letters*, 7(2), 111–117.
<https://doi.org/10.1021/acs.estlett.9b00733>
- Barreto-Rodrigues, M., Silveira, J., Zazo, J. A., & Rodriguez, J. J. (2017). Synthesis, characterization and application of nanoscale zero-valent iron in the degradation of the azo dye Disperse Red 1. *Journal of Environmental Chemical Engineering*, 5(1), 628–634.
<https://doi.org/10.1016/j.jece.2016.12.041>
- Benjamin, M. M., & Lawler, D. F. (2013). *Water Quality Engineering: Physical / Chemical Treatment Processes*. John Wiley & Sons.
- Brack, P., Dann, S. E., & Wijayantha, K. G. U. (2015). Heterogeneous and homogenous catalysts for hydrogen generation by hydrolysis of aqueous sodium borohydride (NaBH_4) solutions. *Energy Science & Engineering*, 3(3), 174–188. <https://doi.org/10.1002/ese3.67>
- Bryjak, M., Kabay, N., Rivas, B. L., & Bundschuh, J. (Eds.). (2016). Removal of trace chromate from contaminated water: Ion-exchange and redox-active sorption processes. In *Innovative Materials and Methods for Water Treatment* (0 ed., pp. 353–388). CRC Press.
<https://doi.org/10.1201/b19577-27>
- Bunzl, K. (1995). Calculation of the Helfferich number to identify the rate-controlling step of ion exchange for a batch process. *Industrial and Engineering Chemistry Research*, 34(8).
<https://doi.org/10.1021/ie00047a005>
- California Manufacturers and Technology Association and Solano County Taxpayers Association v. State Water Resources Control Board., (Superior Court of California 2017).

California Water Boards. (2023, June 29). *Chromium-6 Drinking Water MCL*.

https://www.waterboards.ca.gov/drinking_water/certlic/drinkingwater/Chromium6.html

Carothers, L., & Gorman, C. (2023, April 5). *Non-regenerable SBA-IX Treatment for Cr(VI)*

[Oral presentation]. California-Nevada American Water Works Association Spring Conference 2023.

Chanthapon, N., Sarkar, S., Kidkhunthod, P., & Padungthon, S. (2018). Lead removal by a

reusable gel cation exchange resin containing nano-scale zero valent iron. *Chemical Engineering Journal*, 331, 545–555. <https://doi.org/10.1016/j.cej.2017.08.133>

Chen, A., Lal, V., & Wang, L. (2011). *Arsenic Removal from Drinking Water by Point of*

Entry/Point of Use Adsorptive Media U.S. EPA Demonstration Project at Oregon Institute of Technology at Klamath Falls, OR Final Performance Evaluation Report

(EPA/600/R-11/035).

https://hero.epa.gov/hero/index.cfm/reference/details/reference_id/1372077

Chen, A., Wang, L., Sorg, T. J., & Lytle, D. A. (2020). Removing arsenic and co-occurring

contaminants from drinking water by full-scale ion exchange and point-of-use/point-of-entry reverse osmosis systems. *Water Research*, 172, 115455.

<https://doi.org/10.1016/j.watres.2019.115455>

Clifford, D., & Weber Jr., W. J. (1982). The determinants of divalent/monovalent selectivity in

anion exchangers—ScienceDirect. *Reactive Polymers, Ion Exchangers, Sorbents*, 1(2), 77–89.

Costa, M. (2003). Potential hazards of hexavalent chromate in our drinking water. *Toxicology*

and Applied Pharmacology, 188(1), 1–5. [https://doi.org/10.1016/S0041-008X\(03\)00011-](https://doi.org/10.1016/S0041-008X(03)00011-)

5

- Crittenden, J. C., Trussell, R. R., Hand, D. W., Howe, K. J., & Tchobanoglous, G. (2012). *MWH's Water Treatment: Principles and Design*. John Wiley & Sons.
- Cross, K. M., Lu, Y., Zheng, T., Zhan, J., McPherson, G., & John, V. (2009). Chapter 24—
Water Decontamination Using Iron and Iron Oxide Nanoparticles. In N. Savage, M. Diallo, J. Duncan, A. Street, & R. Sustich (Eds.), *Nanotechnology Applications for Clean Water* (pp. 347–364). William Andrew Publishing. <https://doi.org/10.1016/B978-0-8155-1578-4.50033-0>
- de Dardel, F. (2013a). *Ion exchange resin structure*. http://dardel.info/IX/resin_structure.html
- de Dardel, F. (2013b). *Selectivity*. http://dardel.info/IX/other_info/selectivity_a.html
- Du, Q., Zhang, S., Pan, B., Lv, L., Zhang, W., & Zhang, Q. (2013). Bifunctional resin-ZVI composites for effective removal of arsenite through simultaneous adsorption and oxidation. *Water Research*, *47*(16), 6064–6074. <https://doi.org/10.1016/j.watres.2013.07.020>
- Dummer, A. (2021). *Best Available Technologies (BAT) for Hexavalent Chromium Treatment*. California Water Boards. https://www.waterboards.ca.gov/drinking_water/certlic/drinkingwater/docs/2022/hexavalent_chromium/pr-request.pdf
- Easton, C. D., Kinnear, C., McArthur, S. L., & Gengenbach, T. R. (2020). Practical guides for x-ray photoelectron spectroscopy: Analysis of polymers. *Journal of Vacuum Science & Technology A*, *38*(2), 023207. <https://doi.org/10.1116/1.5140587>
- Fendorf, S. E. (1995). Surface reactions of chromium in soils and waters. *Geoderma*, *67*(1–2), 55–71. [https://doi.org/10.1016/0016-7061\(94\)00062-F](https://doi.org/10.1016/0016-7061(94)00062-F)

- Flint, L. C., Arias-Paić, M. S., & Korak, J. A. (2021). Removal of hexavalent chromium by anion exchange: Non-target anion behavior and practical implications. *Environmental Science: Water Research & Technology*, 7(12), 2397–2413. <https://doi.org/10.1039/D1EW00382H>
- Fu, F., Ma, J., Xie, L., Tang, B., Han, W., & Lin, S. (2013). Chromium removal using resin supported nanoscale zero-valent iron. *Journal of Environmental Management*, 128, 822–827. <https://doi.org/10.1016/j.jenvman.2013.06.044>
- Gao, W., Zhong, D., Xu, Y., Luo, H., & Zeng, S. (2022). Nano zero-valent iron supported by macroporous styrene ion exchange resin for enhanced Cr(VI) removal from aqueous solution. *Journal of Dispersion Science and Technology*, 43(8), 1197–1207. <https://doi.org/10.1080/01932691.2020.1848583>
- Gorman, C., Kennedy, A., Samson, C., Plummer, S., Townsend, E., & Seidel, C. (2023). Improvements in the reduction coagulation filtration process for hexavalent chromium treatment. *AWWA Water Science*, 5(1). <https://doi.org/10.1002/aws2.1315>
- Gorman, C., Seidel, C., Henrie, T., Huang, L., & Robert, T. (2016). Pilot Testing Strong Base Anion Exchange for CrVI Removal. *Journal - American Water Works Association*, 108, E240–E246. <https://doi.org/10.5942/jawwa.2016.108.0028>
- Han, Y., Yang, M. D. Y., Zhang, W., & Yan, W. (2015). Optimizing synthesis conditions of nanoscale zero-valent iron (nZVI) through aqueous reactivity assessment. *Frontiers of Environmental Science & Engineering*, 9(5), 813–822. <https://doi.org/10.1007/s11783-015-0784-z>
- Hauptert, L. M., Pressman, J. G., Speth, T. F., & Wahman, D. G. (2021). Avoiding pitfalls when modeling removal of per- and polyfluoroalkyl substances by anion exchange. *AWWA Water Science*, 3(2). <https://doi.org/10.1002/aws2.1222>

- Haupt, G. W. (1952). An alkaline solution of potassium chromate as a transmittancy standard in the ultraviolet. *Journal of Research of the National Bureau of Standards*, 48(12).
- Hausladen, D. M., Alexander-Ozinskas, A., McClain, C., & Fendorf, S. (2018). Hexavalent Chromium Sources and Distribution in California Groundwater. *Environmental Science & Technology*, 52(15), 8242–8251. <https://doi.org/10.1021/acs.est.7b06627>
- Helffferich, F., & Plesset, M. S. (2004). Ion Exchange Kinetics. A Nonlinear Diffusion Problem. *The Journal of Chemical Physics*, 28(3), 418–424. <https://doi.org/10.1063/1.1744149>
- Henrie, T., Plummer, S., Orta, J., Bigley, S., Gorman, C., Seidel, C., Shimabuku, K., & Liu, H. (2019). Full-scale demonstration testing of hexavalent chromium reduction via stannous chloride application. *AWWA Water Science*, 1(2), e1136. <https://doi.org/10.1002/aws2.1136>
- Huynh, B., & Edjan, E. (2023, April 5). *Reduction/Coagulation/Oxidation/Filtration System for Hexavalent Chromium Removal* [Oral presentation]. California-Nevada American Water Works Association Spring Conference 2023.
- Jiang, Z., Lv, L., Zhang, W., Du, Q., Pan, B., Yang, L., & Zhang, Q. (2011). Nitrate reduction using nanosized zero-valent iron supported by polystyrene resins: Role of surface functional groups. *Water Research*, 45(6), 2191–2198. <https://doi.org/10.1016/j.watres.2011.01.005>
- Jiang, Z., Zhang, S., Pan, B., Wang, W., Wang, X., Lv, L., Zhang, W., & Zhang, Q. (2012). A fabrication strategy for nanosized zero valent iron (nZVI)–polymeric anion exchanger composites with tunable structure for nitrate reduction. *Journal of Hazardous Materials*, 233–234, 1–6. <https://doi.org/10.1016/j.jhazmat.2012.06.025>

- Kabay, N., Bundschuh, J., Hendry, B., & Bryjak, M. (Eds.). (2010). Field experiences with ArsenXnp , a very effective and efficient hybrid media for arsenic removal. In *The Global Arsenic Problem* (0 ed., pp. 229–236). CRC Press.
<https://doi.org/10.1201/b10537-27>
- Kennedy, A. M., Korak, J. A., Flint, L. C., Hoffman, C. M., & Arias-Paic, M. (2018). Pilot-Scale Removal of Total and Hexavalent Chromium From Groundwater Using Stannous Chloride. *Journal - American Water Works Association*, *110*(4), E29–E42.
<https://doi.org/10.1002/awwa.1048>
- Korak, J. A., Mungan, A. L., & Watts, L. T. (2023). Critical review of waste brine management strategies for drinking water treatment using strong base ion exchange. *Journal of Hazardous Materials*, *441*, 129473. <https://doi.org/10.1016/j.jhazmat.2022.129473>
- Lace, A., Ryan, D., Bowkett, M., & Cleary, J. (2019). Chromium Monitoring in Water by Colorimetry Using Optimised 1,5-Diphenylcarbazide Method. *International Journal of Environmental Research and Public Health*, *16*(10), 1803.
<https://doi.org/10.3390/ijerph16101803>
- Leun, D., & SenGupta, A. K. (2000). Preparation and Characterization of Magnetically Active Polymeric Particles (MAPPs) for Complex Environmental Separations. *Environmental Science & Technology*, *34*(15), 3276–3282. <https://doi.org/10.1021/es0010148>
- Li, M., Zhang, B., Zou, S., Liu, Q., & Yang, M. (2020). Highly selective adsorption of vanadium (V) by nano-hydrous zirconium oxide-modified anion exchange resin. *Journal of Hazardous Materials*, *384*, 121386. <https://doi.org/10.1016/j.jhazmat.2019.121386>

- Li, P., & SenGupta, A. K. (2000). Intraparticle diffusion during selective ion exchange with a macroporous exchanger. *Reactive and Functional Polymers*, 44(3), 273–287.
[https://doi.org/10.1016/S1381-5148\(99\)00103-0](https://doi.org/10.1016/S1381-5148(99)00103-0)
- Li, X., & Zhang, W. (2007). Sequestration of Metal Cations with Zerovalent Iron Nanoparticles A Study with High Resolution X-ray Photoelectron Spectroscopy (HR-XPS). *The Journal of Physical Chemistry C*, 111(19), 6939–6946.
<https://doi.org/10.1021/jp0702189>
- Liu, G., Han, C., Kong, M., Abdelraheem, W. H. M., Nadagouda, M. N., & Dionysiou, D. D. (2022). Nanoscale Zero-Valent Iron Confined in Anion Exchange Resins to Enhance Selective Adsorption of Phosphate from Wastewater. *ACS ES&T Engineering*, 2(8), 1454–1464. <https://doi.org/10.1021/acsestengg.1c00506>
- Liu, H., & Yu, X. (2020). Hexavalent chromium in drinking water: Chemistry, challenges and future outlook on Sn(II)- and photocatalyst-based treatment. *Frontiers of Environmental Science & Engineering*, 14(5), 88. <https://doi.org/10.1007/s11783-020-1267-4>
- Liu, Y., Choi, H., Dionysiou, D., & Lowry, G. V. (2005). Trichloroethene Hydrodechlorination in Water by Highly Disordered Monometallic Nanoiron. *Chemistry of Materials*, 17(21), 5315–5322. <https://doi.org/10.1021/cm0511217>
- Marracocco, T., & Kennedy, A. (2023, April 5). *Indio Water Authority Regenerable SBA-IX Treatment for Cr(VI) and Plans for Future Cr(VI) Best Available Technology Treatment Needs* [Oral presentation]. California-Nevada American Water Works Association Spring Conference 2023.

- McLean, J. E., McNeill, L. S., Edwards, M. A., & Parks, J. L. (2012). Hexavalent chromium review, part 1: Health effects, regulations, and analysis. *Journal - American Water Works Association*, 104(6), E348–E357. <https://doi.org/10.5942/jawwa.2012.104.0091>
- Moffat, I., Martinova, N., Seidel, C., & Thompson, C. M. (2018). Hexavalent Chromium in Drinking Water: JOURNAL AWWA. *Journal - American Water Works Association*, 110(5), E22–E35. <https://doi.org/10.1002/awwa.1044>
- Mueller, N. C., Braun, J., Bruns, J., Černík, M., Rissing, P., Rickerby, D., & Nowack, B. (2012). Application of nanoscale zero valent iron (NZVI) for groundwater remediation in Europe. *Environmental Science and Pollution Research*, 19(2), 550–558. <https://doi.org/10.1007/s11356-011-0576-3>
- Najim, I., Brown, N. P., Seo, E., Gallagher, B., Gramith, K., Blute, N., Wu, X., Yoo, M., Liang, S., Maceiko, S., Kader, S., & Lowry, J. (2014). *Impact of Water Quality on Hexavalent Chromium Removal Efficiency and Cost* (4450; pp. 1–174). Water Research Foundation Project.
- Nomura, Y., Inoue, D., & Moritomo, Y. (2022). Control of Fe³⁺ coordination by excess Cl⁻ in alcohol solutions. *RSC Advances*, 12(28), 17932–17936. <https://doi.org/10.1039/D2RA01522F>
- Noubactep, C. (2009). Characterizing the discoloration of methylene blue in Fe0/H2O systems. *Journal of Hazardous Materials*, 166(1), 79–87. <https://doi.org/10.1016/j.jhazmat.2008.11.001>
- Nurmi, J. T., Tratnyek, P. G., Sarathy, V., Baer, D. R., Amonette, J. E., Pecher, K., Wang, C., Linehan, J. C., Matson, D. W., Penn, R. L., & Driessen, M. D. (2005). Characterization and Properties of Metallic Iron Nanoparticles: Spectroscopy, Electrochemistry, and

- Kinetics. *Environmental Science & Technology*, 39(5), 1221–1230.
<https://doi.org/10.1021/es049190u>
- Ouchiyama, N., & Tanaka, T. (1984). Porosity estimation for random packings of spherical particles. *Industrial & Engineering Chemistry Fundamentals*, 23(4), 490–493.
<https://doi.org/10.1021/i100016a019>
- Owlad, M., Aroua, M. K., Daud, W. A. W., & Baroutian, S. (2009). Removal of Hexavalent Chromium-Contaminated Water and Wastewater: A Review. *Water, Air, and Soil Pollution*, 200(1–4), 59–77. <https://doi.org/10.1007/s11270-008-9893-7>
- Oze, C., Bird, D. K., & Fendorf, S. (2007). Genesis of hexavalent chromium from natural sources in soil and groundwater. *Proceedings of the National Academy of Sciences*, 104(16), 6544–6549. <https://doi.org/10.1073/pnas.0701085104>
- Pan, B., Jiang, Z., Zhang, W., Lv, L., Xie, Y., & Zhang, Q. (2015). *Method for regulating the distribution of metallic nanoparticles within the resin support* (United States Patent US9138737B2). <https://patents.google.com/patent/US9138737B2/en>
- Pande, S., Saha, A., Jana, S., Sarkar, S., Basu, M., Pradhan, M., Sinha, A. K., Saha, S., Pal, A., & Pal, T. (2008). Resin-Immobilized CuO and Cu Nanocomposites for Alcohol Oxidation. *Organic Letters*, 10(22), 5179–5181. <https://doi.org/10.1021/ol802040x>
- Park, H., Park, Y., Oh, S., You, K., & Lee, S. (2009). Enhanced reduction of nitrate by supported nanoscale zero-valent iron prepared in ethanol-water solution. *Environmental Technology*, 30(3), 261–267. <https://doi.org/10.1080/09593330802596705>
- Pellerin, C., & Booker, S. M. (2000). Reflections on Hexavalent Chromium: Health Hazards of an Industrial Heavyweight. *Environmental Health Perspectives*, 108(9), A402–A407.
<https://doi.org/10.2307/3434980>

- PubChem. (n.d.). *Sodium metaborate*. Retrieved July 5, 2023, from <https://pubchem.ncbi.nlm.nih.gov/compound/145326>
- Purolite. (n.d.). *Purolite Product: Purolite® A500Plus*. Retrieved July 5, 2023, from <http://www.purolite.com/product/a500plus>
- Qin, G., McGuire, M. J., Blute, N. K., Seidel, C., & Fong, L. (2005). Hexavalent Chromium Removal by Reduction with Ferrous Sulfate, Coagulation, and Filtration: A Pilot-Scale Study. *Environmental Science & Technology*, *39*(16), 6321–6327. <https://doi.org/10.1021/es050486p>
- Ravikumar, K. V. G., Kumar, D., Rajeshwari, A., Madhu, G. M., Mrudula, P., Chandrasekaran, N., & Mukherjee, A. (2016). A comparative study with biologically and chemically synthesized nZVI: Applications in Cr (VI) removal and ecotoxicity assessment using indigenous microorganisms from chromium-contaminated site. *Environmental Science and Pollution Research*, *23*(3), 2613–2627. <https://doi.org/10.1007/s11356-015-5382-x>
- Saha, R., Nandi, R., & Saha, B. (2011). Sources and toxicity of hexavalent chromium. *Journal of Coordination Chemistry*, *64*(10), 1782–1806. <https://doi.org/10.1080/00958972.2011.583646>
- Sarkar, S., Blaney, L. M., Gupta, A., Ghosh, D., & SenGupta, A. K. (2007). Use of ArsenXnp, a hybrid anion exchanger, for arsenic removal in remote villages in the Indian subcontinent. *Reactive and Functional Polymers*, *12*(67), 1599–1611. <https://doi.org/10.1016/j.reactfunctpolym.2007.07.047>
- Sarkar, S., SenGupta, A. K., & Prakash, P. (2010). The Donnan Membrane Principle: Opportunities for Sustainable Engineered Processes and Materials. *Environmental Science & Technology*, *44*(4), 1161–1166. <https://doi.org/10.1021/es9024029>

- Sedman, R. M., Beaumont, J., McDonald, T. A., Reynolds, S., Krowech, G., & Howd, R. (2006). Review of the Evidence Regarding the Carcinogenicity of Hexavalent Chromium in Drinking Water. *Journal of Environmental Science and Health, Part C*, 24(1), 155–182. <https://doi.org/10.1080/10590500600614337>
- Seidel, C. J., & Corwin, C. J. (2013). Total chromium and hexavalent chromium occurrence analysis. *Journal - American Water Works Association*, 105(6), E310–E319. <https://doi.org/10.5942/jawwa.2013.105.0050>
- Seidel, C. J., Najm, I. N., Blute, N. K., Corwin, C. J., & Wu, X. (2013). National and California treatment costs to comply with potential hexavalent chromium MCLs. *Journal - American Water Works Association*, 105(6), E320–E336. <https://doi.org/10.5942/jawwa.2013.105.0080>
- SenGupta, A. K. (2017). *Ion Exchange in Environmental Processes: Fundamentals, Applications and Sustainable Technology*. Wiley.
- Sengupta, A. K., Clifford, D., & Subramonian, S. (1986). Chromate ion-exchange process at alkaline pH. *Water Research*, 20(9), 1177–1184. [https://doi.org/10.1016/0043-1354\(86\)90064-3](https://doi.org/10.1016/0043-1354(86)90064-3)
- Sengupta, D., Saha, J., De, G., & Basu, B. (2014). Pd/Cu bimetallic nanoparticles embedded in macroporous ion-exchange resins: An excellent heterogeneous catalyst for the Sonogashira reaction. *Journal of Materials Chemistry A*, 2(11), 3986–3992. <https://doi.org/10.1039/C3TA14916A>
- Shard, A. G. (2020). Practical guides for x-ray photoelectron spectroscopy: Quantitative XPS. *Journal of Vacuum Science & Technology A*, 38(4), 041201. <https://doi.org/10.1116/1.5141395>

- Shi, J., Yi, S., He, H., Long, C., & Li, A. (2013). Preparation of nanoscale zero-valent iron supported on chelating resin with nitrogen donor atoms for simultaneous reduction of Pb²⁺ and. *Chemical Engineering Journal*, *230*, 166–171.
<https://doi.org/10.1016/j.cej.2013.06.088>
- Song, Y., Zeng, Y., Jiang, T., Chen, J., & Du, Q. (2022). Efficient Removal of Ciprofloxacin from Contaminated Water via Polystyrene Anion Exchange Resin with Nanoconfined Zero-Valent Iron. *Nanomaterials*, *13*(1), 116. <https://doi.org/10.3390/nano13010116>
- Song, Y., Zeng, Y., Liao, J., Chen, J., & Du, Q. (2021). Efficient removal of sulfamethoxazole by resin-supported zero-valent iron composites with tunable structure: Performance, mechanisms, and degradation pathways. *Chemosphere*, *269*, 128684.
<https://doi.org/10.1016/j.chemosphere.2020.128684>
- Sun, Y.-P., Li, X., Cao, J., Zhang, W., & Wang, H. P. (2006). Characterization of zero-valent iron nanoparticles. *Advances in Colloid and Interface Science*, *120*(1–3), 47–56.
<https://doi.org/10.1016/j.cis.2006.03.001>
- Tai, C., She, J., Yin, Y., Zhao, T., & Wu, L. (2016). Degradation of 2,4,6-Trichlorophenol Using Hydrogen Peroxide Catalyzed by Nanoscale Zero-Valent Iron Supported on Ion Exchange Resin. *Journal of Nanoscience and Nanotechnology*, *16*(6), 5850–5855.
<https://doi.org/10.1166/jnn.2016.12415>
- Toli, A., Chalastara, K., Mystrioti, C., Xenidis, A., & Papassiopi, N. (2016). Incorporation of zero valent iron nanoparticles in the matrix of cationic resin beads for the remediation of Cr(VI) contaminated waters. *Environmental Pollution*, *214*, 419–429.
<https://doi.org/10.1016/j.envpol.2016.04.034>

- Toli, A., Mystrioti, C., Avgoustidis, I., & Papassiopi, N. (2021). Fixed-bed flow experiments with supported green nZVI for the remediation of contaminated waters: Effect of pH and background solution composition. *Chemosphere*, 279, 130472.
<https://doi.org/10.1016/j.chemosphere.2021.130472>
- Toli, A., Mystrioti, Ch., Xenidis, A., & Papassiopi, N. (2021). Continuous Flow Process for Cr(VI) Removal from Aqueous Solutions Using Resin Supported Zero-Valent Iron. *Bulletin of Environmental Contamination and Toxicology*, 106(3), 409–414.
<https://doi.org/10.1007/s00128-020-02843-8>
- U.S. Environmental Protection Agency. (2008). *Drinking Water Health Advisory For Boron* (822-R-08–013). U.S. Environmental Protection Agency.
- Xi, Y., Mallavarapu, M., & Naidu, R. (2010). Reduction and adsorption of Pb²⁺ in aqueous solution by nano-zero-valent iron—A SEM, TEM and XPS study. *Materials Research Bulletin*, 45(10), 1361–1367. <https://doi.org/10.1016/j.materresbull.2010.06.046>
- Zhang, Q., Pan, B., Pan, B., Zhang, W., Jia, K., & Zhang, Q. (2008). Selective Sorption of Lead, Cadmium and Zinc Ions by a Polymeric Cation Exchanger Containing Nano-Zr(HPO₃S)₂. *Environmental Science & Technology*, 42(11), 4140–4145.
<https://doi.org/10.1021/es800354b>